

Development of a QMC code to tackle interacting electronic systems in 2D with application to TMD nanoribbons

Francisco Monteiro de Oliveira Brito

Thesis to obtain the Master of Science Degree in
Physics Engineering

Supervisor(s): Prof. Eduardo Filipe Vieira de Castro
Prof. João Manuel Viana Parente Lopes

Examination Committee

Chairperson: Prof. Lorem
Supervisor: Prof. Eduardo Filipe Vieira de Castro
Co-Supervisor: Prof. João Manuel Viana Parente Lopes
Members of the Committee: Dr. Lorem Ipsum

June 2018

The behavior of large and complex aggregates of elementary particles, it turns out, is not to be understood in terms of a simple extrapolation of the properties of a few particles.

P. W. Anderson

Cover picture credit: University of Manchester
www.graphene.manchester.ac.uk (accessed on 12 June 2018)

Acknowledgments

I want to start by thanking my parents Laura and João, and the rest of my family, biological, and non-biological. They did everything they could (and more) to ensure that I had the opportunities that led me to develop this work. They taught me to do things out of love, and that is a lesson I carry with me everyday of my life.

Then, I want to thank Beatriz (não te vou deixar ver isto já)

Of course, I would also like to thank my supervisors Prof. Eduardo Filipe Vieira de Castro, and Prof. João Manuel Viana Parente Lopes for the openness, support, and tireless will to teach me, and learn with me. Not only did they provide valuable scientific insight, but they also showed great humaneness in guiding me through the journey I embarked on during the last year.

I also want to express the gratitude and admiration I feel for my colleagues at Centro de Física do Porto, the Theoretical Physics Center at University of Porto. They worked beside almost daily, discussing and criticizing my work, providing great help, be it by cheering me up in darker times, or by celebrating even the tiniest achievements in my work.

I am grateful for having had great teachers, who inspired me to seek knowledge over the years. I wish to thank all of them. In particular, I want to mention Maria da Luz and Vítor Santos that got me excited about Physics in the first place, and Profs. Joaquim Agostinho Gomes Moreira and João M. B. Lopes dos Santos for sparking my enthusiasm for condensed matter physics. Moreover, I would like to thank Dr. Miklós Lajkó, Dr. Jon Demidio for what they taught during my stay in Lausanne, and Prof. Frédéric Mila for introducing me to the many currents topics of research in condensed matter theory, and sharing valuable insight.

Lastly, I want to thank a number of close friends who constantly support me, of which I will mention a few: Mateus, Carol, Marta, Bárbara, Andreia, Inês Lopes, Inês Viegas, Nuno, Glênio, Angélica, Raquel, Tiago, Miguel, Branca, Pedro, and Isabela.

Abstract

The aim of this work (English)

Keywords

Hubbard Model, Strongly Correlated Electrons, Transition Metal Dichalcogenides, Quantum Monte Carlo (QMC) (English)

Resumo

O objectivo deste trabalho (Português)

Palavras Chave

Palavras-chave (Português)

Contents

1	Introduction	1
1.1	Motivation	2
1.2	Strongly correlated electron systems	2
1.3	State of The Art	5
1.3.1	Beyond graphene: TMD nanoribbons	5
1.3.2	Introduction to Quantum Monte Carlo	7
1.3.3	Monte Carlo Method in Classical Statistical Physics	9
1.3.4	Variational Monte Carlo	15
1.3.5	Diffusion Monte Carlo	16
1.4	Original Contributions	17
1.5	Thesis Outline	17
2	Minimal models of electron correlations in energy bands	19
2.1	Modelling electron correlations	20
2.2	Hubbard model	21
2.2.1	Electron correlations in narrow d -bands	22
2.2.2	Hubbard Hamiltonian	24
2.2.3	Particle-hole symmetry	26
2.3	Mott insulators	27
2.4	Exact solutions for simple cases	30
2.4.1	The purely atomic $\frac{t}{U} = 0$ limit	32
2.4.2	The non-interacting $\frac{t}{U} \rightarrow \infty$ limit	36
2.5	Effective Heisenberg Hamiltonian	38
2.5.1	Two-site calculation	38
2.5.2	Degenerate perturbation theory	41
2.6	Green's functions: Mott gap and spectral function	42
2.7	Magnetism and mean field theory	42
3	Auxiliary Field Quantum Monte Carlo	43
3.1	Trotter-Suzuki Decomposition	44
3.1.1	Hubbard-Stratonovich transformation	44

3.1.1.A	Monte Carlo sampling of the HS-field	53
3.1.1.B	Making measurements	55
3.1.1.C	Correlation functions	58
4	Discussing the algorithm	61
5	Stabilization	63
6	Applications	65
6.1	One-dimensional Hubbard Chain	66
6.2	Square lattice	66
6.3	Honeycomb lattice	66
6.4	Nanoribbon	66
7	Conclusions and Future Work	69
Bibliography		71
Appendix A Hartree-Fock Approximation and the Self Consistent Field Method		A-1
Appendix B Computing the partition function for a quadratic Hamiltonian		B-1
Appendix C Obtaining an effective Heisenberg Hamiltonian as the $U/t \gg 1$ limit of the Hubbard model		C-1

List of Figures

1.1	Graphene monolayer; graphene's dispersion relation.	6
1.2	Fabrication of Transition Metal Dichalcogenide (TMD) nanoribbons	7
1.3	Zigzag edges of a nanoribbon and magnetism.	7
2.1	Graphical comparison between the Ising and the Hubbard models.	20
2.2	Hydrogen atomic wave functions.	22
2.3	Bipartite lattices and antiferromagnetic order.	26
2.4	Configuration of the Hubbard model on the square lattice with a hole and a doubly occupied site.	29
2.5	Electron density in the purely atomic limit of the Hubbard model	34
2.6	Magnetization as a function of the on-site interaction $\langle m^2 \rangle (U)$ in the single site Hubbard model for varying temperature T .	35
2.7	Magnetization as a function of temperature $\langle m^2 \rangle (T)$ in the single site Hubbard model for varying chemical potential μ .	35
6.1	Boundary conditions on the nanoribbon.	67

List of Tables

6.1 Nearest neighbors on the nanoribbon.	68
--	----

Abbreviations

QMC Quantum Monte Carlo

TMD Transition Metal Dichalcogenide

LG Landau Ginzburg

2D Two-dimensional

1D One-dimensional

PBC Periodic boundary condition

OBC Open boundary condition

PHS Particle-hole symmetry

AF Antiferromagnetic

PHT Particle-hole transformation

AFM Atomic Force Microscopy

BSS Blaistenbecker, Scalapino and Sugar

FFT Fast Fourier Transform

1

Introduction

Contents

1.1	Motivation	2
1.2	Strongly correlated electron systems	2
1.3	State of The Art	5
1.4	Original Contributions	17
1.5	Thesis Outline	17

1.1 Motivation

The isolation of graphene in 2004 has led to a growing interest of the scientific community in Two-dimensional (2D) materials revealing extraordinary properties. It might seem surprising that 2D systems were not considered as a real possibility before since they are often idealized in thought experiments, for example when investigating toy models of more complex higher dimensional systems. In fact, their very existence was not expected *a priori* because at first sight they seem to violate the Mermin-Wagner-Hohenberg theorem [1–3], a no-go theorem that forbids ordering below three dimensions at finite temperature¹. Graphene paved the way for the search for similarly stable 2D materials, and since it was isolated, a plethora of these has been discovered. A vast set of open problems remains to be solved within the realm of the fascinating and counterintuitive properties of the now huge variety of existing 2D systems. In particular, in some of these, the effect of electron interactions is non negligible, leading to emergent phenomena. These are collective effects that emerge as a result of the interactions between the individual components of a system. The properties of the system's components do not directly percolate up; instead, they shape the interactions that dictate the system's properties sometimes in rather unexpected ways, leading to unusual behavior.

Interacting electron systems are often tackled by carrying out computer simulations. Quantum Monte Carlo (QMC) is a family of numerical methods that are amply applicable to condensed matter physics problems, and that are particularly well suited to study strongly correlated electrons. Despite the system size being constrained due to limited simulation time, reliable, accurate and unbiased solutions are provided to the otherwise intractable quantum many-body problem. The class of QMC algorithms that is used in this work was introduced in the 1980's in a series of seminal papers by Hirsch and Blankenbecler, Scalapino and Sugar² [4–10], but it saw a recent surge [11–23] due to the increase in computational power, and algorithmic development. As a result, the field is currently very active and method optimization can prove crucial in applications to widely studied physical models of electron interactions. In particular, the recent computational and algorithmic developments allow the study of both larger and lower temperature systems.

In this work, an implementation of determinant QMC based on the BSS algorithm is used to simulate a Transition Metal Dichalcogenide (TMD) nanoribbon, a nanostructure made of this recent member of the 2D materials family.

1.2 Strongly correlated electron systems

Condensed matter physics is concerned with the emergence of the properties of quantum materials from complexity. The central concept within this approach is that of symmetry breaking. When a

¹2D materials are stable because not all the conditions of Mermin-Wagner-Hohenberg theorem are verified, namely the condition of short-ranged interactions. The issue is quite subtle, and is beyond the scope of this work.

²After whom the Blankenbecler, Scalapino and Sugar (BSS) algorithm, on which we based the implementation used in this work, is named.

phase transition occurs, a system is said to condense into a phase of lower symmetry. A simple pictorial example is the transition from a gas to a solid. Statistically, any point within a gas is equivalent, that is, on average, the surroundings of all points look similar. Formally, the system is then said to be fully translationally invariant. On the other hand, in a solid, a point is only equivalent to a discrete set of other points. In fact, a simplified view of a solid consists of a periodic arrangement of atoms occupying the points of a lattice. Any point on the lattice can be reached starting from any other point upon translation by a lattice vector. Thus, a system that makes a transition from the gaseous to the solid state becomes invariant only under a discrete set of translations, rather than a continuous one.

A framework that is commonly used to identify symmetry breaking is the Landau Ginzburg (LG) theory of phase transitions. The theory gives a prescription to discover phase transitions. More precisely, it gives criteria for a symmetry to become manifest. Although this framework is very useful, it turns out that the search for order relies on symmetry ideas well beyond condensed matter. Symmetry breaking gives rise to emergent phenomena. The idea of emergence rests on a constructionist, rather than a reductionist hypothesis: that the behavior of the many does not trivially follow from the behavior of the few. As P.W. Anderson puts it, “The ability to reduce everything to simple fundamental laws does not imply the ability to start from those laws and reconstruct the universe.” [24]

The broad scope of condensed matter comes from the sheer number of possibilities that the symmetry breaking approach affords. For the specific case of the LG theory, one can study the emergence of magnetism, superconductivity, or superfluidity, just to name a few. However, as we shall see, sometimes the LG theory fails to capture a system’s behavior, and we must resort to other theories to identify these, or other eventual properties that might arise. The Landau Ginzburg procedure can be summarized as follows: identify an order parameter reflecting the underlying symmetry of the system, and minimize the free energy in order to deduce conditions for the symmetry to become manifest, leading to a phase transition. The drawback of this *variational* approach is that it might be difficult to identify an order parameter in the first place. Moreover, even if we do manage to find one, the usual procedure may be impossible to perform. It can easily happen that the degree of complexity of the order parameter is simply too high. Additionally, and perhaps more importantly, not all phase transitions can be described by the LG paradigm.

On the one hand, there are systems where a different kind of order arises. A prominent example is that of fractional quantum Hall effect, where (rather surprisingly!) the *quasi-particles* describing the excitations of the quantum Hall fluid carry *fractions* of the electron charge. There is an intimate connection between charge fractionalization and topology, which may be understood in terms of the properties of the Laughlin states describing the quantum Hall fluid. However, while it is tempting to try to characterize the latter in terms of the LG paradigm, it must actually be regarded as a distinct type of matter, where “topological order” arises [25].

On the other hand, for the so called strongly correlated systems we shall focus on in this work, there are phenomena which emerge specifically due to the interacting nature of the problem. They are elusive because a description in terms of the LG paradigm does not yield a behavior consistent with what is observed empirically. Instead, order emerges from the complexity created by the interactions

among all the constituents. The LG theory fails because it ignores these interactions by disregarding fluctuations in the microscopic configuration of the system. This approximation consists of reducing the complex interactions to an effective *mean field*, which is normally determined self consistently. Strongly correlated systems require an approach beyond mean field, which makes them both extremely interesting and notoriously difficult to tackle. The mean field view fails to describe them because it considers each constituent to interact only with an external entity representing the interactions with all other constituents, ignoring collective behavior. In fact, the failure of mean field theory is not limited to correlated systems, and its success in describing a given system depends, for example, on the dimensionality³ and on the range of the particular type of interaction that is considered.

In many cases, mean field theory is too extreme an approximation. Nonetheless, its occasional failure at capturing the whole of a system's properties does not deem it useless. Actually, it is quite the contrary. Mean field is often used as a first approach to build an intuitive physical picture for the general properties and behavior of the system. Of course, this is done while keeping in mind that the description it provides is intrinsically insufficient. Clearly, to extract the features of a correlated system we must extend it to the fully interacting case.

Strongly correlated quantum matter is ubiquitous and is at the heart of today's most advanced electronic materials, namely organic conductors, high T_c (cuprate) superconductors, colossal magnetoresistance materials, and “heavy-fermion”⁴ compounds. Actually, the problem of strong correlations has now expanded beyond condensed matter physics. Quark-gluon plasmas, believed to have been formed just a few microseconds after the Big Bang, also belong to this class of systems. Another example comes from atomic physics: ultracold atoms in optical lattices behave in a very similar way to correlated electrons. In fact, the behavior is so similar that these systems are being used as *de facto* quantum simulators of correlated electron systems [26].

A central piece in the understanding of correlated matter is the Hubbard model. It was introduced to bridge a gap between metals and magnetic insulators, building on the earlier work of Mott. The model is extremely simple. Electrons hop from atom to atom on a lattice, paying an energy penalty when they occupy the same site. This repulsive effect results in correlations beyond those that are always present due to the fermionic nature of the particles obeying the Pauli exclusion principle. In the limit of weak repulsion, the electrons are nearly free, and the system behaves like a metal. Otherwise, the electrons become localized at fixed atomic positions resulting in magnetic insulating behavior. The model is simple to formulate, but already includes correlation effects between all electrons in the solid. Thus, it is not surprising that an exact solution exists only in 1D [27], and higher dimensional versions are still being studied more than 50 years after the model appeared [28].

³Normally, there is an upper critical dimension d_c above which mean field is exact. Below d_c , its predictions might be useful qualitatively, but not quantitatively.

⁴The quasi-particles describing excitations in these materials behave like much heavier electrons, hence the name.

1.3 State of The Art

Solving the many-body problem remains one of the greatest challenges in physics. Following the wealth of attempts at such pursuit, certain phenomena arising due to the strong interactions in quantum systems are explained in different theoretical frameworks, namely superconductivity, the Mott metal-insulator transition, and fractional quantum Hall effect. All of these breakthroughs represented revolutions in their respective fields with significant scientific and technological impact.

Only in very limited cases does an actual analytical solution exist for the Schrödinger equation for a system of interacting particles. One must resort to sophisticated approximation methods to obtain information about the role played by the competing interactions under various conditions in the aforementioned cases. It is then natural that numerical methods have become prominent as a tool for extracting useful information about this type of systems. QMC is amongst the most accurate and extensively studied ones.

The idea of all QMC methods is to reduce the interacting problem to solving a set of integrals, which can be evaluated numerically through a standard stochastic procedure. These integrals are arrived at upon formulating the quantum many-body description of the system using the Schrödinger equation. Hence the name Quantum Monte Carlo, which is used to distinguish it from Classical Monte Carlo. In the classical version, one measures thermal averages, while in the quantum version, one measures expectations of operators over the Hilbert space of the system, corresponding to physical observables that fluctuate with a dynamics given by the Schrödinger equation.

1.3.1 Beyond graphene: TMD nanoribbons

2D materials have steadily been attracting more and more attention since graphene was experimentally isolated from a graphite sample by mechanical exfoliation, yielding a system constituted by a single layer of atoms (Figure 1.1, left). Since then, numerous studies have been made due to the promising properties of these materials, and the interesting as-yet-unseen phenomena occurring within them, for example: unconventional quantum Hall effect, absence of localization, and electrons behaving like massless relativistic particles (Figure 1.1, right), providing a bridge between condensed matter physics and quantum electrodynamics [29].

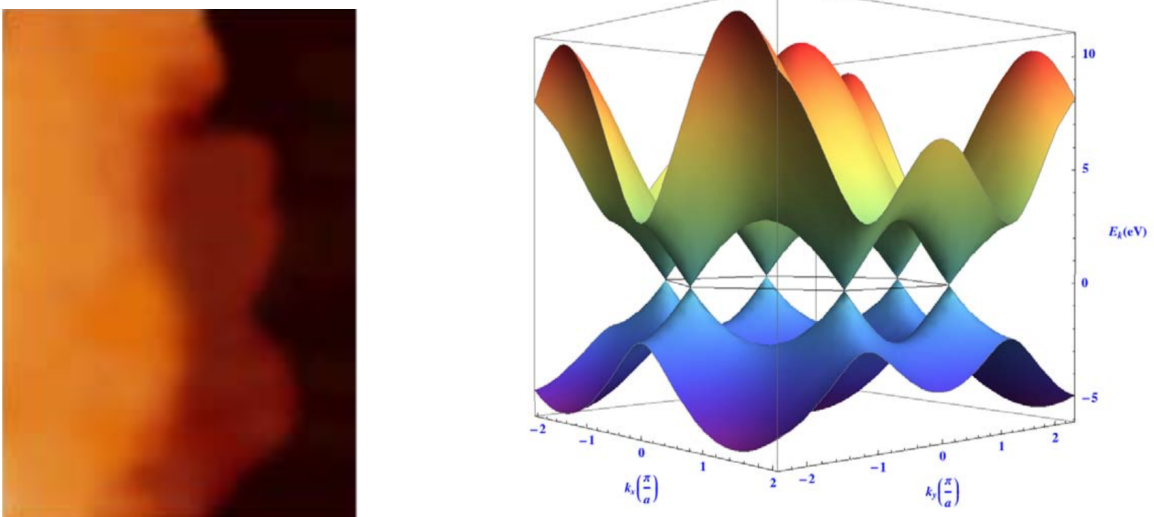


Figure 1.1: Left: Atomic Force Microscopy (AFM) picture of a graphene monolayer. The black area is a substrate used for fabrication purposes. The dark orange area is a monolayer of graphene. Right: Dispersion relation of graphene. The black line represents the Fermi energy. Close to it, the dispersion relation is linear, corresponding to massless excitations (taken from [30]).

On the other hand, TMDs are a recent member of the 2D materials family [31–33]. TMDs have been attracting interest because they seem to overcome some of the drawbacks of graphene in technological applications. For example, monolayer graphene is gapless, while its bilayer counterpart has only a tunable, but small gap of the order of a tenth of an eV. Contrastingly, TMDs have an intrinsic gap in excess of 1 eV, being more promising in designing, for example, transistors. Hole-doped TMDs are expected to show topological superconductivity [34], while the superconducting phase of graphene has been predicted, but is not easily attained. Superconductivity in graphene-like 2D materials is important because it could boost high speed nanoelectronics. Moreover, the presence of transition metal atoms in TMDs suggests the possibility of magnetic ordering [35], which could be very relevant in nanospintronics applications. Both topological superconductivity and magnetic ordering arise due to the effect of strong electron correlations. Thus, to investigate these properties of TMDs when performing simulations, we need a computational method that is robust enough to capture the effects of electron interactions.

A nanoribbon consists of a 2D layer that can be regarded as infinitely long on one direction, but not on the other (Figure 1.2), so that edge states become relevant, and can be controlled to yield interesting properties. For simulation purposes, it is natural to assume translational invariance along the ribbon’s longitudinal direction, and use Periodic boundary conditions (PBCs). On the other direction, we use Open boundary conditions (OBCs), effectively considering zigzag edges (Figure 1.3, left).

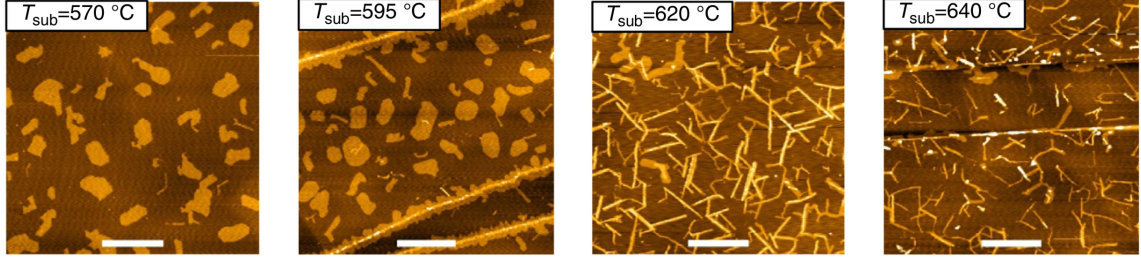


Figure 1.2: Fabrication of TMD nanoribbons. From left to right, we see AFM images showing the appearance of nanostructures ranging from 2D nanoislands to nanoribbons, as the temperature of the substrate is increased. The nanoribbons are grown by taking advantage of the temperature dependence of shape transformations occurring during the nonequilibrium growth of this kind of surface-based nanostructures. (taken from [36])

A high density of low-energy electronic states is localized at the zigzag edges, decaying quickly in the bulk, which suggests the possibility of magnetic ordering. In fact, a mean field solution of the Hubbard model for a graphene nanoribbon shows that magnetic moments are localized at the edges [37] (Figure 1.3, right). QMC has been used to investigate edge-state magnetism beyond mean field in graphene [38–42]. However, edge magnetism in TMD nanoribbons remains unexplored [43].

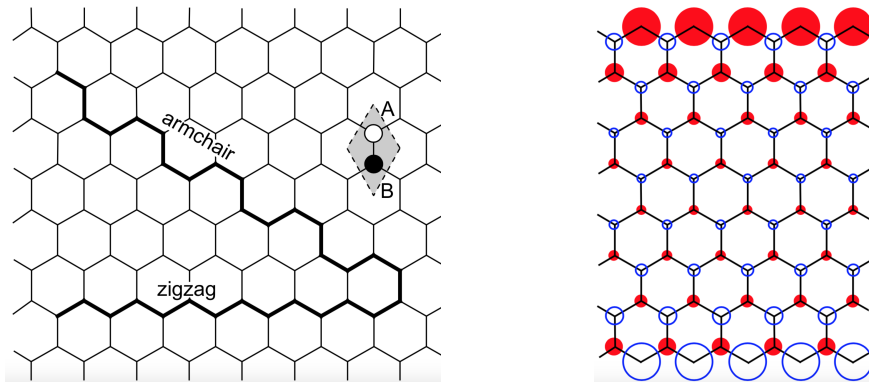


Figure 1.3: Left: Two possible terminations of a TMD nanoribbon condensing in a honeycomb lattice. Right: Local magnetic moments exist on the zigzag edges. The area of the circles corresponds to the magnitude of the magnetic moment, while the color red corresponds to a spin up density, and blue to a spin down density. The accumulation of electronic edge states leads to an AF ground state (opposite edges with opposite magnetic moment). (taken from [37])

While the zigzag graphene nanoribbon antiferromagnetic ground state is semiconducting, a state with interedge ferromagnetic orientation is a metal. An example of an application based on the switching between the two states is a magnetoresistive sensor. This device allows switching between low and high-resistance configurations, corresponding, respectively, to parallel, and antiparallel configurations of ferromagnetic leads at the ends of a nanoribbon. An important application of this project is precisely the investigation of the possibility of edge-state magnetism, as is observed in graphene nanoribbons, for TMD nanoribbons, which could yield similarly innovative applications.

1.3.2 Introduction to Quantum Monte Carlo

In principle, the properties of a quantum many-fermion system can all be deduced by solving an extremely complicated Schrödinger equation that takes into account the coupling of all (identical)

particles of the system. However, for the majority of systems the resulting integrals have no analytic solution, so we solve the problem by numerical integration. But there is a myriad of methods to evaluate integrals numerically. How do we pick the best one for this case? Multi-dimensional integrals are plagued by the curse of dimensionality. Although the Newton-Cotes quadrature formulas (including, for example the Newton method, and Simpson's rules), Gaussian quadrature formulas, or Romberg's method all scale polynomially with the number of integration points, they become impractical as the dimension increases. To use them, one would invoke Fubini's theorem to reduce the multi-dimensional integral to a series of one-dimensional integrals. However, the number of function evaluations required to compute the whole integral grows exponentially with its dimension. Monte Carlo methods preserve the polynomial scaling, thus yielding comparable accuracy with far less function evaluations. It is natural to use them since typically the state space of our quantum system is huge, leading to high dimensional integrals.

The Monte Carlo method is ubiquitous. Its central idea is to use randomness to produce accurate estimates of deterministic integrals. The term was coined by Nicolas Metropolis in 1949, first appearing in a seminal paper, in which it was described as a “statistical approach to the study of differential equations, or more generally, of integro-differential equations that occur in various branches of sciences”[44]. Although it was used as early as 1777 in an experiment known as Buffon’s needle - where one obtains an estimate of the constant π by repeatedly throwing a needle randomly onto a sheet of paper with evenly spaced lines - it was crucially developed in the Los Alamos National Laboratory during World War II where the development of the first atomic bomb was completed, the primary objective of the Manhattan Project. The method is particularly useful when one wants to sample from a probability distribution in an exponentially large state space. In fact, it can in principle be used to solve any problem allowing a probabilistic formulation.

A variety of Quantum Monte Carlo (QMC) methods exists, using a sampling scheme based on the Metropolis algorithm, and variations thereof. Variational and Diffusion QMC are the simplest QMC methods that allow one to capture some properties of correlated systems. Although they already contain the main concepts used in this type of simulations, it is not always possible to use them. We will discuss their flaws and show how further refinement leads to the determinant, or auxiliary field method we ultimately used.

Using the Monte Carlo approach to study a many-fermion system implies overcoming a significant obstacle common to all QMC methods - the so called *fermion-sign problem*. Pauli’s exclusion principle implies that the many-fermion wave function is anti-symmetric, which leads to a sign oscillation that greatly impedes the accurate evaluation of averages of quantum observables. The anti-symmetry constraint implies that a straightforward weight interpretation of the wave function is not possible. In the case of the finite temperature algorithm, the cancellations that occur when computing the average of any physical observable lead to poor statistical properties of the corresponding estimators. This means that a massive amount of samples requiring enormous computer time are needed to obtain meaningful results. In the case of the zero temperature algorithms, the situation is even worse. It might not even be possible to design a stochastic process carrying the system to its ground state, as

normally is done in “projective” methods⁵: the wave function that is used as an initial proposal turns out to converge to a bosonic one, and the fermionic character of the system is lost.

As was proven by Troyer, the *fermion-sign problem* has NP⁶ computational complexity [45]. One of the greatest open questions in computer science is whether $P = NP$. Solving the *fermion-sign problem* would imply finding a solution to $P = NP$, which would constitute a major breakthrough.

1.3.3 Monte Carlo Method in Classical Statistical Physics

Monte Carlo methods form the largest and arguably most useful class of numerical methods used to approach statistical physics problems. Statistical physics often deals with computing quantities that describe the behavior of condensed matter systems. The main difficulty one faces when doing so has to do with the collective nature of these systems. Many identical components comprise these systems, and while the equations that govern the behavior of the whole may be easy to write down, their solution is in general a remarkably laborious mathematical problem.

The exponentially large number of configurations of a typical condensed matter system can be daunting. Analytical solutions are more often than not hopeless and even numerical solutions are seemingly challenging. However, they give valuable information lying between theory and experiment, and connecting them.

Suppose you try to sample uniformly from the probability distribution of all possible configurations of one of the aforementioned systems. Changes are your algorithm will not end before the Universe does. This is the computational complexity hurdle. A related issue is that of finite size effects. We are far from being able to simulate a macroscopically sized system. At best we can simulate a system that has only a minuscule fraction of the actual size of the corresponding real world system. Amazingly there are techniques that allow us to efficiently extract information out of relatively small size simulations. Nonetheless, increasing the system size systematically improves the reliability of a simulation. Thus, the more efficient the algorithm is, the larger the system we can simulate in a fixed time.

The sheer number of equations describing a condensed matter system, and sometimes the strong coupling between them deems the task of finding an exact solution either very tough or even impossible. It is not even clear whether an analytical solution would be of any use in many cases, and a statistical and numerical treatment often allows us to study more effectively the key properties of a system.

Strikingly, we are able to describe a system that is governed by a macroscopically large number of equations in terms of only a few variables. The loss of information in doing so is only apparent. The statistical description is so effective because most of the possible states of the system are extremely improbable when compared to the relevant very narrow part of configuration space. The success of the field is largely attributed to the averaging out that naturally occurs when we measured a property of a macroscopic system.

The law of large numbers affords an approximation to integrals which can be written as an ex-

⁵Methods that iteratively project a trial wave function onto the ground state.

⁶NP or nondeterministic polynomial time, meaning that one can devise an algorithm that verifies the “yes” answer to a decision problem in polynomial time in the system size. Note that the class P - of polynomial time algorithms - is a subclass of NP.

pectation of a random variable. Upon drawing enough independent samples from the corresponding distribution, the sample mean gets arbitrarily close to the integral at stake.

$$\mathbb{E}[f(X)] = \int dx f(x)p(x), \quad (1.1)$$

where $p(x)$ is the distribution of X .

We could simply draw M independent and identically distributed samples $x_{1,\dots,M}$ from $p(x)$ and approximate the integral as

$$\frac{1}{M} \sum_{k=1}^M f(x_k), \quad (1.2)$$

which in most cases converges to the desired expectation, as long as M is large enough. How large?

$$\text{Var}\left(\frac{1}{M} \sum_{k=1}^M f(x_k)\right) = \frac{1}{M} \text{Var}(f(x_1)) \sim \mathcal{O}\left(\frac{1}{M}\right) \quad (1.3)$$

Thus, the correction to the sample mean is of order $\mathcal{O}(\frac{1}{\sqrt{M}})$ as long as $\text{Var}(f(x_1)) \sim 1$.

How do we sample from an arbitrary distribution $p(X)$? The idea is to first make an educated choice of a Markov Chain with the prescribed stationary distribution from which we ultimately desire to sample from, $p(X)$. After a sufficiently high number of steps, a Markov Chain Monte Carlo (MCMC) algorithm generates samples from the target distribution. Imposing some conditions on this Markov Chain, namely that it should be irreducible, aperiodic and positive recurrent, the ergodic theorem guarantees that the empirical measures of the aforementioned sampler approach the target stationary distribution. Another important condition to impose on this Markov Chain is detailed balance. Let the transition matrix be $\mathbf{P} = [P_{\mu \rightarrow \nu}]$, and the state space Ω be $\{\pi_\mu | \mu = 1, \dots, |\Omega|\}$, where $|\Omega|$ is the total number of possible states. Then, the condition of detailed balance is defined for all μ, ν as

$$\pi_\mu P_{\mu \rightarrow \nu} = P_{\nu \rightarrow \mu} \pi_\nu \quad (1.4)$$

Consider a system in state μ that makes transitions to state ν at a rate $R_{\mu \rightarrow \nu}$ (that specifies the system's dynamics) and vice-versa. The probability that a system is in state μ at time t , $p_\mu(t)$, such that $\sum_\mu p_\mu(t) = 1$, is given by the master equation(s):

$$\frac{dp_\mu}{dt} = \sum_\nu [p_\nu(t)R_{\nu \rightarrow \mu} - p_\mu(t)R_{\mu \rightarrow \nu}] \quad \forall \mu \in \Omega \quad (1.5)$$

The equilibrium occupation probabilities at finite temperature T follow the Boltzmann distribution.

$$\pi_\mu = \lim_{t \rightarrow \infty} p_\mu(t) = \frac{1}{Z} e^{-E_\mu/k_B T}, \quad (1.6)$$

where E_μ is the energy of state μ , k_B is Boltzmann's constant, and Z is the partition function, from which we can extract thermodynamic functions in terms of expectations of physical quantities $\langle Q \rangle$, and response functions in terms of their variance σ_Q^2 .

Imposing the condition of stationarity on equation (1.5), $d_t p_\mu = 0$, and noting that $P_{\mu \rightarrow \nu} =$

$R_{\mu \rightarrow \nu} dt$, we obtain the equilibrium condition

$$\sum_{\nu} \pi_{\mu} P_{\mu \rightarrow \nu} = \sum_{\nu} P_{\nu \rightarrow \mu} \pi_{\nu} \iff \pi_{\mu} \sum_{\nu} P_{\mu \rightarrow \nu} = \sum_{\nu} P_{\nu \rightarrow \mu} \pi_{\nu} \iff \pi_{\mu} = \sum_{\nu} P_{\nu \rightarrow \mu} \pi_{\nu} \quad (1.7)$$

This condition is enough to ensure convergence to an equilibrium of the dynamics of the Markov process. However, it does not guarantee that the reached distribution is our desired one, $\boldsymbol{\pi}$, after running the process for long enough. The probability of a state evolves according to

$$\pi_{\nu}(t+1) = \sum_{\mu} P_{\mu \rightarrow \nu} \pi_{\mu}(t) \iff \boldsymbol{\pi}(t+1) = \mathbf{P}\boldsymbol{\pi}(t) \quad (1.8)$$

The stationary distribution of a Markov chain obeys

$$\boldsymbol{\pi}(\infty) = \mathbf{P}\boldsymbol{\pi}(\infty), \quad (1.9)$$

however, condition (1.7) also allows for limit cycles of length n , where $\boldsymbol{\pi}$ rotates around a number of configurations:

$$\boldsymbol{\pi}(\infty) = \mathbf{P}^n \boldsymbol{\pi}(\infty), \quad (1.10)$$

where \mathbf{P}^n is the n -th power of \mathbf{P} .

Detailed balance is a stronger requirement than the equilibrium condition, which eliminates limit cycles, thus ensuring that our sampler draws configurations from the desired distribution. Intuitively, detailed balance corresponds to incorporating time-reversal symmetry in a simulation. The condition imposes a constraint on the Markov transition probabilities:

$$\frac{P_{\mu \rightarrow \nu}}{P_{\nu \rightarrow \mu}} = \frac{\pi_{\nu}}{\pi_{\mu}} = e^{-\beta(E_{\nu} - E_{\mu})} \quad (1.11)$$

Crucially, Monte Carlo methods employ *importance sampling*. It turns out that we can improve upon our estimate of $\mathbb{E}[f(X)]$ by introducing a separate distribution $q(x)$, and defining the weight function as $w(x) = p(x)/q(x)$. Then, we can rewrite equation (1.1):

$$\mathbb{E}[f(X)] = \int dx f(x) q(x) w(x) = \mathbb{E}[f(Y) w(Y)], \quad (1.12)$$

with $Y \sim q$, i.e. the random variable Y follows the distribution $q(Y)$.

It appears as though we didn't gain anything. However, by choosing q wisely, we can actually reduce the variance we computed in equation (1.3):

$$\text{Var}\left(\frac{1}{M} \sum_{k=1}^M f(y_k) w(y_k)\right) = \frac{1}{M} \text{Var}\left(f(y_1) w(y_1)\right) \quad (1.13)$$

Since we didn't make any assumptions about $q(Y)$, it may be chosen so as to minimize the variance, hence the error of the Monte Carlo estimator, improving the approximation of the expectation.

However, note that the error remains proportional to $\frac{1}{\sqrt{M}}$. In practice, we devise a method to select the portion of state space which contains states contributing more significantly to the average. This procedure ensures that $\text{Var}(f(y_1)w(y_1)) \sim 1$, improving the efficiency of our sampler. The choice of the weight function translates to the averaging process by changing the estimator. Explicitly computing the average

$$\langle Q \rangle = \frac{\sum_{\mu} Q_{\mu} e^{-\beta E_{\mu}}}{\sum_{\mu} e^{-\beta E_{\mu}}} \quad (1.14)$$

is only tractable for very small systems. In practice, we choose a subset of M states $\{\mu_1, \mu_2, \dots, \mu_M\}$, and estimate the average as

$$Q_M = \frac{\sum_{i=1}^M Q_{\mu_i} \pi_{\mu_i}^{-1} e^{-\beta E_{\mu_i}}}{\sum_{j=1}^M \pi_{\mu_j}^{-1} e^{-\beta E_{\mu_j}}} \quad (1.15)$$

The estimate improves as N increases, and when $N \rightarrow \infty$, $Q_M \rightarrow \langle Q \rangle$. The accuracy of the estimator depends on the choice of the probabilities $\boldsymbol{\pi}$, which is related to the aforementioned variance. For example, if $\boldsymbol{\pi}$ corresponds to the uniform distribution, i.e. $\pi_{\mu} = \frac{1}{|\Omega|} \forall \mu \in \Omega$, we have

$$Q_M = \frac{\sum_{i=1}^M Q_{\mu_i} e^{-\beta E_{\mu_i}}}{\sum_{j=1}^M e^{-\beta E_{\mu_j}}}, \quad (1.16)$$

which turns out to be a poor choice since most of the visited states contribute negligibly to the average, leading to an inaccurate estimate. The sum is dominated by a small subset of states, which we would like to access. The idea of the Quantum (Classical) Monte Carlo method is to simulate the random quantum (thermal) fluctuations of a system, as it oscillates between states in a given time frame [46]. Instead of visiting these states uniformly, the most relevant part of the phase space is sampled more frequently, overcoming the seemingly exponential complexity of computing a sample mean numerically. Even though only a small fraction of the system's states are sampled, we then obtain an accurate estimate of physical quantities of interest, namely energy, and correlation functions. This is implemented via a proposal-acceptance scheme.

To exploit the freedom given by condition (1.11), we note that we can always introduce a non-zero “stay-at-home” probability $P_{\mu \rightarrow \mu} \in [0, 1]$. Regardless of its value, detailed balance is satisfied. Similarly, any adjustment in $P_{\mu \rightarrow \nu}$ must be compensated by changing $P_{\nu \rightarrow \mu}$ to preserve their ratio. Break the transition probability into a selection probability and an acceptance ratio, respectively:

$$\frac{P_{\mu \rightarrow \nu}}{P_{\nu \rightarrow \mu}} = \frac{G_{\mu \rightarrow \nu} A_{\mu \rightarrow \nu}}{G_{\nu \rightarrow \mu} A_{\nu \rightarrow \mu}} \quad (1.17)$$

The Markov process now consists of generating a chain of states according to $G_{\mu \rightarrow \nu}$, which are then accepted or rejected depending on $A_{\mu \rightarrow \nu}$. Since we want to make the algorithm as efficient as possible, we want to make the acceptance ratio as close to one as possible to avoid useless steps. The most common way to do this is to fix the largest of them to one, and adjust the other accordingly. The acceptance ratio will be close to one more often if $G_{\mu \rightarrow \nu}$ includes most of the dependence of $P_{\mu \rightarrow \nu}$ on the characteristics of the states μ, ν . Ideally, states would always be selected with the correct transition

probability, and the acceptance ratio would be fixed to unity. Good algorithms approach this situation, and much effort has been directed at optimizing them to do so.

By far, the most common sampling scheme choice is the Metropolis-Hastings algorithm, which we now describe.

We select the transition probability to be uniform, and impose detailed balance through the choice of the acceptance ratios:

$$\frac{P_{\mu \rightarrow \nu}}{P_{\nu \rightarrow \mu}} = \frac{A_{\mu \rightarrow \nu}}{A_{\nu \rightarrow \mu}} = e^{-\beta(E_\nu - E_\mu)} \quad (1.18)$$

Suppose that $E_\mu < E_\nu$. Then, $A(\nu \rightarrow \mu) > A(\mu \rightarrow \nu)$, and since only the acceptance ratio is fixed, we may freely set $A(\nu \rightarrow \mu) = 1$, which fixes $A(\mu \rightarrow \nu) = e^{-\beta(E_\nu - E_\mu)}$. This choice maximizes the efficiency of the algorithm. In short, we propose a random new state uniformly, and then we accept it with probability $A_{\mu \rightarrow \nu} = \min(1, e^{-\beta(E_\nu - E_\mu)})$.

Before we can use the states generated by our sampler to measure averages of physical quantities, we must reach the stationary distribution of the Markov process. We consider this condition to be satisfied after a time τ_{eq} , measured in steps of the algorithm. When we consider a lattice model with a discrete set of states at each site $i = 1, 2, \dots, N$, we say that a *sweep* is completed whenever N Monte Carlo steps are performed. Thus, the number of “warm-up” sweeps is $W = \tau_{\text{eq}}/N$.

Before running a simulation, we need to decide how many sweeps we need to get an accurate estimate of the average. The problem is that we need uncorrelated samples to average over. To clarify, let us choose a specific model. The paradigmatic model of statistical physics is the Ising model, a classical model of a magnet, which consists of considering spins-1/2 on a lattice, interacting only with their nearest neighbors. Since each spin can only take on two values, say ± 1 , there are 2^N possible states. The Hamiltonian reads

$$H = -J \sum_{\langle i,j \rangle} s_i s_j - B \sum_i s_i, \quad (1.19)$$

where $\langle i,j \rangle$ means that i, j are nearest neighbors on the lattice.

A simple strategy to sample configurations of the Ising model is single-spin-flip dynamics. We start with a random configuration of the spins, and then propose new configurations at each step by flipping a single spin at a given site. A sweep is completed after we propose a spin flip at every site on the lattice.

Consecutive configurations generated by this chain differ only slightly. Thus, it takes some time for the system to reach a configuration which is significantly different from the initial one. This characteristic time is called the correlation time τ_c . A rigorous manner to estimate τ_c is through the time-displaced auto-correlation function associated to some quantity being measured. An example of a relevant quantity for the case of the Ising model is the magnetization per site:

$$m = \frac{1}{N} \sum_i s_i \quad (1.20)$$

Its associated time-displaced auto-correlation is

$$\chi_m(t) = \int dt' \left(m(t') - \langle m \rangle \right) \left(m(t'+t) - \langle m \rangle \right) = \int dt' \left(m(t')m(t'+t) - \langle m \rangle^2 \right) \quad (1.21)$$

giving a measure of how correlated two measurements of the magnetization separated by a simulation time t are.

The typical time-scale on which $\chi_m(t)$ falls off is a measure of the correlation time of the simulation. In particular, at long times it falls off exponentially. The definition of τ_c stems from this characteristic long-time behavior: $\chi_m(t) \sim e^{-t/\tau_c}$. In practice, after waiting for $2\tau_c$, the measurements are virtually uncorrelated. Let A be the number of sweeps roughly corresponding to $2\tau_c$ steps. Then, if we make S sweeps of the lattice during the simulation, the number of measurements (waiting for A sweeps between them) is

$$M = \frac{S - W}{A} \quad (1.22)$$

There are many ways to estimate τ_c from $\chi_m(t)$. The simplest consists of making an exponential fit in a given range of times. However, this might be unreliable since the estimate depends strongly on the chosen range. An alternative is to compute the “integrated” correlation time:

$$\int_0^\infty dt \frac{\chi_m(t)}{\chi_m(0)} = \int_0^\infty dt e^{-t/\tau_c} = \tau_c, \quad (1.23)$$

which is less sensitive, but not perfect either since the error that is introduced when the assumption that “long-time” behavior has been reached is arbitrary and introduces an uncontrolled error. Moreover, the very long-time behavior of the auto-correlation is rather noisy and must be excluded.

Using measured data for the magnetization at evenly-spaced times, we may construct the time-displaced auto-correlation function up to an unimportant constant, which does not affect the estimate of the correlation time:

$$\chi_m(t) = \frac{1}{t_{\max} - t} \sum_{t'=0}^{t_{\max}-t} m(t')m(t'+t) - \frac{1}{t_{\max} - t} \sum_{t'=0}^{t_{\max}-t} m(t') \frac{1}{t_{\max} - t} \sum_{t'=0}^{t_{\max}-t} m(t'+t), \quad (1.24)$$

where t_{\max} is the total simulation time.

One should be careful when using this expression at very long times. As t approaches t_{\max} , the upper limit of the sums decreases, and the integration interval becomes narrower. Since $m(t)$ fluctuates randomly at very long times, the statistical error associated to $\chi_m(t)$ becomes more prominent as t approaches t_{\max} . This turns out not to be problematic since typical simulations run for many correlation times. Thus, the tails of the auto-correlation may safely be neglected because the correlations will have already vanished, by definition.

To finish our discussion on the issue of correlations, we note that if we have a total of n_s samples of, for instance, magnetization data, the complexity of computing χ_m is $\mathcal{O}(n_s^2)$. It is possible to speed

up this process by computing its Fourier transform $\tilde{\chi}_m(\omega)$, and inverting to recover $\chi_m(t)$. This can be done via a standard Fast Fourier Transform (FFT) algorithm in $\mathcal{O}(2n_s \log n_s)$ flops. To do this, we apply the following trick

$$\begin{aligned}\tilde{\chi}_m(\omega) &= \int dt e^{i\omega t} \int dt' \left(m(t') - \langle m \rangle \right) \left(m(t' + t) - \langle m \rangle \right) \\ &= \int dt \int dt' e^{-i\omega t'} \left(m(t') - \langle m \rangle \right) e^{i\omega(t'+t)} \left(m(t' + t) - \langle m \rangle \right) \\ &= \tilde{m}'(\omega) \tilde{m}'(-\omega) = |\tilde{m}'(\omega)|^2,\end{aligned}\tag{1.25}$$

where $\tilde{m}'(\omega)$ is the Fourier transform of $m'(t) = m(t) - \langle m \rangle$ ⁷.

1.3.4 Variational Monte Carlo

Variational techniques rely on an educated guess for the wave function of the system. One introduces a set of variational parameters α that are then tuned according to a variational principle. Then, we may use the optimized trial wave function to compute physical quantities of interest using Monte Carlo. The method is used to obtain zero temperature properties of a given model. Note that it requires prior knowledge about the system to propose an approximate wave function in the first place.

A particularly relevant observable is the variational energy E_V associated to a trial ground state. Let \mathbf{r} be the $3N$ spatial coordinates of the N electrons. Given the Hamiltonian of the system \mathcal{H} , and a trial wave function $\psi(\mathbf{r})$ - a guess of the wave function representing the ground state - one can compute the corresponding variational energy.

$$E_V = \frac{\langle \psi | \mathcal{H} | \psi \rangle}{\langle \psi | \psi \rangle} = \frac{\int d\mathbf{r} |\psi(\mathbf{r})|^2 E_L(\mathbf{r})}{\int d\mathbf{r} |\psi(\mathbf{r})|^2} = \int d\mathbf{r} \rho(\mathbf{r}) E_L(\mathbf{r}),\tag{1.26}$$

where the local energy $E_L(\mathbf{r})$ is defined as

$$E_L = \frac{\mathcal{H}\psi(\mathbf{r})}{\psi(\mathbf{r})}\tag{1.27}$$

and the probability distribution $\rho(\mathbf{r})$ is defined as

$$\rho(\mathbf{r}) = \frac{|\psi(\mathbf{r})|^2}{\int d\mathbf{r}' |\psi(\mathbf{r}')|^2}\tag{1.28}$$

Note that we managed to recast the variational energy as an average of the *local* energy, $\langle E_L \rangle$, over the the distribution ρ . This may be computed using the Monte Carlo method by sampling M points \mathbf{r}_k from distribution $\rho(\mathbf{r})$:

$$E_V \approx \bar{E}_L = \frac{1}{M} \sum_{k=1}^M E_L(\mathbf{r}_k),\tag{1.29}$$

where \bar{X} denotes a sample mean of the random variable X .

Let the ground state energy be E_0 . Then, states are optimized according to the variational principle:

⁷The only difference between $\tilde{m}'(\omega)$ and $\tilde{m}(\omega)$, is that $\tilde{m}'(0) = 0$, while $\tilde{m}(0) \neq 0$. Thus, one can also compute $\tilde{m}(\omega)$ and then set its $\omega = 0$ component to zero.

$$E_V(\boldsymbol{\alpha}) = \frac{\langle \psi_{\boldsymbol{\alpha}} | \mathcal{H} | \psi_{\boldsymbol{\alpha}} \rangle}{\langle \psi_{\boldsymbol{\alpha}} | \psi_{\boldsymbol{\alpha}} \rangle} \geq E_0, \quad (1.30)$$

where $\psi_{\boldsymbol{\alpha}}$ is the trial ground state wave function for the set of variational parameters $\boldsymbol{\alpha}$.

By varying $\boldsymbol{\alpha}$ we aim to obtain a variational energy that is as close as possible to the true ground state energy. Since $E_V(\boldsymbol{\alpha})$ is bounded from below, this is equivalent to minimizing it in the hope that $E_V(\boldsymbol{\alpha}_{min}) \gtrsim E_0$, i.e. the bound is tight.

The finite sampling size M , of course, introduces a statistical error common to all Monte Carlo methods. However, the use of an approximate wave function introduces a systematic error that is hard to control since trial wave functions are generally introduced based on approximate, or heuristic arguments.

1.3.5 Diffusion Monte Carlo

Variational Monte Carlo is severely limited by the use of a trial wave function $\psi_{\boldsymbol{\alpha}}(\mathbf{r})$ because we may even not have enough information to even construct a reliable variational wave function.

Diffusion QMC allows the simulation of a many-body system while having only a limited knowledge of the system's physical properties. While it is exact for many-boson systems, it is only approximate for many-fermion systems. The idea is to map the Schrödinger equation into an imaginary-time diffusion equation. Excited states are then filtered out by a diffusion process as we advance in imaginary-time. In imaginary-time $\tau = -it$, the solution to the Schrödinger equation in terms of a formal series expansion in the eigenfunctions of the hamiltonian becomes a series of transients $e^{-E_n \tau}$, $n \in \mathbb{N}$. The longest lasting of these is the ground state [47].

The idea of the diffusion method is to generate samples using the exact ground state wave function $\psi_0(\mathbf{r})$ [48]. The associated exact energy E_0 is the matrix element of the hamiltonian calculated using a trial wave function and the ground state wave function.

$$E_0 = \frac{\langle \psi_0 | E_0 \mathbb{1} | \psi \rangle}{\langle \psi_0 | \psi \rangle} = \frac{\langle \psi_0 | \mathcal{H} | \psi \rangle}{\langle \psi_0 | \psi \rangle} = \frac{\int d\mathbf{r} \psi_0^*(\mathbf{r}) \psi(\mathbf{r}) E_L(\mathbf{r})}{\int d\mathbf{r} \psi_0^*(\mathbf{r}) \psi(\mathbf{r})} \quad (1.31)$$

Note that using this trick we avoid the computation of $\mathcal{H}\psi_0 = E_0\psi_0$, that is, the ground state energy. Instead, we approximate the integral by considering M configuration samples $\mathbf{r}_{k=1,\dots,N}$ in a similar spirit to that of Variational QMC. Notice that the integral consists of a local energy of the trial wave function $E_L(\mathbf{r}) = \frac{\mathcal{H}\psi(\mathbf{r})}{\psi(\mathbf{r})}$ averaged over a mixed distribution from which we draw a sample of points $\mathbf{r}_{k=1,\dots,M}$:

$$f(\mathbf{r}) = \frac{\psi_0^*(\mathbf{r}) \psi(\mathbf{r})}{\int d\mathbf{r} \psi_0(\mathbf{r}) \psi(\mathbf{r})} \quad (1.32)$$

Although the method is, of course, aimed at probing many-body systems, let us consider a single particle in One-dimensional for simplicity for illustrating the method. Performing a Wick rotation - effectively going to imaginary time - and shifting the energy, the Schrödinger equation becomes

$$\frac{\partial\psi(x,\tau)}{\partial\tau}=-\frac{1}{2m}\frac{\partial^2\psi(x,\tau)}{\partial x^2}-\left[V(x)-E_T\right]\psi(x,\tau) \quad (1.33)$$

The exact ground state wave function $\psi_0(x)$ is obtained as the longest lasting transient state in imaginary time: we are interested in the asymptotic behavior of the series expansion constituting the formal solution of the Schrödinger equation

$$\psi(x,\tau)=\sum_{n=0}^{\infty}c_n\psi_n(x)e^{-(E_n-E_T)\tau} \quad (1.34)$$

Imaginary time evolution is governed by

$$\begin{aligned} |\psi(t)\rangle &= \lim_{\tau\rightarrow\infty}\sum_i e^{-(E_i-E_T)\tau}|\psi_i\rangle\langle\psi_i|\psi\rangle = \\ &= \lim_{\tau\rightarrow\infty}e^{-(E_0-E_T)\tau}|\psi_0\rangle\langle\psi_0|\psi\rangle \end{aligned} \quad (1.35)$$

If $E_T > E_0$ the wave function diverges exponentially fast: $\lim_{\tau\rightarrow\infty}\psi(x,\tau)=\infty$. Similarly, for $E_T < E_0$ it vanishes exponentially fast: $\lim_{\tau\rightarrow\infty}\psi(x,\tau)=0$. However, if $E_T = E_0$ the wave function converges to the ground state one up to a constant factor.

$$\lim_{\tau\rightarrow\infty}\psi(x,\tau)=c_0\psi_0(x) \text{ , or } \lim_{\tau\rightarrow\infty}|\psi(\tau)\rangle\propto|\psi_0\rangle \quad (1.36)$$

Diffusion QMC makes use of equation (1.36), approximating $\phi_0(x)$ by $\psi(x,\tau)$ for sufficiently long time. The only requirement is that $\psi(x,\tau)$ and $\psi_0(x)$ overlap significantly so that c_0 is large enough to be numerically measurable, and we can always center a positive trial wave function in a region where $\psi_0(x)$ is large enough. Of course, this is always possible for a single particle, but note that it might fail for a many-fermion system, for which the wave function crosses a number of nodes due to its anti-symmetric nature.

1.4 Original Contributions

The major contribution of this work has been the development of a general determinant QMC code in C++, which can be used to simulate low-dimensional Hubbard-like models with different geometries.

The code was then applied to study the properties of a TMD nanoribbon providing insight into its magnetic properties.

Lastly, we characterized and compared different options to stabilize the matrix products needed to perform the simulations.

1.5 Thesis Outline

In this thesis, we first aim to review the existing literature on QMC methods for fermions, then become acquainted with some of the existing libraries so as to develop a code to tackle a specific problem of interacting electrons. The second part of this work has to do with the application to TMD

nanoribbons and physical interpretation of results. The last phase of this project shall then consist in performing various measurements using the built QMC code, and interpreting the results in light of the relevant literature.

Review of Classical Monte Carlo

Build benchmarks for simple examples

Review of main 2D materials results and TMD's

Explore relevant QMC methods, start writing thesis

Review open source libraries, namely QUEST, Alps, Monte Python , ALF

Implement QMC code, application to simple models

Determine which are the main quantities to measure for TMD nanoribbons

Implement measurements and test the code on more complex models

Start performing QMC measurements

Compile and interpret results

Finish writing thesis, review and editing

2

Minimal models of electron correlations in energy bands

Contents

2.1	Modelling electron correlations	20
2.2	Hubbard model	21
2.3	Mott insulators	27
2.4	Exact solutions for simple cases	30
2.5	Effective Heisenberg Hamiltonian	38
2.6	Green's functions: Mott gap and spectral function	42
2.7	Magnetism and mean field theory	42

We start with an overview of the Hubbard model and in the following chapters we provide details on how to simulate it numerically using Quantum Monte Carlo. In particular, we discuss the original motivation provided by Hubbard to introduce the model and show how its Hamiltonian arises as an approximate representation of the Coulomb repulsion between electrons in a solid. Then, we present exact solutions for particular limiting cases, which will be used to crosscheck our simulations. In particular, we show that, in the limit where the interaction is large, the effective Hamiltonian at half filling corresponds to an atomic Heisenberg model defined in the appropriate Hilbert space with one electron per site.

2.1 Modelling electron correlations

The Hubbard model appeared in 1963 as one of the first attempts to include electron interaction effects in a quantum mechanical description of a solid. Originally, it was introduced to explain the behavior of the electrons in the narrow, partially filled d -bands of transition metals [28]. Correlation phenomena due to the Coulomb repulsion between the electrons in these bands lead to a behavior reminiscent of the atomic picture of a solid. In fact, the model may simply be regarded as a minimal model of interacting electrons in an energy band of a solid, where only on-site interactions are considered. We have come a long way since the introduction of the Hubbard model and it is now arguably as paradigm-defining in many-body theory as the Ising model in statistical physics [49–51].

Although the Hubbard model was initially applied to transition metal monoxides like FeO, NiO, and CoO, which are antiferromagnetic insulators (and not metallic, as was initially thought)¹, it is a minimal model giving insight on insulating, magnetic, and even superconducting phases arising due to the effect of electron interactions in a variety of quantum systems.

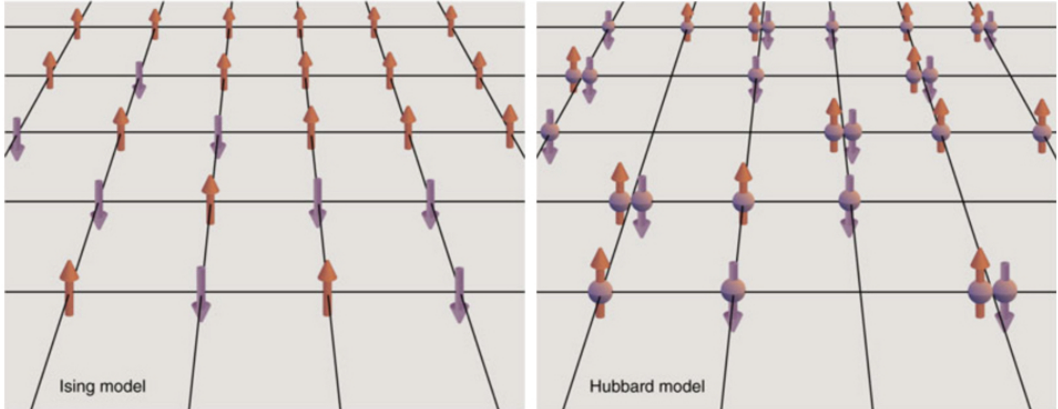


Figure 2.1: Unlike the Ising model, where either an up or a down spin live at each site, in the Hubbard model, there are four possible states at each site: a "hole" (absence of an electron), either an up spin electron or a down spin electron, or two electrons of opposite spins. The idea behind the model is to consider that the electrons interact, repelling each other, only when they are on the same site (taken from [52]).

Of course, Figure (2.1) is only a simplified view presented for the sake of analogy. The Hubbard model is actually defined in terms of a Hamiltonian acting on electron wave functions centered in the

¹They were predicted to be metals by band theory until they were found not to behave like metals empirically.

sites of a lattice. Ultimately, we wish to determine, or at least approximate, the wave function describing the full electronic system. To do so, we must consider a Hamiltonian that allows simultaneous charge and spin fluctuations. It turns out that the *many-body* wave function we seek is not, in general, a simple combination of products of one electron wave functions, as in the interaction-free case.

When Hubbard's seminal paper came out, it followed a trend that arose in the 1950's when people were working on a theory of correlation effects in the free electron gas [53–58]. Hubbard devised a simple model for the (at the time) seemingly intractable problem of interacting electrons in a band. His work explained qualitatively some properties of compounds containing transition metals, in which electron correlations are non negligible. It turns out that the mathematical formulation of the interaction problem for correlated electrons in a band is not prohibitively complicated, and is relatively amenable to both analytical and numerical computations after some controlled approximations are introduced. Notably, the model is particularly adapted to computer simulations because of its simple approximate Hamiltonian. Moreover, it has been shown to be very relevant in the description of Mott insulators, and high T_c superconductors². In fact, the Hubbard model has found many applications, describing successfully a variety of quantum systems [59]; nonetheless, even the simplified picture it offers is in general difficult to approach analytically. There exists an exact, albeit not very transparent solution in one dimension via Bethe ansatz [27], however the more general higher dimensional case is often solved numerically. An example of particular relevance for the work of this thesis is the study carried out by Hirsch [7]. In the following chapters, we will discuss how to simulate the Hubbard model using a numerical approach that is based on this seminal paper, and essentially follows the ideas introduced in it.

2.2 Hubbard model

The nearly free electron gas models the conduction bands of metals and alloys fairly accurately. The high mobility of the electrons compared to the ions justifies two equivalent approximations, both giving essentially the same results [60]. The first idea is to treat the periodic potential created by the *virtually* fixed ions (compared to the electrons) as a perturbation on the free electron gas. Equivalently, we may imagine the system as a collection of tightly bond atoms, in which the electrons in the higher energy band hop from atom to atom. Both these approaches lead to band theory, a framework which allows us to predict whether a material is a conductor or a insulator. From the tight binding point of view, the effect of the electron mobility is the broadening of the atomic energy levels: the electrons in the solid occupy energy bands, rather than levels. The partially filled band of highest energy is called the conduction band, since it is the band occupied by conduction electrons hopping from atom to atom. However, in transition metal and rare-earths, as in some compounds containing these elements, apart from the conduction bands there are partially filled bands: d – or f –bands. The partial filling of these bands and the electron correlations within them are responsible for the characteristic properties of these solids. Some of these properties are not explained by band theory, namely the Mott metal-insulator

²In this context, T_c is the critical temperature associated with the transition to a superconducting phase.

transition [61–63].

2.2.1 Electron correlations in narrow d –bands

First, note that the effects of correlations cannot possibly be the same in narrow energy bands and in the free electron gas. To see this, we may simply recall the shape of a d –wave function. In a d –orbital, the electron charge density is concentrated near the nucleus. In a solid, the electronic charge density should then also be concentrated near the nuclei, as long as the atomic description is useful, even if not completely correct³. It is much smaller between atoms so that electrons do seem to belong to individual atoms in some sense. For a d –band, we assume this description to hold to some extent since the band is narrow. Thus, the fact that we may speak with some meaning of an electron belonging to a particular atom motivates a description from which the atomic characteristics of the solid emerge, in spite of the fact that the bandwidth of a d –band is still appreciable. The point is that electrons in d –bands are certainly not well described by a free electron gas, which cannot possibly account for atomic-like behavior.

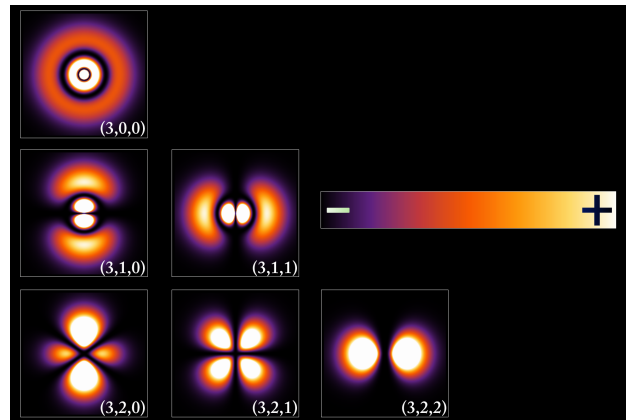


Figure 2.2: Probability density plots for different hydrogen orbital wave functions corresponding to quantum numbers (n, l, m) for $n = 3$. d -wave functions correspond to $l = 2$. Note that the probability density is always higher in a region near the nucleus, and has a complicated shape, which will lead to a non-uniform distribution of electronic charge, as opposed to the case of the free electron gas. (adapted from [64])

Experimentally, d –electrons of transition metals show a hybrid behavior: sometimes they are accurately described by an ordinary band model, but there are occasions in which the atomic model is better. For example, we see spin wave phenomena in ferromagnetic transition metals, and the susceptibilities of some of these metals depend strongly on temperature. This is characteristic of an atomic (Heisenberg) model. On the other hand, the d –electrons contribute significantly to the low temperature specific heat and sometimes the magnetic moments per atom of some transition metal ferromagnets are not integer multiples of the Bohr magneton. This is characteristic of band theory⁴.

³The electronic charge density is, of course, not actually defined in terms of a squared norm of the d –wave function for a narrow band. There is some broadening of the corresponding atomic energy level, and the wave function describing an electron is a Bloch wave function. Since the band is narrow, we assume that the atomic wave function description is still somewhat useful in a given range and we use it to provide a heuristic motivation for the non validity of the free electron assumption.

⁴Think, for example, of a tight binding model. Electrons hop from atom to atom, and in general the spin of each atom depends on the particular electrons “belonging” to it at a given time. If we take an average of the total spin of each atom, we will in general not necessarily obtain an integer multiple of the Bohr magneton. If we simply had a collection of atoms, Hund’s rule would apply, and each atom would have its spin aligned in a given direction. The average spin

Our theory of correlations should describe this balance between band-like and atomic-like behavior.

The atomic picture of a solid consists of an electron gas where ions are immersed. The ions then interact in much the same way as they do in salts. This extreme scenario is surely not even close to the true state of affairs since the number of d -electrons per atom is in general not an integer. This motivates us to introduce a less restrictive model, which is not too far from the atomic model. We shall assume that while d -electrons still have some band motion, they are strongly correlated with each other so that the metal retains some atomic-like behavior. The correlations between electrons on different atoms are likely much weaker and we neglect them.

Let us now look at an example of the aforementioned circumstance. Take a partially filled d -band of non-interacting electrons. The spin of any given atom in the solid is just the total spin of all electrons on that atom. It fluctuates both in magnitude and in direction, with a characteristic time that depends on how frequently d -electrons hop. We can estimate the time interval between d -electron hopping events between atoms as a being of the order \hbar/Δ , where Δ is the d -electron bandwidth. The spin can thus be thought of as being associated to each individual (and constantly hopping) d -electron.

How do the electron interactions affect this picture? We start by recalling Hund's rule: the nature of the interactions between atoms leads to an alignment of the spins on each atom. Since the atomic picture seems to prevail in our metal, we have reason to expect a similar effect to occur. An atom with a total spin in some direction at a given time will tend to attract electrons with the spin on that direction and repel those with opposite spin. This mechanism makes it unlikely for the spin of an atom to change much over time.

If the interactions between atoms are strong enough, the correlations become considerable, and to state it more precisely, the total spin of an atom will persist for a time that is long compared with the d -electron hopping time. Note that it is not the localization of the electrons that causes the spin state of the atom to persist. The specific electrons belonging to a given atom change all the time as long as their spin is consistent with the total spin requirement imposed by Hund's rule. For strong enough correlations, we may think of the spin as being associated to each atom, which opens up the possibility to describe the system using an atomic (Heisenberg) model, as we shall see later.

A theory of electron correlations in a narrow energy band should reduce to an atomic model in the appropriate limit, for example atoms that are so far apart on a lattice that they interact only very weakly. Although we always keep in mind that we are focusing on d -electrons, we shall consider s -electrons in what follows for the sake of simplicity. The important conclusions will not differ significantly. We will use the "atomicity" of the electronic distribution to introduce an approximate representation of the electron interaction. It turns out that this representation is mathematically much simpler to handle than the Coulomb interaction itself.

In short, our picture is the following: electrons hop rapidly from atom to atom in a band-like fashion, but their motion is correlated in such a way that atomic characteristics emerge. The extent of atomic behavior depends, of course, on the strength of the interaction.

would then tend to be an integer multiple of the Bohr magneton.

2.2.2 Hubbard Hamiltonian

Imagine a hypothetical partially filled narrow s -band with n electrons per atom. Suppose you have obtained Bloch wave functions $\psi_{\mathbf{k}}$ corresponding to energies $\varepsilon_{\mathbf{k}}$ by solving the Schrödinger equation for some spin-independent Hartree-Fock potential that accounts for the average interaction of the s -band electrons with electrons on other bands, and the interaction with the other s -electrons. The electrons on the band evolve according to the Hamiltonian:

$$\mathcal{H} = \sum_{\mathbf{k}\sigma} \left(\varepsilon_{\mathbf{k}} - \sum_{\mathbf{k}'} (2V_{\mathbf{k}\mathbf{k}'}^{\mathbf{k}\mathbf{k}'} - V_{\mathbf{k}'\mathbf{k}'}^{\mathbf{k}\mathbf{k}'}) \nu_{\mathbf{k}'} \right) c_{\mathbf{k}\sigma}^\dagger c_{\mathbf{k}\sigma} + \frac{1}{2} \sum_{\substack{\mathbf{k}_1 \mathbf{k}_2 \\ \mathbf{k}'_1 \mathbf{k}'_2 \sigma_1 \sigma_2}} V_{\mathbf{k}'_1 \mathbf{k}'_2}^{\mathbf{k}_1 \mathbf{k}_2} c_{\mathbf{k}_1 \sigma_1}^\dagger c_{\mathbf{k}_2 \sigma_2}^\dagger c_{\mathbf{k}'_2 \sigma_2} c_{\mathbf{k}'_1 \sigma_1}, \quad (2.1)$$

where the \mathbf{k} -sums run over the first Brillouin zone.

The integrals are defined by

$$V_{\mathbf{k}'_1 \mathbf{k}'_2}^{\mathbf{k}_1 \mathbf{k}_2} \equiv \left\langle \mathbf{k}_1 \mathbf{k}_2 \left| \frac{e^2}{r} \right| \mathbf{k}'_1 \mathbf{k}'_2 \right\rangle = e^2 \int \frac{\psi_{\mathbf{k}_1}^*(\mathbf{x}) \psi_{\mathbf{k}_1}(\mathbf{x}) \psi_{\mathbf{k}_2}^*(\mathbf{x}') \psi_{\mathbf{k}_2}(\mathbf{x}')}{|\mathbf{x} - \mathbf{x}'|} d\mathbf{x} d\mathbf{x}' \quad (2.2)$$

The first term represents the band energies of the electrons minus their potential energy in the part of the Hartree-Fock field due to the electrons of the s -band itself. The latter ensures that we do not overestimate the magnitude of the interactions between the electrons of the band: the Hartree-Fock field that specifies $\varepsilon_{\mathbf{k}}$ is computed taking into account these interactions, so if we didn't subtract it, we would count the energy of these interactions twice since they reappear in the last term. The last term represents the interactions among all electrons in the system. Furthermore, we assume that up and down spins are occupied equally, and $\nu_{\mathbf{k}}$ are the occupation numbers of the states of the band in the Hartree-Fock calculation.

The term that we subtract in equation (2.1) corresponds to the part of the interaction term which is already accounted for by the first diagonal “mean field” term. Thus, it corresponds to the mean field expansion of the interaction term. A generic way of writing the interaction term by gathering the \mathbf{k}, σ indexes into a single index μ is

$$V_{\text{int}} = \frac{1}{2} V_{\nu' \mu'}^{\nu \mu} c_\nu^\dagger c_\nu c_\mu^\dagger c_\mu, \quad (2.3)$$

where the summation over repeated indexes is implied.

In appendix A, we obtain the mean field form of V_{int} in the Hartree-Fock approximation.

Now consider the Wannier functions

$$\phi(\mathbf{x}) = N^{-1/2} \sum_{\mathbf{k}} \psi_{\mathbf{k}}(\mathbf{x}), \quad (2.4)$$

where N is the number of atoms.

We may write $\psi_{\mathbf{k}}$ as a combination of Wannier functions localized at each atom.

$$\psi_{\mathbf{k}}(\mathbf{x}) = N^{-1/2} \sum_i e^{i\mathbf{k} \cdot \mathbf{R}_i} \phi(\mathbf{x} - \mathbf{R}_i), \quad (2.5)$$

where the sum runs over all atomic positions \mathbf{R}_i .

Introducing the annihilation (creation) operators of an electron of spin σ in the Wannier state $\phi(\mathbf{x} - \mathbf{R}_i)$ localized at site i , $c_{i\sigma}^{(\dagger)}$, we may write

$$c_{k\sigma}^{(\dagger)} = N^{-1/2} \sum_i e^{i\mathbf{k}\cdot\mathbf{R}_i} c_{i\sigma}^{(\dagger)} \quad (2.6)$$

Thus, the Hamiltonian becomes

$$\mathcal{H} = \sum_{ij\sigma} K_{ij} c_{i\sigma}^\dagger c_{j\sigma} + \sum_{ijkl\sigma\sigma'} \left[\frac{1}{2} V_{kl}^{ij} c_{i\sigma}^\dagger c_{j\sigma'}^\dagger c_{l\sigma'} c_{k\sigma} - \left(2V_{kl}^{ij} - V_{lk}^{ij} \right) \nu_{jl} c_{i\sigma}^\dagger c_{k\sigma} \right], \quad (2.7)$$

where

$$K_{ij} = N^{-1} \sum_{\mathbf{k}} \varepsilon_{\mathbf{k}} e^{i\mathbf{k}\cdot(\mathbf{R}_i - \mathbf{R}_j)}, \text{ and } \nu_{jl} = N^{-1} \sum_{\mathbf{k}} e^{i\mathbf{k}\cdot(\mathbf{R}_j - \mathbf{R}_l)} \quad (2.8)$$

Now comes the crucial approximation. For a narrow energy band, the Wannier functions ϕ nearly coincide with atomic s -functions. For small bandwidth, these s -functions form an atomic shell whose radius is small compared with the spacing between atoms, that is, the lattice constant. Thus, the integral $U = \langle ii | e^2/r | ii \rangle$ should turn out to be much larger than all other integrals. This suggests the seemingly crude approximation of neglecting all other integrals. However, this approximation is not so radical as it could seem at first sight since the other integrals are indeed much smaller than U . In fact, for example, for $3d$ electrons of transition metals they are smaller by about two orders of magnitude [28]. Keeping only the terms in U in the interaction part, we obtain

$$\mathcal{H} = \sum_{ij\sigma} K_{ij} c_{i\sigma}^\dagger c_{j\sigma} + \frac{U}{2} \sum_{i\sigma} n_{i\sigma} n_{i,-\sigma} - U \sum_{i,\sigma} \nu_{i,i} n_{i,\sigma} \quad (2.9)$$

where $n_{i\sigma} = c_{i\sigma}^\dagger c_{i\sigma}$. Note that $\nu_{i,i} = N^{-1} \sum_{\mathbf{k}} \nu_{\mathbf{k}} = n/2$, where n is the electron density, which means that the last term is constant and may be dropped. Now, the hopping matrix \mathbf{K} can, in principle, be found by inverse Fourier transforming the dispersion relation $\varepsilon_{\mathbf{k}}$ of the equivalent interaction-free system, that we can imagine to be obtained experimentally.

In the purely tight binding view (with no U -term), we have a well defined crystal wavevectors that depends on the symmetry of the lattice, which may be written as Fourier transforms

$$|\mathbf{k}\rangle \equiv \frac{1}{N} \sum_{\mathbf{r}} e^{i\mathbf{k}\cdot\mathbf{r}} |\mathbf{r}\rangle \quad (2.10)$$

Recalling the form of the hopping Hamiltonian (or the kinetic energy part in the Hubbard model)

$$\mathcal{H}_K = - \sum_{\mathbf{rr}'} K(\mathbf{r} - \mathbf{r}') |\mathbf{r}'\rangle \langle \mathbf{r}| \quad (2.11)$$

we can obtain the dispersion relation.

$$-\mathcal{H}_K |\mathbf{k}\rangle = \frac{1}{\sqrt{N}} \sum_{\mathbf{r}\mathbf{r}'} K(\mathbf{r} - \mathbf{r}') e^{i\mathbf{k}\cdot\mathbf{r}} |\mathbf{r}'\rangle = \frac{1}{\sqrt{N}} \left(\sum_{\mathbf{R}} K(\mathbf{R}) e^{i\mathbf{k}\cdot\mathbf{R}} \right) \left(\sum_{\mathbf{r}'} e^{i\mathbf{k}\cdot\mathbf{r}'} |\mathbf{r}'\rangle \right) = \varepsilon_{\mathbf{k}} |\mathbf{k}\rangle \quad (2.12)$$

and here we recognize the dispersion relation as the (negative) Fourier transform of the hopping

$$\varepsilon_{\mathbf{k}} = - \sum_{\mathbf{R}} K(\mathbf{R}) e^{i\mathbf{k}\cdot\mathbf{R}} \quad (2.13)$$

This gives us an interpretation of the \mathbf{K} matrix: given the dispersion relation, and considering the solid to be well described by a tight binding model, we can easily obtain the matrix elements K_{ij} .

Let us now suppose that we have the simplest uniform nearest neighbor hopping model. Going back to equation (2.8), and recalling that the sum on \mathbf{k} is restricted to the first Brillouin zone, we obtain the usual tight binding result: $K_{\langle ij \rangle} = -t \in \mathbb{R}$ and 0 otherwise (i.e. \mathbf{K} is a very sparse matrix that is only non-zero for i, j nearest neighbors). The Hubbard Hamiltonian is then

$$\mathcal{H} = -t \sum_{\langle i,j \rangle, \sigma} \left(c_{i,\sigma} c_{j,\sigma}^\dagger + c_{j,\sigma} c_{i,\sigma}^\dagger \right) + U \sum_i n_{i,\uparrow} n_{i,\downarrow} \quad (2.14)$$

2.2.3 Particle-hole symmetry

In this section we examine a particularly relevant and unique symmetry of the Hubbard model. The main idea is that, at half filling, the Hubbard Hamiltonian is invariant under a transformation which turns particles into holes and vice-versa. Particle-hole symmetry (PHS) allows us to relate the properties of the Hubbard Hamiltonian at different values of the parameters. Moreover, it allows us to devise a mapping between the attractive ($U < 0$) and the repulsive ($U > 0$) models. We will see later that this mapping is important in QMC simulations [65].

We start our discussion with the concept of a bipartite lattice. A lattice is said to be bipartite if it can be divided into two sublattices \mathcal{A} and \mathcal{B} , such that the set of neighbors of a site in sublattice \mathcal{A} belongs to sublattice \mathcal{B} . For example, the square and honeycomb lattices are bipartite, whereas the triangular lattice is not.

In a bipartite lattice, Antiferromagnetic (AF) order is favored. In contrast, AF order is frustrated on the triangular and other non bipartite lattices.

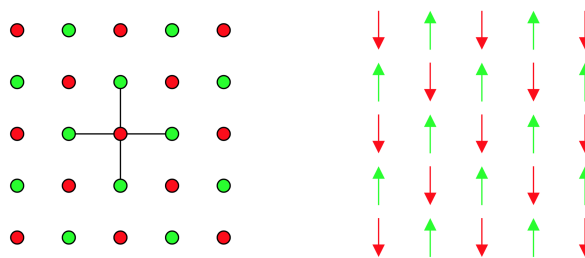


Figure 2.3: On the left, we see that the square lattice is bipartite. The neighbors of a particular site in the red sublattice all belong to the green sublattice. The picture on the right is meant to give some intuition on why the bipartite lattice favors AF order. We represent a configuration where fermions of a given spin have as their neighbors only fermions of opposite spin, which would be favored by Heisenberg exchange (taken from [65]).

Introducing a Particle-hole transformation (PHT),

$$d_{i,\sigma}^\dagger = (-1)^i c_{i,\sigma}, \quad (2.15)$$

we exchange the role of annihilation and creation operators.

In fact, particles become holes and vice-versa: $d_{i,\sigma}^\dagger d_{i,\sigma} = 1 - c_{i,\sigma}^\dagger c_{i,\sigma}$, and the occupations $n = 0, 1$ are interchanged.

Consider a bipartite lattice. Since in that case the factor $(-1)^i$ takes on -1 on one sublattice and 1 on the other, the kinetic part of the Hamiltonian is invariant under a PHT:

$$c_{i,\sigma}^\dagger c_{j,\sigma} + c_{j,\sigma}^\dagger c_{i,\sigma} \mapsto (-1)^{i+j} (d_{i,\sigma}^\dagger d_{j,\sigma} + d_{j,\sigma}^\dagger d_{i,\sigma}) = d_{j,\sigma}^\dagger d_{i,\sigma} + d_{i,\sigma}^\dagger d_{j,\sigma} \quad (2.16)$$

The PHS of the kinetic term can be incorporated into the interaction term by a shift in the chemical potential and by adding a constant to the Hamiltonian. First, note that the term

$$U \left(n_{i,\uparrow} - \frac{1}{2} \right) \left(n_{i,\downarrow} - \frac{1}{2} \right)$$

is unchanged under a PHT.

Expanding this term, we obtain $U n_{i,\uparrow} n_{i,\downarrow} - \frac{U}{2} (n_{i,\uparrow} + n_{i,\downarrow}) + \frac{U}{4}$, which indeed differs from the original interaction term by a shift in the chemical potential plus a constant. Thus, the particle-hole symmetric form of the Hamiltonian

$$\mathcal{H} = -t \sum_{\langle i,j \rangle, \sigma} \left(c_{i,\sigma} c_{j,\sigma}^\dagger + c_{i,\sigma}^\dagger c_{j,\sigma} \right) + U \sum_i \left(n_{i,\uparrow} - \frac{1}{2} \right) \left(n_{i,\downarrow} - \frac{1}{2} \right) - \mu \sum_i \left(n_{i,\uparrow} + n_{i,\downarrow} \right) \quad (2.17)$$

is completely equivalent to the original Hamiltonian.

Under a PHT, the density transforms as $\rho \mapsto 2 - \rho$. The Hamiltonian changes only in the chemical potential term: $\mu \mapsto -\mu$. Thus, we have that $\rho(\mu) = 2 - \rho(-\mu)$, and at $\mu = 0$, we have half filling: $\rho = 1$. This reasoning is valid for any β , t , or U , which implies that the phase diagram of the Hubbard model must be symmetric about half filling. Suppose you added next nearest neighbor (NNN) hoppings t' ⁵. Then, PHS would be broken, and the phase diagram would no longer be symmetric about $\mu = 0$. Indeed, a modified version of the Hubbard model with NNN hoppings is often used to model cuprate superconductors, and this lack of symmetry is consistent with the fact that hole- and electron-doped cuprates have different properties.

2.3 Mott insulators

Band theory was found to be flawed soon after it was introduced. The picture it proposes is simple and generally works pretty well. It is based on considering the electrons to be independently moving under the constant background potential created by the ions. The solutions of the Schrödinger for free electrons in a periodic potential $U(\mathbf{r})$, such that $U(\mathbf{r}) = U(\mathbf{r} + \mathbf{R})$,

⁵On the square lattice, this corresponds to connecting sites across the diagonal of each square.

$$\left[-\frac{1}{2m} \nabla^2 + U(\mathbf{r}) \right] \psi(\mathbf{r}) = \varepsilon \psi(\mathbf{r}) \quad (2.18)$$

are given by Bloch's theorem: $\psi_{\mathbf{k}}(\mathbf{r}) = e^{i\mathbf{k}\cdot\mathbf{r}} u_{\mathbf{k}}(\mathbf{r})$. Note that we made $\hbar = 1$. Replacing this wave function in equation (2.18), we obtain a differential equation for $u_{\mathbf{k}}(\mathbf{r})$, which has in general an infinite number of solutions. We label them with an index n , which we call the band index. To each solution there corresponds a function $\varepsilon_{n\mathbf{k}}$. The set of these functions is known as the band structure. Since electrons are taken to be independent in band theory, the N-electron eigenstates are obtained by placing an electron in each quantum state. Each state is labelled by its energy $\varepsilon_{n\mathbf{k}\sigma}$. Since our model Hamiltonian does not couple spins (via an electron interaction, for example) and assuming there is no external magnetic field and that the system has an inversion center, we have $\varepsilon_{n\mathbf{k}\uparrow} = \varepsilon_{n\mathbf{k}\downarrow}$. In general there might be energies for which there is no corresponding $\varepsilon_{n\mathbf{k}\sigma}$. These form intervals called forbidden bands⁶. Thus, the ground state of our model may be obtained by filling the energy levels starting from the lowest energy state. Two cases are particularly relevant:

- Every band is either fully occupied or empty. The first excited state differs from the ground state by Δ , the separation between the last fully occupied band and the first empty band. It is then impossible to induce the motion of the electrons by applying an arbitrarily small voltage. This is what it means to be an *insulator*. Since there $2N$ states per band, this is not possible unless the number of electrons per unit cell is an even integer.
- One or more of the bands are partially filled. The energy of occupied state of higher energy is named the Fermi energy ε_F . In this case, the separation between the ground state and the first excited state tends to 0 in the thermodynamic limit, $N \rightarrow \infty$. The system may then respond to infinitesimal excitations, which is the definition of a metal.

Band theory made it possible to predict whether a solid would be a metal or an insulator. However, its success rests crucially on the independent electron approximation. Thus, it is not surprising that for compounds with strongly correlated electrons the theory might fail [66]. The Coulomb interaction is in general non negligible, and the effects it leads to are not captured by a mean field approach. One must resort to many-body theory. An example of a many-body effect that band theory doesn't capture is superconductivity. However, this does not deem band theory useless. In fact, the superconducting phase arises due to an instability of a state that is itself well described by band theory [67]. A far greater failure of band theory is that predicts certain compounds with an odd number of electrons per unit cell, such as NiO and La₂CuO₄, to be metals, while in fact they turn out to be (Mott) insulators. Mott devised a simple argument to justify this failure. It is based on considering the elementary electronic excitations of a solid composed by hydrogen atoms as a function of the distance between atoms.

Consider a hypothetical solid consisting of a square lattice with hydrogen atoms on its points. Each unit cell has one hydrogen atom, and consequently one electron. Band theory would predict such a solid to be a metal. However, if the lattice parameter a is large enough, the solid cannot remain a

⁶We disregard surface states that may have energies that fall in the forbidden bands of band theory.

metal. There must be some value of the lattice parameter $a = a_c$ for which the system becomes an insulator. When current flows through a sample of this solid, electrons hop consecutively, reaching positions that can be quite far on the lattice. For a metal, this process occurs even when exciting the system with an infinitesimal amount of energy. How much energy do we need to provide for this process to occur?

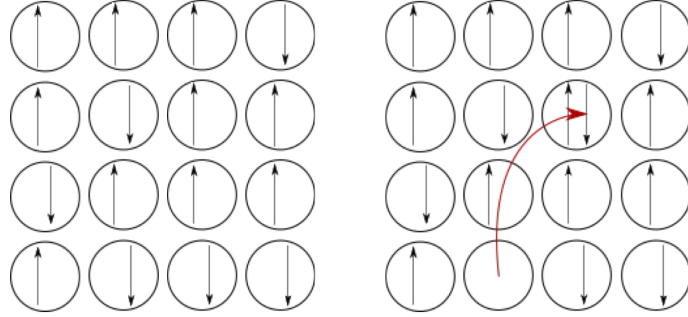


Figure 2.4: On the right, a configuration of hydrogen atoms on a square lattice with a hole and a doubly occupied site obtained by delocalization of the spin down electron on the left.

If a is large, we have essentially one electron per site at the start. When an electron is displaced, we end up with a hole and a doubly occupied site. The potential energy of such a state is

$$E_{H^-} + E_{H^+} - 2E_H \quad (2.19)$$

Due to the Coulomb repulsion between the two electrons in H^- , this quantity is strictly positive. Call it $U > 0$. On the other hand, the system also has kinetic energy: both the hole and the doubly occupied site can delocalize. Let W be the bandwidth corresponding to the delocalization of an electron on the lattice. Both the hole and the doubly occupied will stay at the bottom of the band and gain an energy $W/2$ (assuming that this delocalization is of the same order of magnitude). The dominant transfer integral $-t$ is between nearest neighbors. The dispersion relation then reads

$$\varepsilon_{\mathbf{k}} = -2t(\cos k_x + \cos k_y) \quad (2.20)$$

The bandwidth is then $W = 8t$. The energy of a configuration with a hole and a doubly occupied site is

$$\Delta_c = U - W, \quad (2.21)$$

where U is practically independent of the lattice parameter a . The bandwidth W , however, depends strongly on a . When $a \gg a_0$, where a_0 is the Bohr radius, the transfer integral is exponentially small, because only the exponential tails of the wave functions are relevant. In this limit, $\Delta_c \approx U$ is a large, positive number, and the system is an insulator. This type of insulator is called a Mott insulator, and Δ_c is called the charge gap. As a decreases, t increases, and there must be a critical value $a_c \sim a_0$, for which $U = W$. Below this value, the computation of Δ_c is not valid anymore because the gap cannot be negative. Thus, there must be a metal-insulator transition. It is possible to see this transition if we

apply enough pressure to a Mott insulator so as to decrease a and increase t . A transition of this type was first seen in the 1970's for V_2O_3 ⁷. There is a fundamental difference between a band insulator and a Mott insulator. While we must pay an energy Δ_c to make a charge excitation, there is no cost for making a spin excitation: we can flip the spin of an electron without creating a doubly occupied site. The fluctuations of both charge and spin due to the electron interactions may then lead to magnetic behavior characteristic of correlated systems.

2.4 Exact solutions for simple cases

In PHS form, the Hubbard Hamiltonian may then be written as a sum of kinetic, chemical and potential energy terms, respectively:

$$\mathcal{H} = \mathcal{H}_K + \mathcal{H}_\mu + \mathcal{H}_V, \quad (2.22)$$

defined as

$$\mathcal{H}_K = -t \sum_{\langle i,j \rangle, \sigma} \left(c_{i,\sigma} c_{j,\sigma}^\dagger + c_{j,\sigma}^\dagger c_{i,\sigma} \right), \quad \mathcal{H}_\mu = -\mu \sum_i \left(n_{i,\uparrow} + n_{i,\downarrow} \right), \quad \mathcal{H}_V = U \sum_i \left(n_{i,\uparrow} - \frac{1}{2} \right) \left(n_{i,\downarrow} - \frac{1}{2} \right), \quad (2.23)$$

where:

- i and j label sites on the lattice.
- $c_{i,\sigma}^{(\dagger)}$ is an operator that annihilates (creates) an electron with spin σ on site i .
- $n_{i,\sigma}$ is the number operator counting the number of electrons of spin σ on site i (either 0 or 1).
- t is the hopping parameter related to the kinetic energy of the electrons. It is determined by the overlap of the atomic wave functions on neighboring sites $\langle i,j \rangle$.
- U is the on-site Coulomb repulsion between electrons. Whenever a site i has two electrons, there is a local repulsion between them corresponding to an energy cost $Un_{i\uparrow}n_{i\downarrow}$ (up to an additive constant).
- μ is the chemical potential controlling the electron number (or density).

A given physical observable of interest \mathcal{O} , such as the spin-spin correlation, or the magnetic susceptibility may be computed formally by

$$\langle \mathcal{O} \rangle = \text{Tr}(\mathcal{O}\mathcal{P}) \quad (2.24)$$

where

⁷Of course, the transition is not so easy to describe. We should consider the Hubbard model! However, this simple argument provides an intuitive picture.

$$\mathcal{P} \equiv \frac{1}{Z} e^{-\beta \mathcal{H}}, \text{ with } Z = \text{Tr}(e^{-\beta \mathcal{H}}) \quad (2.25)$$

The trace is taken over the Hilbert space corresponding to all possible configurations of the lattice occupation. Defining an orthonormal basis of this Hilbert space $\{|\psi_\alpha\rangle | \alpha = 1, \dots, D\}$, where D is the dimension of the Hilbert space, the partition function reads

$$\text{Tr}(e^{-\beta \mathcal{H}}) = \sum_{\alpha} \langle \psi_{\alpha} | e^{-\beta \mathcal{H}} | \psi_{\alpha} \rangle \quad (2.26)$$

There are four possible states at each site in the Hubbard model: $| \rangle$, $|\uparrow\rangle$, $|\downarrow\rangle$, $|\uparrow\downarrow\rangle$, corresponding, respectively, to no electron, a spin up or spin down electron, and two electrons of opposite spin occupying the site. The potential energy operator acts as follows

$$U(n_{i\uparrow} - \frac{1}{2})(n_{i\downarrow} - \frac{1}{2}) \begin{cases} | \rangle = \frac{U}{4} | \rangle \\ |\uparrow\rangle = -\frac{U}{4} |\uparrow\rangle \\ |\downarrow\rangle = -\frac{U}{4} |\downarrow\rangle \\ |\uparrow\downarrow\rangle = \frac{U}{4} |\uparrow\downarrow\rangle \end{cases} \quad (2.27)$$

Singly occupied states ($|\uparrow\rangle$, $|\downarrow\rangle$) have lower energy and are thus more likely to occur. They correspond to nonzero magnetization $m = n_{\uparrow} - n_{\downarrow}$, which is favored by the Hubbard interaction U . A relevant question is whether or not the spins order in space when $t \neq 0$ and to what extent.

Let us now establish our notations for second quantized operators to introduce a different representation of electronic states on the lattice. The fermionic annihilation and creation operators anticommute: $\{c_{j\sigma}, c_{l\sigma'}^\dagger\} = \delta_{jl}\delta_{\sigma\sigma'}$. The c -operator algebra is further defined by the vanishing of all other anticommutators: $\{c_{j\sigma}^{(\dagger)}, c_{l\sigma'}^{(\dagger)}\} = 0$. Note that taking $l = j$ and $\sigma = \sigma'$ in this equation for the c^\dagger -operators, we recover Pauli's exclusion principle since $(c_{j\sigma}^\dagger)^2 = 0$. If we omit the site i and spin σ indices, a convenient way of specifying states on the lattice is

$$|0\rangle : \text{unoccupied state - no electron} \quad |1\rangle : \text{occupied state - one electron} \quad (2.28)$$

so that a generic state may be written as a product of the states above $\otimes_{i=1}^N \otimes_{\sigma=\pm 1/2} |n\rangle_{i,\sigma}$ at each site for each spin state, where $n = 0, 1$. For example, one such state is

$$|0\rangle_{1,\uparrow} |1\rangle_{1,\downarrow} |1\rangle_{2,\uparrow} |1\rangle_{2,\downarrow} |0\rangle_{3,\uparrow} |0\rangle_{3,\downarrow} \dots |1\rangle_{N,\uparrow} |0\rangle_{N,\downarrow}, \quad (2.29)$$

where N is the number of sites on the lattice. Site 1 has a single spin-down electron, while site 2 is doubly occupied, site 3 is unoccupied, and so on, until we reach site N , which has a single spin-up electron.

The creation and annihilation operators act as follows

$$c|0\rangle = 0 \quad c^\dagger|0\rangle = |1\rangle \quad c|1\rangle = |0\rangle \quad c^\dagger|1\rangle = 0 \quad (2.30)$$

Thus, the eigenstates of the number operator are $|0\rangle, |1\rangle$: $n|0\rangle = 0$, $n|1\rangle = |1\rangle$.

Moreover, the operator $c_i^\dagger c_{i+1}^\dagger$, corresponding to the hopping from site $i+1$ to i , i.e. to the kinetic energy of the electrons on neighboring sites, acts as follows (ignoring spin):

$$c_i^\dagger c_{i+1}^\dagger \begin{cases} |00\rangle = 0 \\ |10\rangle = 0 \\ |01\rangle = |10\rangle \\ |11\rangle = c_i^\dagger |10\rangle = 0 \end{cases} \quad (2.31)$$

The operator annihilates the particle at $i+1$ and creates it back at i , i.e. the electron hops from $i+1$ to i .

2.4.1 The purely atomic $\frac{t}{U} = 0$ limit

When $t = 0$, the site index may be omitted since the Hamiltonian is a sum of operators solely at site i . Hence, we have $[\mathcal{H}, n_{i,\sigma}] = 0 \forall i = 1, 2, \dots, N$, and the eigenstates of \mathcal{H} are also eigenstates of all number operators at the different sites in the lattice. Thus, in the single site limit, we obtain

$$\mathcal{H} = U \left(n_\uparrow - \frac{1}{2} \right) \left(n_\downarrow - \frac{1}{2} \right) - \mu (n_\uparrow + n_\downarrow) \quad (2.32)$$

which acts as follows (using the eigenstates of n_σ)

$$\mathcal{H} \begin{cases} |\rangle = \frac{U}{4} |\rangle \\ |\uparrow\rangle = \left(\frac{U}{4} - (\mu + \frac{U}{2}) \right) |\uparrow\rangle \\ |\downarrow\rangle = \left(\frac{U}{4} - (\mu + \frac{U}{2}) \right) |\downarrow\rangle \\ |\uparrow\downarrow\rangle = \left(\frac{U}{4} - 2\mu \right) |\uparrow\downarrow\rangle \end{cases} \quad (2.33)$$

Thus, the Hamiltonian is diagonal in the basis $\{|\psi_\alpha\rangle\} = |\rangle, |\uparrow\rangle, |\downarrow\rangle, |\uparrow\downarrow\rangle$:

$$\mathcal{H} \rightsquigarrow \mathbf{H} = \text{diag} \left(\frac{U}{4}, \frac{U}{4} - (\mu + \frac{U}{2}), \frac{U}{4} - (\mu + \frac{U}{2}), \frac{U}{4} - 2\mu \right), \quad (2.34)$$

which means that $e^{-\beta\mathcal{H}}$ is also diagonal:

$$e^{-\beta\mathcal{H}} \rightsquigarrow e^{-\beta U/4} \text{diag} \left(1, e^{\beta(\mu+\frac{U}{2})}, e^{\beta(\mu+\frac{U}{2})}, e^{2\beta\mu} \right) \quad (2.35)$$

and this is one of the rare situations in which it is possible to explicitly write down a closed form for the partition function.

$$Z = \text{Tr}[e^{-\beta\mathcal{H}}] = \sum_\alpha \langle \psi_\alpha | e^{-\beta\mathcal{H}} | \psi_\alpha \rangle = e^{-\beta U/4} \left(1 + 2e^{\beta(\mu+\frac{U}{2})} + e^{2\beta\mu} \right) \quad (2.36)$$

Moreover, some of the observables that were mentioned before are explicitly computable. This is because due to the diagonal form of \mathcal{H} , the expressions defining these observables greatly simplify.

$$\begin{aligned}
\mathcal{H}e^{-\beta\mathcal{H}} &\rightsquigarrow e^{-\beta U/4} \text{diag}\left(\frac{U}{4}, (-\mu - \frac{U}{4})e^{\beta(\mu + \frac{U}{2})}, (-\mu - \frac{U}{4})e^{\beta(\mu + \frac{U}{2})}, (\frac{U}{4} - 2\mu)e^{2\beta\mu}\right) \\
n_{\uparrow}e^{-\beta\mathcal{H}} &\rightsquigarrow e^{-\beta U/4} \text{diag}\left(0, e^{\beta(\mu + \frac{U}{2})}, 0, e^{2\beta\mu}\right) \\
n_{\downarrow}e^{-\beta\mathcal{H}} &\rightsquigarrow e^{-\beta U/4} \text{diag}\left(0, 0, e^{\beta(\mu + \frac{U}{2})}, e^{2\beta\mu}\right) \\
n_{\uparrow}n_{\downarrow}e^{-\beta\mathcal{H}} &\rightsquigarrow e^{-\beta U/4} \text{diag}\left(0, 0, 0, e^{2\beta\mu}\right)
\end{aligned} \tag{2.37}$$

From these we can compute some traces which we shall find useful to obtain averages of various observables.

$$\begin{aligned}
\text{Tr} \left[\mathcal{H}e^{-\beta\mathcal{H}} \right] &= e^{-\beta U/4} \left(\frac{U}{4} + 2(-\mu - \frac{U}{4})e^{\beta(\mu + \frac{U}{2})} + (\frac{U}{4} - 2\mu)e^{2\beta\mu} \right) \\
\text{Tr} \left[(n_{\uparrow} + n_{\downarrow})e^{-\beta\mathcal{H}} \right] &= e^{-\beta U/4} \left(2(-\mu - \frac{U}{4})e^{\beta(\mu + \frac{U}{2})} + (\frac{U}{4} - 2\mu)e^{2\beta\mu} \right) \\
\text{Tr} \left[n_{\uparrow}n_{\downarrow} \right] &= e^{-\beta U/4} e^{2\beta\mu}
\end{aligned} \tag{2.38}$$

The bottom line is that we are able to obtain *exact* expressions for

1. the one-site density $\rho = \langle n_{\uparrow} \rangle + \langle n_{\downarrow} \rangle$, measuring the average occupation of each site.

$$\rho = \frac{\text{Tr}[(n_{\uparrow} + n_{\downarrow})e^{-\beta\mathcal{H}}]}{Z} = \frac{2e^{\beta(\frac{U}{2} + \mu)} + 2e^{2\beta\mu}}{1 + 2e^{\beta(\mu + \frac{U}{2})} + e^{2\beta\mu}} \tag{2.39}$$

Note that when there is no chemical potential $\mu = 0$, we have $\rho = 1$ for any U , or β . This corresponds to half filling: the density of electrons is half its maximum possible value.

In figure (2.5), we plot $\rho(\mu)$ for varying temperature, and fixed on-site interaction. It allows us to get some insight into the Mott insulating gap. At $T = 0.25$, the curve owes its step-like shape to the small thermal fluctuations. As T increases, the curve starts losing this tendency, and by $T = 2.0$, it is no longer possible to identify it. This is a consequence of the now larger thermal fluctuations that are present at higher temperature.

We denote the flat region between $\mu = -U/2$ and $\mu = U/2$ “Mott Plateau”. As the chemical potential is increased, the density remains small until a threshold is exceeded at $\mu = -\frac{U}{2}$. Then, it rises very rapidly to $\rho = 1$ (half filling), and again stays almost constant. It is not until μ jumps by U that we fill the site ($\rho = 2$). This Mott insulating gap appears because the presence of a fermion in the site blocks the addition of a second due to the on-site interaction. One needs a sufficiently large chemical potential to overcome this effect. As we shall see, this feature of the model remains present as the number of sites increases. Note that in the Mott gap, the compressibility vanishes: $\kappa = \frac{\partial\rho}{\partial\mu} = 0$.

Just as thermal fluctuations can destroy the sharp jumps corresponding to the gap, so can quantum fluctuations. The hopping term in the Hamiltonian introduces such fluctuations, leading

to an effect similar to that of figure (2.5).

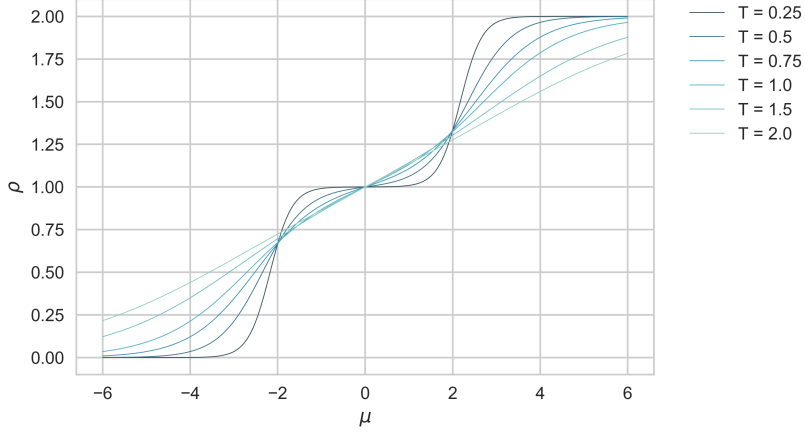


Figure 2.5: Electron density ρ for varying chemical potential μ and temperature $T = \beta^{-1}$, but fixed $U = 4$. As the temperature decreases, a “Mott plateau” sets in. The Mott insulating gap already seen here is an important feature of the Hubbard model.

2. the one-site energy $E = \langle \mathcal{H} \rangle$.

$$\begin{aligned}
E &= \frac{\text{Tr}\left(\mathcal{H}e^{-\beta\mathcal{H}}\right)}{Z} = \frac{\frac{U}{4} + 2(-\mu - \frac{U}{4})e^{\beta(\frac{U}{2}+\mu)} + (\frac{U}{4} - 2\mu)e^{2\beta\mu}}{1 + 2e^{\beta(\frac{U}{2}+\mu)} + e^{2\beta\mu}} \\
&= \frac{\frac{U}{4}(1 + 2e^{\beta(\frac{U}{2}+\mu)} + e^{2\beta\mu})}{1 + 2e^{\beta(\frac{U}{2}+\mu)} + e^{2\beta\mu}} + \frac{2(-\mu - \frac{U}{4})e^{\beta(\frac{U}{2}+\mu)} - 2\mu e^{2\beta\mu} - 2\frac{U}{4}e^{\beta(\frac{U}{2}+\mu)}}{1 + 2e^{\beta(\frac{U}{2}+\mu)} + e^{2\beta\mu}} \\
&= \frac{U}{4} - \frac{(2\mu - U)e^{\beta(\frac{U}{2}+\mu)} + 2\mu e^{2\beta\mu}}{1 + 2e^{\beta(\frac{U}{2}+\mu)} + e^{2\beta\mu}}
\end{aligned} \tag{2.40}$$

which at half filling becomes

$$E = \frac{U}{4} - \frac{U}{2(1 + e^{-\beta U/2})} \tag{2.41}$$

3. the double occupancy $\langle n_{\uparrow}n_{\downarrow} \rangle$.

$$\langle n_{\uparrow}n_{\downarrow} \rangle = \frac{\text{Tr}[n_{\uparrow}n_{\downarrow}]}{Z} = \frac{e^{2\beta\mu}}{1 + 2e^{\beta(\frac{U}{2}+\mu)} + e^{2\beta\mu}} \tag{2.42}$$

which, at half filling, simplifies to

$$\langle n_{\uparrow}n_{\downarrow} \rangle = \frac{1}{2(1 + e^{\beta U/2})} \tag{2.43}$$

Note that as either U or β increase the double occupancy tends to zero.

As was motivated in the previous chapter, we are interested in studying magnetism in correlated systems. For the Hubbard model, the relevant quantity is the local moment

$$\langle m^2 \rangle = \langle (n_{\uparrow} - n_{\downarrow})^2 \rangle = \langle n_{\uparrow} - n_{\downarrow} \rangle - 2 \langle n_{\uparrow}n_{\downarrow} \rangle = \rho - 2 \langle n_{\uparrow}n_{\downarrow} \rangle \tag{2.44}$$

In figures (2.6, 2.7), we show how $\langle m^2 \rangle$ varies as a function of U for different temperatures, and how $\langle m^2 \rangle$ varies with T , for different values of the chemical potential, respectively. At low temperature or for large on-site interaction, local moments tend to develop, which leads to magnetic ordering: $\langle m^2 \rangle \rightarrow 1$ (in the half-filled case). Since the double occupancy is zero in this case, if we do not consider thermal fluctuations, the magnetization corresponds to the spin of the electron occupying the site.

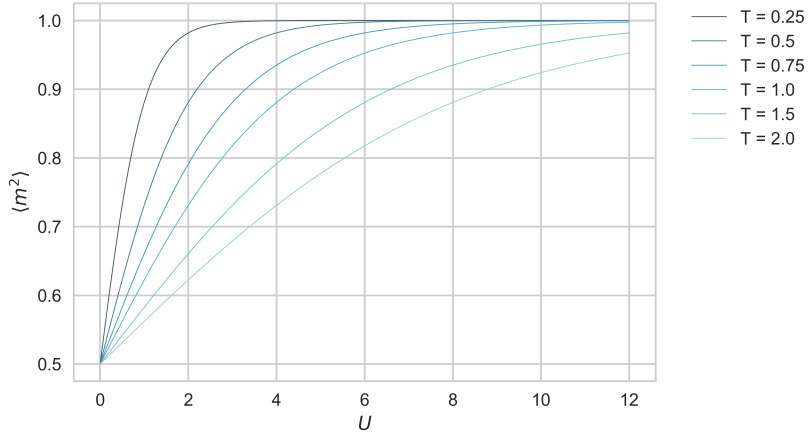


Figure 2.6: Magnetization as a function of the on-site interaction $\langle m^2 \rangle$ (U) in the single site Hubbard model for varying temperature T . Local moments are favored by the on-site interaction, and are more likely to develop at lower temperatures, when thermal fluctuations are smaller. Here we consider half filling: $\mu = 0$.

In figure(2.6), we see thermal fluctuations destroying magnetic ordering. As what happens for the Mott plateau, quantum fluctuations (i.e. introducing a hopping term in the Hamiltonian) change the behavior of the magnetization, and perfect moments ($\langle m^2 \rangle = 1$) do not form anymore at zero temperature for finite on-site interaction.

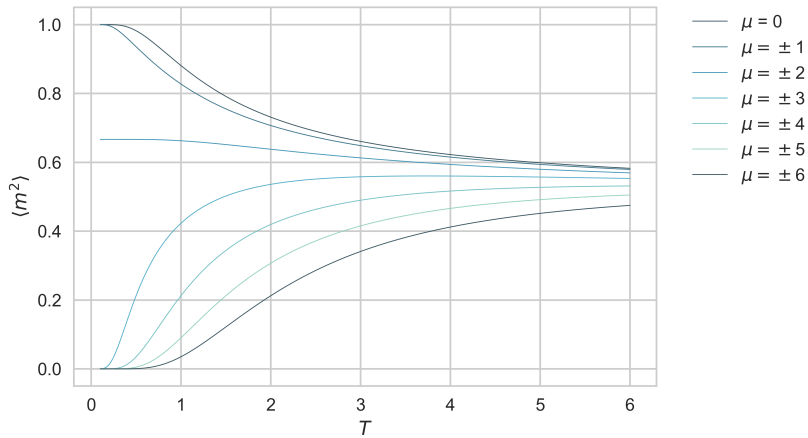


Figure 2.7: Magnetization as a function of temperature $\langle m^2 \rangle$ (T) in the single site Hubbard model for varying chemical potential μ . Local moments develop at lower temperature. However, as we increase the chemical potential, the situation is reversed. At low temperatures, the site is doubly occupied and so the magnetization goes to zero. Thermal fluctuations allow the occupation of the site to fluctuate, and the magnetization to become nonzero.

2.4.2 The non-interacting $\frac{t}{U} \rightarrow \infty$ limit

In the $\frac{t}{U} \rightarrow \infty$ limit, the spin spaces become independent, and they may be considered separately. Thus, we omit the spin indices of the operators in the Hamiltonian:

$$\mathcal{H} = -t \sum_{\langle i,j \rangle} \left(c_i^\dagger c_j + c_j^\dagger c_i \right) - \mu \sum_i n_i = \mathbf{c}^\dagger \left(-t\mathbf{K} - \mu\mathbf{I} \right) \mathbf{c}, \quad (2.45)$$

where we casted the Hamiltonian as a bilinear form, and defined

$$\mathbf{c} = \begin{bmatrix} c_1 & c_2 & \dots & c_N \end{bmatrix}^T \quad \mathbf{c}^\dagger = \begin{bmatrix} c_1^\dagger & c_2^\dagger & \dots & c_N^\dagger \end{bmatrix}, \quad (2.46)$$

and where \mathbf{I} is the identity matrix. We also defined a matrix of zeros and ones specifying the hopping geometry, \mathbf{K} . The elements of the hopping matrix are simply defined by the indicator function: $K_{ij} = \mathbb{1}_{\langle j_i \rangle}(i)$, where $\langle j_i \rangle$ is the set of neighbors j of site i . When writing down \mathbf{K} , we must specify the boundary conditions. Periodic boundary conditions (PBCs) preserve a system's translational invariance and are advantageous because they reduce finite size effects. An example of a quantity which is measured more accurately is energy. In the thermodynamic limit, $N \rightarrow \infty$, the measured energy differs from the actual value by a correction of order $\mathcal{O}(\frac{1}{N^2})$ with PBCs, while for Open boundary conditions (OBCs), the correction is of order $\mathcal{O}(\frac{1}{N})$ [68]. Additionally, PBCs have the property of giving site independent observables. For example, the electron density per site does not vary with the distance to the edges of the lattice with PBCs, but it does when we use OBCs.

For concreteness, let us consider a rectangular two-dimensional lattice with $N_x \times N_y$ sites. Then, we have $\dim(\mathbf{K}) = N_x N_y \times N_x N_y$, and

$$\mathbf{K} = \mathbf{I}_y \otimes \mathbf{K}_x + \mathbf{I}_x \otimes \mathbf{K}_y, \quad (2.47)$$

where $\mathbf{I}_{x,y}$ are identity matrices of dimension $N_{x,y} \times N_{x,y}$, respectively, and $\mathbf{K}_{x,y}$ are the hopping matrices in the x and y -directions.

For lattices in 1D or 2D, it is possible to find an exact eigendecomposition

$$\mathbf{K} = \mathbf{F}^T \boldsymbol{\Lambda} \mathbf{F} \quad \text{with} \quad \mathbf{F}^T \mathbf{F} = \mathbf{I}, \quad (2.48)$$

where $\boldsymbol{\Lambda} = \text{diag}(\lambda_{\mathbf{k}})$ is a diagonal matrix of eigenvalues of \mathbf{K} . The Hamiltonian is diagonalized:

$$\mathcal{H} = \tilde{\mathbf{c}}^\dagger \left(-t\mathbf{K} - \mu\mathbf{I} \right) \tilde{\mathbf{c}} = \sum_{\mathbf{k}} \varepsilon_{\mathbf{k}} \tilde{n}_{\mathbf{k}}, \quad (2.49)$$

where $\tilde{\mathbf{c}} = \mathbf{F}\mathbf{c}$ and $\tilde{\mathbf{c}}^\dagger = (\mathbf{F}\mathbf{c})^\dagger$, and

$$\varepsilon_{\mathbf{k}} = -t\lambda_{\mathbf{k}} - \mu \quad \tilde{n}_{\mathbf{k}} = \tilde{c}_{\mathbf{k}}^\dagger \tilde{c}_{\mathbf{k}} \quad (2.50)$$

This is equivalent to performing a canonical transformation on the annihilation (creation) operators, that preserves not their Poisson brackets, as in classical mechanics, but their anti-commutators. Finding the eigendecomposition is equivalent to changing to Fourier space:

$$\tilde{c}_{\mathbf{k}}^\dagger = \frac{1}{\sqrt{N}} \sum_{\mathbf{j}} e^{i\mathbf{k}\cdot\mathbf{j}} c_{\mathbf{j}}^\dagger, \quad (2.51)$$

a transformation which indeed preserves the anti-commutation relations, and the total number operator, i.e., $n = \sum_{\mathbf{j}} n_{\mathbf{j}} = \tilde{n} = \sum_{\mathbf{k}} n_{\mathbf{k}}$.

The \tilde{c} -operators are equally valid electron creation/annihilation operators, obeying the same anti-commutation relations as the original operators c_i , and the total number operator is unchanged under our transformation. While the original operators create/annihilate particles at specific (spatial) sites, the new ones create/annihilate particles with momentum \mathbf{k} . Both sets of operators describe the same physics. Why can't procedure be applied to the interacting case? For instance, the interaction term in the Hubbard model is fairly complex to write in momentum space so it is not possible to apply this procedure to diagonalize it.

Now, it turns out that it is easy to evaluate the partition function for quadratic Hamiltonians. If $\mathcal{H} = \mathbf{c}^\dagger \mathbf{H} \mathbf{c}$, where \mathbf{H} is a $N \times N$ Hermitian matrix, then we have that

$$\text{Tr}[e^{-\beta \mathcal{H}}] = \prod_{i=1}^N (1 + e^{-\beta \lambda_i}), \quad (2.52)$$

where λ_i are the eigenvalues of \mathbf{H} . We present a proof of this result in appendix B.

This result suggests that if we are able to devise some approximation to transform the quartic term of the interacting Hubbard model in a quadratic form, then we can solve it. While this idea is essentially correct, the procedure is not straightforward. Actually, we explore this in the next chapter to derive the simulation method that is at the basis of the entire thesis.

To complete the solution of the non-interacting case we apply the result of equation (2.52) to compute the partition function corresponding to the quadratic Hamiltonian defined in equation (2.49):

$$Z = \prod_{\mathbf{k}} (1 + e^{-\beta(\varepsilon_{\mathbf{k}} - \mu)}) \quad (2.53)$$

Now that we have found a closed form solution for Z , it is again possible to find closed form expressions for observables of interest as well, namely:

1. the density, or average occupation of each site, ρ .

$$\rho = \langle n \rangle = \langle \tilde{n} \rangle = \frac{1}{N} \sum_{\mathbf{k}} \langle \tilde{n}_{\mathbf{k}} \rangle = \frac{1}{N} \sum_{\mathbf{k}} \frac{1}{1 + e^{\beta(\varepsilon_{\mathbf{k}} - \mu)}} = \frac{1}{N} \sum_{\mathbf{k}} f_{\mathbf{k}} \quad (2.54)$$

2. the energy $E = \langle \mathcal{H} \rangle$.

$$E = \frac{1}{N} \sum_{\mathbf{k}} \frac{\varepsilon_{\mathbf{k}} - \mu}{1 + e^{\beta(\varepsilon_{\mathbf{k}} - \mu)}} = \sum_{\mathbf{k}} (\varepsilon_{\mathbf{k}} - \mu) f_{\mathbf{k}} \quad (2.55)$$

3. the equal-time Green's function, which plays a key role in computing other quantities, such as correlation functions.

$$G_{\mathbf{l}\mathbf{j}} = \langle c_{\mathbf{l}} c_{\mathbf{j}}^\dagger \rangle = \frac{1}{N} \sum_{\mathbf{k}} e^{i\mathbf{k}\cdot(\mathbf{l}-\mathbf{j})} (1 - f_{\mathbf{k}}), \quad (2.56)$$

where $f_{\mathbf{k}} = (1 + e^{\beta(\varepsilon_{\mathbf{k}} - \mu)})^{-1}$ is the Fermi-Dirac distribution (of course, here we consider half filling: $\mu = 0$). Note that the Green's function, like the Hamiltonian, is translationally invariant: $G_{l,j} = G_{l-j}$. If we use PBCs, no site is singled out, they are all equivalent and this behavior of the Green's function should become apparent in our simulations.

From our analysis, we draw an important conclusion: that solving the single-particle problem, that is obtaining $\varepsilon_{\mathbf{k}}$ gives us all the information we need about all particle sectors (any number of particles, which is controlled via the chemical potential). When the on-site interaction is “turned off”, the fermions simply occupy the one-particle states according to Pauli’s exclusion principle. The single-particle sector allows us to extrapolate to obtain the behavior of a system for any number of particles simply because $U = 0$; even if the hoppings were not uniform, this would hold. The hoppings need not even be only between nearest neighbors, and in general we could even consider a chemical potential varying from site to site. All we require is that the Hamiltonian is a quadratic form of the fermion operators.

2.5 Effective Heisenberg Hamiltonian

As we have already seen, Mott insulators allow low energy magnetic excitations (spin flips) without energy cost. We concluded that their insulating phase corresponds to a configuration where each atom has an odd number of electrons, let’s say one. This electron may have its spin up or down. In the purely atomic limit $\frac{t}{U} \rightarrow 0$, the atoms are infinitely far, and the excitation spectrum is very simple. The ground state is highly degenerate: every configuration with one electron per site is a ground state. As a matter of fact, the ground state is 2^N -fold degenerate. The first excited state corresponds to configurations with a hole and a doubly occupied site. Let us set the energy of the ground state to zero in our conventions. The energy of these configurations is then U , and there are $N(N-1)2^{N-2}$ of them. This process of generating higher energy excitations may be continued.

When the atoms are brought together, the first effect is the lifting of the degeneracy of the ground state, i.e. the splitting of the subspace of energy $E = 0$ in more subspaces. The effective hamiltonian describing the lifting of the degeneracy of the lowest energy band is obtained by applying degenerate perturbation theory [66] to the kinetic term of the Hubbard Hamiltonian⁸

$$\mathcal{H}_0 = -t \sum_{\langle i,j \rangle, \sigma} (c_{i\sigma}^\dagger c_{j\sigma} + c_{j\sigma}^\dagger c_{i\sigma}) \quad (2.57)$$

2.5.1 Two-site calculation

The effect of the hopping term is best understood in a minimal two-site example. There are four one-particle quantum states, represented by the action of the operators $c_{1,\uparrow}^\dagger$, $c_{1,\downarrow}^\dagger$, $c_{2,\uparrow}^\dagger$, $c_{2,\downarrow}^\dagger$ on the vacuum state. There are six two-particle states in the Fock space $|n_{1\uparrow} n_{1\downarrow} n_{2\uparrow} n_{2\downarrow}\rangle$:

⁸An alternative method would be to use a canonical transformation technique.

$$\begin{aligned}
|1\rangle &\equiv |1, 0, 1, 0\rangle = c_{1\uparrow}^\dagger c_{2\uparrow}^\dagger |0\rangle & |2\rangle &\equiv |0, 1, 0, 1\rangle = c_{1\downarrow}^\dagger c_{2\downarrow}^\dagger |0\rangle \\
|3\rangle &\equiv |1, 0, 0, 1\rangle = c_{1\uparrow}^\dagger c_{2\downarrow}^\dagger |0\rangle & |4\rangle &\equiv |0, 1, 1, 0\rangle = c_{1\downarrow}^\dagger c_{2\uparrow}^\dagger |0\rangle \\
|5\rangle &\equiv |1, 1, 0, 0\rangle = c_{1\uparrow}^\dagger c_{1\downarrow}^\dagger |0\rangle & |6\rangle &\equiv |0, 0, 1, 1\rangle = c_{2\uparrow}^\dagger c_{2\downarrow}^\dagger |0\rangle
\end{aligned} \tag{2.58}$$

The two-site Hamiltonian

$$\mathcal{H}_2 = -t \left(c_{1\uparrow}^\dagger c_{2\uparrow} + c_{2\uparrow}^\dagger c_{1\uparrow} + c_{1\downarrow}^\dagger c_{2\downarrow} + c_{2\downarrow}^\dagger c_{1\downarrow} \right) + U \left(n_{1\uparrow} n_{1\downarrow} + n_{2\uparrow} n_{2\downarrow} \right) \tag{2.59}$$

acts on the states of the Fock space as follows

$$\begin{aligned}
\mathcal{H}_2 |1\rangle &= 0 \\
\mathcal{H}_2 |2\rangle &= 0 \\
\mathcal{H}_2 |3\rangle &= -t(c_{2\uparrow}^\dagger c_{1\uparrow} + c_{1\downarrow}^\dagger c_{2\downarrow}) c_{1\uparrow}^\dagger c_{2\downarrow}^\dagger |0\rangle = -t(|5\rangle + |6\rangle) \\
\mathcal{H}_2 |4\rangle &= -t(c_{1\uparrow}^\dagger c_{2\uparrow} + c_{2\downarrow}^\dagger c_{1\downarrow}) c_{1\downarrow}^\dagger c_{2\uparrow}^\dagger |0\rangle = t(|5\rangle + |6\rangle) \\
\mathcal{H}_2 |5\rangle &= \left[-t(c_{2\uparrow}^\dagger c_{1\uparrow} + c_{2\downarrow}^\dagger c_{1\downarrow}) + Un_{1\uparrow} n_{1\downarrow} \right] c_{1\uparrow}^\dagger c_{1\downarrow}^\dagger |0\rangle = U|5\rangle - t(|3\rangle - |4\rangle) \\
\mathcal{H}_2 |6\rangle &= \left[-t(c_{1\uparrow}^\dagger c_{2\uparrow} + c_{1\downarrow}^\dagger c_{2\downarrow}) + Un_{2\uparrow} n_{2\downarrow} \right] c_{2\uparrow}^\dagger c_{2\downarrow}^\dagger |0\rangle = U|6\rangle - t(|3\rangle - |4\rangle)
\end{aligned} \tag{2.60}$$

When we act on the first two states we obtain 0 because every term of the Hamiltonian gives a term $(c^\dagger)^2$, which is 0 due to Pauli's exclusion principle. The minus signs that appear on the hopping terms stem from the fermion anticommutation relations.

Let us now diagonalize the Hamiltonian in the subspace spanned by $\{|3\rangle, |4\rangle, |5\rangle, |6\rangle\}$. If we add states $|3\rangle$ and $|4\rangle$, we get 0 when acting with the Hamiltonian.

$$\mathcal{H}_2(|3\rangle + |4\rangle) = 0 \tag{2.61}$$

On the other hand, if we subtract $|5\rangle$ and $|6\rangle$, we obtain

$$\mathcal{H}_2(|5\rangle - |6\rangle) = U(|5\rangle - |6\rangle) \tag{2.62}$$

We have found two more eigenvalues (the first two were trivially found to be zero). The others are found by subtracting $|3\rangle$ and $|4\rangle$ and adding $|5\rangle$ and $|6\rangle$.

$$\begin{aligned}
\mathcal{H}_2(|3\rangle + |4\rangle) &= -2t(|5\rangle + |6\rangle) \\
\mathcal{H}_2(|5\rangle - |6\rangle) &= -2t(|3\rangle - |4\rangle) + U(|5\rangle + |6\rangle)
\end{aligned} \tag{2.63}$$

The characteristic equation allowing us to find the rest of the eigenvalues in the rotated subspace spanned by $\{|3\rangle \pm |4\rangle, |5\rangle \pm |6\rangle\}$ is

$$E(E - U) - 4t^2 = 0 \iff E_{\pm} = \frac{U \pm \sqrt{U^2 + 16t^2}}{2} \quad (2.64)$$

Taylor expanding the square root up to second order, we obtain

$$E_- = -\frac{4t^2}{U} \quad E_+ = U + \frac{4t^2}{U} \quad (2.65)$$

Thus, we have obtained the complete energy spectrum. The ground state is a non-degenerate state of energy $-\frac{4t^2}{U}$, while the first excited state is a 3-fold degenerate state with energy 0. The two other excited states have energies of the order of U , the first one being exactly U and the second $U + \frac{4t^2}{U}$.

There are four states for which the energy would be 0 if the hopping term vanished, corresponding to the four states with one electron per site. The effect of the hopping term is to lift the degeneracy by splitting the 4-fold degenerate zero energy state into a singlet of energy $-\frac{4t^2}{U}$ and a triplet of energy 0. This is what we obtain my minimizing a Heisenberg Hamiltonian of the form

$$\mathcal{H} = \frac{4t^2}{U} \left(\mathbf{S}_1 \cdot \mathbf{S}_2 - \frac{1}{4} \right) \quad (2.66)$$

for two spins- $\frac{1}{2}$. However, it turns out that this result is yet more general. For an arbitrary number of sites, this is is the form of the effective Hamiltonian at second order (see appendix (C) for details).

It is easy to extend this analysis beyond half filling to compare it to our solution for the single site case. The latter gave us some insight into how the on-site interaction gives rise to magnetic ordering, and about the development of the Mott plateau. Adding in the hopping we can understand the interplay between kinetic and potential energy, and the magnetic correlations between sites. In fact, we will outline the simplest nontrivial method to solve Hubbard-type Hamiltonians: *exact diagonalization*, which is a competitor of QMC.

Since the two-site Hamiltonian of equation (2.59) commutes with n_{σ} , it conserves the number of up and down fermions, and the $2^4 = 16$ states can be divided into 9 sectors of varying dimension d : $(n_{\uparrow}, n_{\downarrow}, d) = (0, 0, 1), (1, 0, 2), (2, 0, 1), (0, 1, 2), (1, 1, 4), (2, 1, 2), (0, 2, 1), (1, 2, 2), (2, 2, 1)$. There are four sectors of dimension 1: the empty lattice, the fully filled lattice, and the lattices with two-like spin fermions. All these sectors have zero kinetic energy: in the first, there are no electrons present to hop, and in the second Pauli's exclusion principle blocks hopping. The sectors with $n_{\sigma} = 2$ have energy $-U/2$, while the ones with $n_{\uparrow} = n_{\downarrow}$ have energy $U/2$.

The four sectors of dimension are also simple. One and three particle sectors must have the spectrum due to Particle-hole symmetry (PHS). They have eigenenergies $\pm t$. A single fermion can hop between sites, while out of the three fermions, the two with like-spin are blocked and can't hop to the same site, leaving a single fermion free to hop. We have already solved the most complicated $n_{\uparrow} = n_{\downarrow} = 1$ sector, while tackling the half filled case. By determining the complete spectrum of the two-site Hubbard model, we demonstrated that the eigenenergies in the $U \neq 0$ case can't be deduced solely from considering the single-particle sector. The low temperature properties of the model are determined by the lowest energy eigenvalues, which all seem to fall in the half filled sectors. Subtracting $U/2$ to the energies we obtained in the half filled sectors is equivalent to considering the PHS form of

the Hamiltonian. At half filling, we end up with four states with energies around $-U/2$ (the so called lower Hubbard band), and two states with energies around $U/2$ (the so called upper Hubbard band). The lower Hubbard band controls the low temperature physics. In the next section, we show that the Heisenberg Hamiltonian that seems to govern the behavior of the electrons in the lower Hubbard band is in fact the effective $U/t \gg 1$ Hamiltonian.

2.5.2 Degenerate perturbation theory

To first order in \mathcal{H} , the matrix elements of its effective Hamiltonian coincide in the ground state subspace, by definition.

$$\langle m | \mathcal{H}_{\text{eff}} | n \rangle = \langle m | \mathcal{H}_0 | n \rangle, \quad (2.67)$$

where $|m\rangle$, and $|n\rangle$ belong to the ground state subspace. Since we are considering the system to be at half filling in our calculations, $|m\rangle$, and $|n\rangle$ must have one electron per site. The hopping Hamiltonian \mathcal{H}_0 makes an electron hop, leaving its previous site empty, and the site it hops to doubly occupied. This implies that all the matrix elements in the previous equation must be 0.

To second order, the matrix elements of the effective Hamiltonian are

$$\langle m | \mathcal{H}_{\text{eff}} | n \rangle = \sum_{|k\rangle} \frac{\langle m | \mathcal{H}_0 | k \rangle \langle k | \mathcal{H}_0 | n \rangle}{E_0 - E_k} = -\frac{1}{U} \sum_{|k\rangle} \langle m | \mathcal{H}_0 | k \rangle \langle k | \mathcal{H}_0 | n \rangle, \quad (2.68)$$

where $|k\rangle$ are the states that are not in the ground state subspace. In the second equality we simply noted that \mathcal{H}_0 creates a doubly occupied site. The energy cost of creating a doubly occupied site is U .

The identity operator in the in the subspace of states with one doubly occupied site

$$\sum_{|k\rangle} |k\rangle \langle k|$$

may be written in a more convenient form in another representation:

$$\sum_j n_{j,\sigma} n_{j,-\sigma}$$

so that the effective Hamiltonian becomes

$$\mathcal{H}_{\text{eff}} = -\mathcal{H}_0 \frac{\sum_j n_{j,\sigma} n_{j,-\sigma}}{U} \mathcal{H}_0 \quad (2.69)$$

In appendix (C), we find the Heisenberg model as the effective Hamiltonian in this $\frac{U}{t} \gg 1$ limit. This is consistent since the Heisenberg model couples spins on different sites, thus it is an *atomic* model.

$$\mathcal{H}_{\text{eff}} = J \sum_{\langle i,j \rangle} \mathbf{S}_i \cdot \mathbf{S}_j, \quad (2.70)$$

with $J = 4t^2/U$. Since $J > 0$, the model favors configurations with antiparallel adjacent spins.

There is an intuitive physical picture for this result: if two electrons on neighboring sites have parallel spins, none of the two can hop to the neighboring site due to Pauli's exclusion principle. If adjacent sites have antiparallel spins, however, it is possible for any of the two electrons to hop to the neighboring site, and an exchange process allows the system to lower its energy.

2.6 Green's functions: Mott gap and spectral function

2.7 Magnetism and mean field theory

3

Auxiliary Field Quantum Monte Carlo

Contents

3.1 Trotter-Suzuki Decomposition	44
--	----

The interactions between the electrons in a solid give rise to effects that arise specifically due to the many-body nature of the system. The Hubbard model is a minimal model that encapsulates electron correlations. It goes beyond the periodic ionic potential perturbation to the free electron gas or tight binding approaches, which lead to band theory. As we have seen, one obtains the Hubbard Hamiltonian by adding the simplest possible electron-electron interaction term to a tight binding Hamiltonian: an on-site interaction term that penalizes double occupancy of a site. From it, we can make predictions about properties of a strongly correlated system, namely magnetic and superconducting behavior, and metal-insulator transitions.

Auxiliary-field, or Determinant Quantum Monte Carlo ¹ is a simulation method that is commonly used to simulate the Hubbard model, allowing one to capture the elusive effects of electron correlations, for example in the two-dimensional graphene-like nanostructures we are concerned with.

Among the various methods belonging to the family of QMC methods, AFQMC has the advantage of allowing us to circumvent the sign problem for the half filled Hubbard model. The sign problem is an uncontrolled numerical error due to the antisymmetry of the many-electron wave function, leading to oscillations in the sign of the quantities that we are interested in measuring. These oscillations deem the algorithm exponentially complex in the size of the system, in general, but it is possible to overcome this hurdle for a class of models, namely the Hubbard model at half filling. The difficulty lies in computing averages of a quantity X that is very close to zero, on average, but has a large variance, i.e. $\sigma_X / \langle X \rangle \gg 1$.

3.1 Trotter-Suzuki Decomposition

We seek a computable approximation of the projection operator \mathcal{P} defined in equation (2.25). As we shall see, it is found by using a discrete Hubbard-Stratonovich transformation. This transformation introduces an auxiliary field (consisting basically of Ising spins), and we use Monte Carlo to sample configurations from the distribution corresponding to this *classical* configuration space.

For now, let us assume half filling $\mu = 0$, so that there is no sign problem. In fact, many interesting phenomena occur at half filling, for example magnetic ordering and the Mott metal-insulator transition.

3.1.1 Hubbard-Stratonovich transformation

In section ??, we found exact solutions for particular instances of the Hubbard model by finding a closed form for the partition function [68]. When devising a numerical method, a good sanity check is to verify that it satisfactorily approximates the partition function.

The operators \mathcal{H}_K and \mathcal{H}_V of equation (2.22) do not commute. This impedes us from factorizing the exponential of their sum $e^{-\beta(\mathcal{H}_K + \mathcal{H}_V)}$ exactly. The Trotter-Suzuki decomposition leads to the sought approximate factorization that is used to approximate the partition function. Quantum states evolve according to

¹AFQMC or DQMC, respectively.

$$|\psi(\tau)\rangle = e^{-\tau\mathcal{H}} |\psi(0)\rangle, \quad (3.1)$$

where $\tau = it$ is the imaginary time. Recall that Diffusion Monte Carlo is based on this imaginary time evolution, filtering out the ground state as the state that takes longer to vanish exponentially. We now seek a finite temperature method. To find it, we invoke an analogy with the evolution of a quantum system according to the previous equation.

Taking the scalar product with a position eigenstate $\langle \mathbf{x}|$, we obtain $\psi(\mathbf{x}, \tau) = \langle \mathbf{x} | \psi(\tau) \rangle$. Using the closure relation $\int d\mathbf{y} |\mathbf{y}\rangle \langle \mathbf{y}| = 1$, we get

$$\psi(\mathbf{x}, \tau) = \int d\mathbf{y} \langle \mathbf{x} | e^{-\tau\mathcal{H}} |\mathbf{y}\rangle \psi(\mathbf{y}, 0) \quad (3.2)$$

The wave function at position \mathbf{x} and time t may be obtained by this equation as long as we know the wave function at $\tau = 0$, $\psi(\mathbf{y}, 0)$ for all points in space \mathbf{y} . The evolution operator matrix element, or Green function,

$$G(\mathbf{x}, \tau | \mathbf{y}, 0) \equiv \langle \mathbf{x} | e^{-\tau\mathcal{H}} |\mathbf{y}\rangle, \quad (3.3)$$

as the wave function, satisfies the Schrödinger equation, with the initial condition $\psi(\mathbf{y}, 0) = \delta(\mathbf{x} - \mathbf{y})$. It is then the probability of presence at \mathbf{x}, t of a wave packet centered at \mathbf{y} at $t = 0$. Note that the solution of the Schrödinger equation is then analogous to that of a diffusion equation (that in turn one may obtain as the continuum limit of a random walk). We may write G as a linear combination of the eigenstates of the Hamiltonian

$$G(\mathbf{x}, \tau | \mathbf{y}, 0) = \sum_{\alpha} \psi_{\alpha}^*(\mathbf{y}) \psi_{\alpha}(\mathbf{x}) e^{-E_{\alpha}\tau}, \quad (3.4)$$

where we immediately note a striking similarity with equation (2.26). The correspondence $\psi(\mathbf{x}, \tau) \mapsto Z_{\beta}$, where $\tau \mapsto \beta$, with respect to section ?? makes the analogy evident. \mathbf{x} has no correspondence because it is not a parameter, it is just an arbitrary position that we fixed for the sake of the argument.

Computing the partition function at finite temperature

$$Z_{\beta} = \text{Tr}(e^{-\beta\mathcal{H}}) \quad (3.5)$$

is analogous to computing the Green function of a quantum system evolving in imaginary time. The inverse temperature β now represents the imaginary time $\tau = it$, and Z_{β} may be simply thought of as the wave function of the analogous quantum system at imaginary time (temperature) β .

This expression is not very amenable to numerical computation since it contains an exponential of a sum of operators $\mathcal{H}_K + \mathcal{H}_V$, which is not factorizable and involves computing an infinite number of commutators containing these two operators, as per the Zassenhaus formula, valid for any two generic operators X and Y :

$$e^{\delta(X+Y)} = e^{\delta X} e^{\delta Y} e^{-\frac{\delta^2}{2}[X,Y]} e^{\frac{\delta^3}{6}(2[Y,[X,Y]]+[X,[X,Y]])} \\ e^{-\frac{\delta^4}{24}([[X,Y],X],X)+3[[[X,Y],X],Y]+3[[[X,Y],Y],Y]} \dots, \quad (3.6)$$

where $\delta \in \mathbb{C}$ is an expansion parameter.

Dividing the imaginary time interval $[0, \beta]$ into L equal sub-intervals of width $\Delta\tau = \beta/L$, we obtain

$$Z = \text{Tr} \left(\prod_{l=1}^L e^{-\Delta\tau \mathcal{H}} \right), \quad (3.7)$$

which is now a product of exponentials of operators multiplied by a constant that can be made small by increasing L . The Trotter-Suzuki decomposition follows from truncating equation (3.6), and keeping only the first order term in t , i.e. the one in $\Delta\tau$ in our case.

$$Z = \text{Tr} \left(\prod_{l=1}^L e^{-\Delta\tau \mathcal{H}_K} e^{-\Delta\tau \mathcal{H}_V} \right) + \mathcal{O}(\Delta\tau^2) \quad (3.8)$$

The kinetic energy term is quadratic in the fermion operators, and is spin-independent and thus may be separated into spin up and spin down components

$$e^{-\Delta\tau \mathcal{H}_K} = e^{-\Delta\tau \mathcal{H}_{K\uparrow}} e^{-\Delta\tau \mathcal{H}_{K\downarrow}}, \quad (3.9)$$

where $\mathcal{H}_{K_\sigma} = -t \mathbf{c}_\sigma^\dagger \mathbf{K} \mathbf{c}_\sigma$.

The potential energy term, however, is quartic. Surprisingly, it is possible to express it in quadratic form by introducing an extra degree of freedom, the so called *Hubbard-Stratonovich (HS) field* $\mathbf{h} \equiv (h_i)_{i=1}^N$, in which each element is essentially an Ising spin. First, note that number operators on different sites commute, so that we have

$$e^{-\Delta\tau \mathcal{H}_V} = e^{-U \Delta\tau \sum_{i=1}^N (n_{i\uparrow} - 1/2)(n_{i\downarrow} - 1/2)} \\ = \prod_i e^{-U \Delta\tau (n_{i\uparrow} - 1/2)(n_{i\downarrow} - 1/2)} \quad (3.10)$$

Now we introduce the discrete Hubbard Stratonovich transformation for $U > 0$ that allows us to recast the equation above in terms of a non-interacting quadratic term $(n_{i\uparrow} - n_{i\downarrow})$.

$$e^{-U \Delta\tau (n_{i\uparrow} - 1/2)(n_{i\downarrow} - 1/2)} = c_U \sum_{h_i=\pm 1} e^{\nu h_i (n_{i\uparrow} - n_{i\downarrow})}, \quad (3.11)$$

where $c_U = \frac{1}{2} e^{-\frac{U\Delta\tau}{4}}$ and $\nu = \text{arcosh}(e^{\frac{U\Delta\tau}{2}})$.

To prove this identity, let us write down how the operators $(n_{i\uparrow} - 1/2)(n_{i\downarrow} - 1/2)$ and $(n_{i\uparrow} - n_{i\downarrow})$ act on a state on a given site.

$$(n_{i\uparrow} - 1/2)(n_{i\downarrow} - 1/2) \begin{cases} |\rangle = \frac{1}{4} |\rangle \\ |\uparrow\rangle = -\frac{1}{4} |\uparrow\rangle \\ |\downarrow\rangle = -\frac{1}{4} |\downarrow\rangle \\ |\uparrow\downarrow\rangle = \frac{1}{4} |\uparrow\downarrow\rangle \end{cases} \quad (3.12)$$

$$(n_{i\uparrow} - n_{i\downarrow}) \begin{cases} |\rangle = 0 |\rangle \\ |\uparrow\rangle = |\uparrow\rangle \\ |\downarrow\rangle = |\downarrow\rangle \\ |\uparrow\downarrow\rangle = 0 |\uparrow\downarrow\rangle \end{cases}$$

Now we simply compare the action of the operators on the left hand side and on the right hand side of equation (3.11) and find the desired relation by defining

$$\cosh \nu = \frac{e^\nu + e^{-\nu}}{2} \equiv e^{\frac{U\Delta\tau}{2}} \quad (3.13)$$

$$e^{-U\Delta\tau(n_{i\uparrow}-1/2)(n_{i\downarrow}-1/2)} |\psi\rangle = e^{-\frac{U\Delta\tau}{4}} |\psi\rangle, |\psi\rangle = |\rangle, |\uparrow\downarrow\rangle$$

$$e^{-U\Delta\tau(n_{i\uparrow}-1/2)(n_{i\downarrow}-1/2)} |\uparrow(\downarrow)\rangle = e^{\frac{U\Delta\tau}{4}} |\uparrow(\downarrow)\rangle$$

$$c_U \sum_{h_i=\pm 1} e^{\nu h_i (n_{i\uparrow} - n_{i\downarrow})} |\psi\rangle = e^{-\frac{U\Delta\tau}{4}} |\psi\rangle, |\psi\rangle = |\rangle, |\uparrow\downarrow\rangle \quad (3.14)$$

$$c_U \sum_{h_i=\pm 1} e^{\nu h_i (n_{i\uparrow} - n_{i\downarrow})} |\uparrow(\downarrow)\rangle = \frac{e^\nu + e^{-\nu}}{2} e^{-\frac{U\Delta\tau}{4}} |\uparrow(\downarrow)\rangle$$

Note that we require $U > 0$ so that there exists $\nu \in \mathbb{R}$ such that $\cosh \nu = e^{U\Delta\tau/2}$. A similar reasoning could be made for $U < 0$. Additionally, other transformations that recast other types of quartic terms in terms of quadratic ones exist, but we shall not need them in what follows [8]. The transformation we derived is the one we will use throughout.

We have now made progress. At the expense of introducing an extra N -dimensional HS-field \mathbf{h} , we obtained an *exact* representation of the quartic term in terms of quadratic terms [68].

$$e^{-\Delta\tau\mathcal{H}_V} = \prod_{i=1}^N \left(c_U \sum_{h_i=\pm 1} e^{\nu h_i (n_{i\uparrow} - n_{i\downarrow})} \right), \quad (3.15)$$

which can be manipulated to arrive at a more compact form.

$$\begin{aligned}
e^{-\Delta\tau\mathcal{H}_V} &= (c_U)^N \sum_{h_i=\pm 1} e^{\nu h_i(n_{1\uparrow}-n_{1\downarrow})} \sum_{h_i=\pm 1} e^{\nu h_i(n_{2\uparrow}-n_{2\downarrow})} \\
&\quad \cdots \sum_{h_i=\pm 1} e^{\nu h_i(n_{N\uparrow}-n_{N\downarrow})} \\
&= (c_U)^N \sum_{h_i=\pm 1} e^{\sum_{i=1}^N [(\nu h_i(n_{i\uparrow}-n_{i\downarrow})]} \\
&\equiv (c_U)^N \text{Tr}_h e^{\sum_{i=1}^N [(\nu h_i(n_{i\uparrow}-n_{i\downarrow})]} \\
&= (c_U)^N \text{Tr}_h e^{\sum_{i=1}^N \nu h_i n_{i\uparrow}} e^{-\sum_{i=1}^N \nu h_i n_{i\uparrow}} \\
&= (c_U)^N \text{Tr}_h (e^{\mathcal{H}_{V\uparrow}} e^{\mathcal{H}_{V\downarrow}}),
\end{aligned} \tag{3.16}$$

where the spin up and spin down operators $\mathcal{H}_{V\sigma}$ are defined as follows

$$\mathcal{H}_{V\sigma} = \sum_{i=1}^N \nu h_i n_{i\sigma} = \sigma \nu \mathbf{c}_\sigma^\dagger \mathbf{V}(\mathbf{h}) \mathbf{c}_\sigma, \tag{3.17}$$

with $\mathbf{V}(\mathbf{h})$ being simply the HS-field put into a diagonal $N \times N$ matrix: $\mathbf{V}(\mathbf{h}) \equiv \text{diag}(h_1, h_2, \dots, h_N)$.

For each imaginary time slice l (where $l \in [1, L]$) we may define a HS-field \mathbf{h}_l , which in turn specifies \mathbf{V}_l and $\mathcal{H}_{V_\sigma}^l$. We may now replace the result of equation (3.16) in equation (3.8), and exchange the traces to obtain

$$\begin{aligned}
Z_h &= (c_U)^{NL} \text{Tr}_h \text{Tr} \left[\underbrace{\prod_{l=1}^L \left(e^{-\Delta\tau\mathcal{H}_{K\uparrow}} e^{\mathcal{H}_{V\uparrow}^l} \right)}_{B_{l,\uparrow}(\mathbf{h}_l)} \right. \\
&\quad \left. \underbrace{\left(e^{-\Delta\tau\mathcal{H}_{K\downarrow}} e^{\mathcal{H}_{V\downarrow}^l} \right)}_{B_{l,\downarrow}(\mathbf{h}_l)} \right], \tag{3.18}
\end{aligned}$$

where all operators are now quadratic in the fermion operators:

$$\begin{aligned}
\mathcal{H}_{K\sigma} &= -t \mathbf{c}_\sigma^\dagger \mathbf{K} \mathbf{c}_\sigma \\
\mathcal{H}_{V_\sigma}^l &= \sigma \nu \mathbf{c}_\sigma^\dagger \mathbf{V}_l(\mathbf{h}_l) \mathbf{c}_\sigma
\end{aligned} \tag{3.19}$$

for $\sigma = \pm 1$ and $\mathbf{V}_l(\mathbf{h}_l) = \text{diag}(h_{l,1}, h_{l,2}, \dots, h_{l,N})$.

Furthermore, we have defined the \mathbf{B} -matrices

$$\mathbf{B}_{l,\sigma}(\mathbf{h}_l) = e^{t\Delta\tau\mathbf{K}} e^{\sigma \nu \mathbf{V}_l(\mathbf{h}_l)} \tag{3.20}$$

Note that the argument of the first exponential is positive since \mathbf{K} is defined so that its entries are 0's and 1's; otherwise (defining \mathbf{K} with 0's and -1 's) it would be negative.

The problem of computing the partition has been reduced to computing the trace of a product of exponentials of quadratic forms. Thus, we may still rewrite equation (3.18) by making use of the following identity.

Let \mathcal{H}_l be quadratic forms of the fermion operators:

$$\mathcal{H}_l = c_i^\dagger (H_l)_{ij} c_j, \quad (3.21)$$

where the summation is implied, and where H_l are real matrices. Then, the following identity holds

$$\text{Tr} [e^{-\mathcal{H}_1} e^{-\mathcal{H}_2} \dots e^{-\mathcal{H}_L}] = \det(\mathbf{I} + e^{-H_L} e^{-H_{L-1}} \dots e^{-H_1}) \quad (3.22)$$

For simplicity, we present the proof for a simpler case, corresponding to a single \mathbf{B} -matrix, i.e. a product of exponentials of two quadratic operators [7]. It could then be easily extended to the more general case. Let the two arbitrary real matrices be \mathbf{M} and \mathbf{N} . Then, a particular case of the previous identity is

$$\text{Tr} [e^{-c_i^\dagger M_{ij} c_j} e^{-c_i^\dagger N_{ij} c_j}] = \det(\mathbf{I} + e^{-\mathbf{M}} e^{-\mathbf{N}}), \quad (3.23)$$

where a summation over repeated indices is implied, as it will be throughout this proof.

To prove this identity, we start by proving that

$$e^{-c_i^\dagger M_{ij} c_j} e^{-c_i^\dagger N_{ij} c_j} = e^{-\sum_\nu c_\nu^\dagger \rho_\nu c_\nu}, \quad (3.24)$$

where $\lambda_\nu = e^{-\rho_\nu}$ are the eigenvalues of the matrix $e^{-\mathbf{M}} e^{-\mathbf{N}}$.

The proof consists of showing that any many-particle state are propagated in the same way when acted upon by any of these two operators, i.e. the LHS operator leads the system to the same state as the RHS operator.

A generic single-particle state reads

$$|\phi\rangle = \sum_j a_j c_j^\dagger |0\rangle, \quad (3.25)$$

where a_j are arbitrary coefficients, and $|0\rangle$ is the vacuum state.

Let $\{|\mu\rangle\}$ be the basis in which the matrix \mathbf{N} is diagonal. Using Dirac notation, we then have

$$\mathbf{N} = \sum_\mu |\mu\rangle n_\mu \langle \mu| \quad (3.26)$$

Defining new fermionic operators

$$\begin{aligned} c_\mu &= \sum_j \langle \mu | j \rangle c_j \\ c_\mu^\dagger &= \sum_j \langle j | \mu \rangle c_j^\dagger, \end{aligned} \quad (3.27)$$

which may be inverted to obtain

$$\begin{aligned} c_j &= \sum_{\mu} \langle j | \mu \rangle c_{\mu} \\ c_j^{\dagger} &= \sum_{\mu} \langle \mu | j \rangle c_{\mu}^{\dagger}, \end{aligned} \tag{3.28}$$

Now we prove yet another identity that goes into proving equation (3.24).

$$e^{-c_i^{\dagger} N_{ij} c_j} = \prod_{\mu} [\mathbb{1} + (e^{-n_{\mu}} - 1) c_{\mu}^{\dagger} c_{\mu}] \tag{3.29}$$

$$\begin{aligned} \exp(-c_i^{\dagger} N_{ij} c_j) &= \exp\left(-\sum_{\mu\nu} \langle \mu | i \rangle c_{\mu}^{\dagger} N_{ij} \langle j | \nu \rangle c_{\nu}\right) \\ &= \exp\left(-\sum_{ij} \sum_{\mu\nu\sigma} \langle \mu | i \rangle \langle i | \sigma \rangle c_{\mu}^{\dagger} n_{\sigma} \langle \sigma | j \rangle \langle j | \nu \rangle c_{\nu}\right), \\ &\quad (\text{using the closure relation } \sum_i |i\rangle \langle i| = \mathbb{1}) \\ &= \exp\left(-\sum_{\mu\nu\sigma} \overbrace{\langle \mu | \sigma \rangle}^{\delta_{\mu\sigma}} c_{\mu}^{\dagger} n_{\sigma} \overbrace{\langle \sigma | \nu \rangle}^{\delta_{\sigma\nu}} c_{\nu}\right) \\ &= \exp\left(-\sum_{\mu} c_{\mu}^{\dagger} n_{\mu} c_{\mu}\right) \\ &= \prod_{\mu} e^{-n_{\mu} \hat{n}_{\mu}} \\ &= \prod_{\mu} [\mathbb{1} + (-n_{\mu} \hat{n}_{\mu} + \frac{n_{\mu}^2}{2!} \hat{n}_{\mu}^2 - \frac{n_{\mu}^3}{3!} \hat{n}_{\mu}^3 + \dots)] \\ &= \prod_{\mu} [\mathbb{1} + (-n_{\mu} + \frac{n_{\mu}^2}{2!} - \frac{n_{\mu}^3}{3!} + \dots) \hat{n}_{\mu}] \\ &\quad (\text{since } \hat{n} = \hat{n}^k \text{ for all } k \in \mathbb{N} \text{ for fermions since } n = 0, 1) \\ &= \prod_{\mu} [\mathbb{1} + (e^{-n_{\mu}} - 1) c_{\mu}^{\dagger} c_{\mu}] \quad \square \end{aligned}$$

Let

$$|\phi\rangle = \sum_j a_j c_j^{\dagger} |0\rangle \tag{3.30}$$

be an arbitrary many-particle state.

Now we use the previous identity to prove that applying the operator of equation (3.29) to $|\phi\rangle$ we obtain

$$e^{-c_i^{\dagger} N_{ij} c_j} |\phi\rangle = \sum_j a'_j c_j^{\dagger} |0\rangle, \tag{3.31}$$

with

$$a'_j = \sum_i (e^{-B})_{ji} a_i \tag{3.32}$$

We start by writing $|\phi\rangle$ in the basis $\{|\mu\rangle\}$ (in which N is diagonal).

$$|\phi\rangle = \sum_{i,\mu} a_i \langle \mu | i \rangle c_\mu^\dagger |0\rangle \quad (3.33)$$

Then, we apply the RHS of equation (3.29) to $|\phi\rangle$ written in this basis.

$$\begin{aligned} & \sum_\nu \left[\mathbb{1} + (e^{-n_\mu} - 1)c_\nu^\dagger c_\nu \right] c_\mu^\dagger |0\rangle \\ &= \left[\mathbb{1} + (e^{-n_\mu} - 1)c_\mu^\dagger c_\mu \right] c_\mu^\dagger |0\rangle \\ &= c_\mu^\dagger |0\rangle + (e^{-n_\mu-1} - 1)c_\mu^\dagger |0\rangle \\ &= c_\mu^\dagger e^{-n_\mu} |0\rangle \end{aligned} \quad (3.34)$$

$$\begin{aligned} & \sum_\nu \left[\mathbb{1} + (e^{-n_\mu} - 1)c_\nu^\dagger c_\nu \right] |\phi\rangle \\ &= \sum_{i\mu} \langle \mu | i \rangle a_i e^{-n_\mu} c_\mu^\dagger \\ &= \sum_{j\mu i} \langle j | \mu \rangle e^{-n_\mu} \langle \mu | i \rangle a_i |j\rangle \\ &= \sum_{ji} \underbrace{\sum_{\mu\nu} \langle j | \mu \rangle e^{-N_{\mu\nu}} \langle \nu | i \rangle a_i}_{(e^{-\mathbf{N}})_{ji}} |j\rangle \\ &= \sum_j a'_j c_j^\dagger |0\rangle \end{aligned} \quad (3.35)$$

Similarly, by repeating the procedure performing a change of basis to the eigenbasis of \mathbf{M} , we obtain the more general relation

$$\begin{aligned} & e^{-c_i^\dagger M_{ij} c_j} e^{-c_i^\dagger N_{ij} c_j} |\phi\rangle = \sum_j a''_j c_j^\dagger |0\rangle \\ & a''_j = \sum_i (e^{-\mathbf{M}} e^{-\mathbf{N}})_{ji} a_i \end{aligned} \quad (3.36)$$

The amplitude of a propagated state is given by multiplying the initial amplitude by the matrix $e^{-\mathbf{M}} e^{-\mathbf{N}}$, whichever the basis we choose. Then, since equation (3.36) holds in particular for the choice of the eigenbasis of $e^{-\mathbf{M}} e^{-\mathbf{N}}$ as our basis of single-particle states, if we start with an eigenstate

$$|\phi\rangle = c_\nu^\dagger |0\rangle, \quad (3.37)$$

then the amplitude of the propagated state will be given by

$$(e^{-\mathbf{M}} e^{-\mathbf{N}})_{\nu\nu} = e^{-\rho_\nu}, \quad (3.38)$$

the same as we would obtain from equation (3.24). Clearly, if we start with a state that is an arbitrary combination of states of the eigenbasis, we would obtain the identity (3.24).

The identity was proven for a single-particle state. Does it generalize to more than one particle? As we did before, we start with propagation by a single factor $e^{-\mathbf{N}}$. Take a two-particle state

$$|\phi\rangle = c_{\mu_1}^\dagger c_{\mu_2}^\dagger |0\rangle \quad (3.39)$$

Now propagate it with \mathbf{N} , i.e.

$$\begin{aligned} e^{-c_i^\dagger N_{ij} c_j} |\phi\rangle &= \prod_\mu \left[1 + (e^{-n_\mu} - 1) c_\mu^\dagger c_\mu \right] c_{\mu_1}^\dagger c_{\mu_2}^\dagger |0\rangle \\ &= e^{-n_{\mu_1}} e^{-n_{\mu_2}} c_{\mu_1}^\dagger c_{\mu_2}^\dagger |0\rangle, \end{aligned} \quad (3.40)$$

where we simply note that by similar reasoning to the previous case, we would in equation (3.34) keep two terms corresponding to $\mu_1 \neq \mu_2$. If $\mu_1 = \mu_2$, then both sides are equal to zero due to Pauli's exclusion principle and the equality holds trivially. This reasoning clearly generalizes to an arbitrary superposition of many-particle states. Moreover, we proved the result for a product of two factors $e^{-\mathbf{M}} e^{-\mathbf{N}}$, but it is also easy to see that by successive changes of basis, we could extend our result to an arbitrary number of factors.

To complete our proof of the identity (3.23) that is so crucial in formulating AFQMC, we use the auxiliar identity we just proved (3.24).

$$\begin{aligned} \text{Tr} \left[e^{-\sum_\nu c_\nu^\dagger \rho_\nu c_\nu} \right] &= \text{Tr} \left[\prod_\nu e^{-c_\nu^\dagger \rho_\nu c_\nu} \right] \text{ since } [\hat{n}_\mu, \hat{n}_\nu] = 0 \\ &= \prod_\nu (1 + e^{-\rho_\nu}) = \det[\mathbf{I} + e^{-\mathbf{M}} e^{-\mathbf{N}}], \quad \square \end{aligned} \quad (3.41)$$

where the last equality stems from the fact that the determinant of a diagonal matrix is just the product of the eigenvalues.

When applied to our problem, equation (3.22) essentially makes the computation of the trace possible! Note that if we were to compute it naively, we would soon run out of computer memory. The dimension of the Hilbert space of the Hubbard model is exponential in N (actually 4^N), where N is the number of lattice sites. The determinant is calculated for a matrix whose size is polynomial in N .

Equation (3.22) allows us to write the partition function (3.18) in computable form

$$\begin{aligned} Z_{\mathbf{h}} &= \text{Tr}_{\mathbf{h}} \left[(c_U)^{NL} \det[\mathbf{M}_\uparrow(\mathbf{h})] \det[\mathbf{M}_\downarrow(\mathbf{h})] \right] \\ &\equiv \text{Tr}_{\mathbf{h}} \left[\tilde{\rho}_{\text{eff}}(\mathbf{h}) \right], \end{aligned} \quad (3.42)$$

where the fermion matrices \mathbf{M}_σ are defined in terms of the \mathbf{B} -matrices for a given spin σ and a given HS-field \mathbf{h} :

$$\mathbf{M}_\sigma(\mathbf{h}) = \mathbf{I} + \mathbf{B}_{L,\sigma}(h_L) \mathbf{B}_{L-1,\sigma}(h_{L-1}) \dots \mathbf{B}_{1\sigma}(h_1) \quad (3.43)$$

Equation (3.42) defines an effective density matrix (now a function!) $\tilde{\rho}_{\text{eff}}(\mathbf{h})$ in the HS-field space.

The computable approximation of the distribution operator \mathcal{P} corresponding to this partition function is

$$P(\mathbf{h}) = \frac{A}{Z_h} \det[\mathbf{M}_\uparrow(\mathbf{h})] \det[\mathbf{M}_\downarrow(\mathbf{h})], \quad (3.44)$$

where $A = (c_U)^{NL}$ is a normalization constant. This is now a distribution function over configurations \mathbf{h} since the problem is classical!

For the particular case of no interactions $U = 0$, we have that $\nu = 0$, and $\mathbf{M}_\sigma(\mathbf{h})$ are constant matrices, independent of the HS-field. The Trotter-Suzuki approximation then becomes exact and the Hubbard Hamiltonian may be simulated exactly after evaluating $\mathbf{M}_\sigma(\mathbf{h})$ a single time. No updates are required.

As a final remark, note that we managed to map a quantum problem to a classical problem in higher dimension. The degrees of freedom of the quantum problem correspond to the i indices of the c -operators. In our formulation, an additional imaginary time slice index l was introduced, leading to a mapping that is not specific to the Hubbard model, but that actually applies very generally for any quantum system.

3.1.1.A Monte Carlo sampling of the HS-field

The computational problem is now that of sampling configurations of the \mathbf{h} field drawn from the distribution $P(\mathbf{h})$ using *Classical* Monte Carlo. The size of the state space has been (hopefully) reduced to 2^{NL} (assuming that $L < N$).

It remains to choose a dynamics and a sampling scheme. The simplest strategy to change from a configuration \mathbf{h} to a new one \mathbf{h}' is single spin-flip dynamics. We choose a random point (l, i) , and we flip the spin at that “site”

$$h'_{l,i} = -h_{l,i}, \quad (3.45)$$

keeping all others unchanged.

The most common scheme to ensure that the distribution of the accepted sample is $P(\mathbf{h})$ is the Metropolis-Hastings algorithm.

After the warm-up steps, i.e. after we ensure that we are correctly sampling from the required distribution, we may perform measurements, waiting for some (Monte Carlo) time before each of them to ensure that the correlations within the sample are negligible. Let the total number of Monte Carlo steps (warm-up W + measurement M) be $S = W + M$. The idea is that we run the algorithm for W steps, before starting the measurements. Then we measure the state of the system every 2τ steps, where τ is the correlation time, i.e. the time it takes for some representative correlation function to drop to e^{-1} its original value.

The Metropolis acceptance/rejection scheme leads to a rank-one update of the matrices $\mathbf{M}_\sigma(\mathbf{h})$, which affords an efficient evaluation of the acceptance ratio $a_{l,i}$ [68].

Algorithm 3.1 Auxiliary Field Quantum Monte Carlo

```

Initialize HS field  $\mathbf{h}$ 
Initialize hoppings  $\mathbf{K}$ 
 $(h_{l,i}) = (\pm 1)_{l=1,i=1}^{L,N}$ 
 $(l, i) \leftarrow (1, 1)$ 
5: for step = 1 to  $S$  do
    Propose new configuration by flipping a spin
     $h'_{l,i} = -h_{l,i}$ 
    Compute the acceptance ratio  $a_{l,i}$ 
     $\frac{\det[\mathcal{M}_\uparrow(\mathbf{h}')]\det[\mathcal{M}_\downarrow(\mathbf{h}')]}{\det[\mathcal{M}_\uparrow(\mathbf{h})]\det[\mathcal{M}_\downarrow(\mathbf{h})]}$ 
    Metropolis step
    Draw random number  $r \in [0, 1]$ 
10:   if  $r \leq \min(1, a_{l,i})$  then
         $\mathbf{h} = \mathbf{h}'$ 
    else
         $\mathbf{h} = \mathbf{h}$ 
    end if
15:   Next site
    if  $i < N$  then
         $l = l, i = i + 1$ 
    else
        if  $l < L$  then
             $l = l + 1, i = 1$ 
        end if
        if  $l = L$  then
             $l = 1, i = 1$ 
        end if
25:   end if
end for

```

Consider two matrices $\mathbf{A}_1, \mathbf{A}_2$ written in the form

$$\mathbf{A}_{1,2} = \mathbf{I} + \mathbf{F}\mathbf{V}_{1,2}, \quad (3.46)$$

where \mathbf{F} is some matrix. $\mathbf{V}_{1,2}$ are diagonal and non-singular and differ only in the (1, 1) entry, so that

$$\mathbf{V}_1^{-1}\mathbf{V}_2 = \mathbf{I} + \alpha_1 \mathbf{e}_1 \mathbf{e}_1^T, \quad (3.47)$$

where \mathbf{e}_1 is a vector corresponding to the first column of the identity matrix \mathbf{I} , and

$$\alpha_1 = \frac{V_2(1, 1)}{V_1(1, 1)} - 1$$

Then, \mathbf{A}_2 is clearly a rank-one update of \mathbf{A}_1 .

$$\begin{aligned} \mathbf{A}_2 &= \mathbf{I} + \mathbf{F}\mathbf{V}_1 + \mathbf{F}\mathbf{V}_1(\mathbf{V}_1^{-1}\mathbf{V}_2 - \mathbf{I}) \\ &= \mathbf{A}_1 + \alpha_1(\mathbf{A}_1 - \mathbf{I})\mathbf{e}_1\mathbf{e}_1^T \\ &= \mathbf{A}_1[\mathbf{I} + \alpha_1(\mathbf{I} - \mathbf{A}_1^{-1})\mathbf{e}_1\mathbf{e}_1^T] \end{aligned}$$

Using the identity $\det[\mathbf{I} + \mathbf{x}\mathbf{y}^T] = 1 + \mathbf{y}^T\mathbf{x}$ for any two column vectors, we may write the ratio of the determinants of matrices \mathbf{A}_1 and \mathbf{A}_2 as

$$r_1 = \frac{\det[\mathbf{A}_2]}{\det[\mathbf{A}_1]} = 1 + \alpha_1(1 - \mathbf{e}_1^T \mathbf{A}_1^{-1} \mathbf{e}_1), \quad (3.48)$$

which reduces the computation of the ratio r_1 to computing the $(1, 1)$ entry of \mathbf{A}^{-1} .

Now we generalize this idea for a sequence of matrices $\mathbf{A}_1, \mathbf{A}_2, \dots, \mathbf{A}_i, \dots, \mathbf{A}_n$ generated by successive rank-one updates: $\mathbf{A}_{i+1} = \mathbf{I} + \mathbf{F}\mathbf{V}_{i+1}$, $i = 1, 2, \dots, n - 1$, with

$$\mathbf{V}_i^{-1}\mathbf{V}_{i+1} = \mathbf{I} + \alpha_i \mathbf{e}_i \mathbf{e}_i^T \quad \alpha_i = \frac{\mathbf{V}_{i+1}(1, 1)}{\mathbf{V}_i(1, 1)} - 1 \quad (3.49)$$

The Sherman-Morrison-Woodbury formula gives an expression for the inverse of \mathbf{A}_2 as a rank-one update of \mathbf{A}_1^{-1} .

$$\begin{aligned} \mathbf{A}_2^{-1} &= \left[\mathbf{I} - \frac{\alpha_1}{r_1} (\mathbf{I} - \mathbf{A}_1^{-1}) \mathbf{e}_1 \mathbf{e}_1^T \right] \mathbf{A}_1^T \\ &= \mathbf{A}_1^{-1} - \frac{\alpha_1}{r_1} \mathbf{u}_1 \mathbf{w}_1^T, \end{aligned} \quad (3.50)$$

where

$$\mathbf{u}_1 = (\mathbf{I} - \mathbf{A}_1^{-1}) \mathbf{e}_1 \quad \mathbf{w}_1 = (\mathbf{A}_1^{-1})^T \mathbf{e}_1$$

Using equation (3.48), we find the updates

$$\begin{aligned} r_i &= \frac{\det[\mathbf{M}_{i+1}]}{\det[\mathbf{M}_i]} = 1 + \alpha_i (1 - \mathbf{e}_i^T \mathbf{A}_i^{-1} \mathbf{e}_i), \text{ and} \\ \mathbf{M}_{i+1}^{-1} &= \mathbf{M}_i^{-1} - \frac{\alpha_i}{r_i} \mathbf{u}_i \mathbf{w}_i^T, \end{aligned} \quad (3.51)$$

where $\mathbf{u}_i = (\mathbf{I} - \mathbf{A}_i^{-1}) \mathbf{e}_i$ and $\mathbf{w}_i = (\mathbf{A}_i^{-1})^T \mathbf{e}_i$.

It is possible to generalize this procedure to compute the inverse of \mathbf{M}_k as a rank- $(k - 1)$ update of \mathbf{A}_1^{-1} :

$$\mathbf{M}_k^{-1} = \mathbf{M}_1^{-1} - \mathbf{U}_{k-1} \mathbf{D}_k \mathbf{W}_{k-1}^T, \quad (3.52)$$

where

$$\mathbf{U}_k = [\mathbf{u}_1, \mathbf{u}_2, \dots, \mathbf{u}_{k-1}] \quad \text{and} \quad \mathbf{W} = [\mathbf{w}_1, \mathbf{w}_2, \dots, \mathbf{w}_{k-1}], \quad (3.53)$$

and $\mathbf{D}_k = \text{diag}(\alpha_1/r_1, \alpha_2/r_2, \dots, \alpha_{k-1}/r_{k-1})$.

3.1.1.B Making measurements

In QMC simulations, physical observables are extracted by measuring them directly over the course of the sampling of the configuration space. The single-particle (equal time) Green's Function is useful to obtain quantities such as density and kinetic energy. It turns out that it is simply the inverse of the \mathbf{M} -matrix that we already compute to obtain the acceptance ratio at each step.

$$\begin{aligned}
G_{ij}^\sigma &= \left\langle c_{i\sigma} c_{j\sigma}^\dagger \right\rangle_{\mathbf{h}} \\
&= \left(M_\sigma^{-1}(\mathbf{h}) \right)_{ij} \\
&= \left([\mathbf{I} + \mathbf{B}_{L,\sigma}(h_L) \mathbf{B}_{L-1,\sigma}(h_{L-1}) \dots \mathbf{B}_{1,\sigma}(h_1)]^{-1} \right)_{ij}
\end{aligned} \tag{3.54}$$

The equal time Green's function is a fermion average for a given HS-field configuration [69]. The corresponding thermal average is given by

$$\begin{aligned}
\left\langle c_i c_j^\dagger \right\rangle &= \frac{1}{Z} \text{Tr} \left[e^{-\beta \mathcal{H}} c_i c_j^\dagger \right] \\
&= \frac{1}{Z} \text{Tr}_{\mathbf{h}} \text{Tr} \left[c_{i\sigma} c_{j\sigma}^\dagger \prod_{l=1}^L B_{l,\uparrow}(\mathbf{h}_l) B_{l,\downarrow}(\mathbf{h}_l) \right],
\end{aligned} \tag{3.55}$$

The density matrix $e^{-\beta \mathcal{H}}$ may be written as a trace over HS-field configurations of a product of L factors corresponding to each imaginary time slice. Recall equation (3.18): the partition function Z is just the trace over the Hilbert space of the aforementioned density matrix. Equivalently, it may be thought of as a trace over HS-field configurations of the effective density matrix $\hat{\rho}_{\text{eff}}(\mathbf{h})$ defined in equation (3.42).

The Green's function is defined for fixed \mathbf{h} . Omitting the spin index σ , without loss of generality, we obtain

$$\begin{aligned}
G_{ij} &\equiv \left\langle c_i c_j^\dagger \right\rangle_{\mathbf{h}} = \frac{\text{Tr}[\mathbf{B}_L(h_l) \mathbf{B}_{L-1}(h_{l-1}) \dots \mathbf{B}_1(h_1) c_i c_j^\dagger]}{\tilde{\rho}_{\text{eff}}} \\
&= \frac{\text{Tr}[\mathbf{B}_L \mathbf{B}_{L-1} \dots \mathbf{B}_1 c_i c_j^\dagger]}{\text{Tr}[\mathbf{B}_L \mathbf{B}_{L-1} \dots \mathbf{B}_1]}
\end{aligned} \tag{3.56}$$

The trace is evaluated by changing to a basis $\{|\alpha\rangle\}$, where c_i is diagonal and then repeating the procedure for c_j^\dagger , now changing again to a basis $\{|\beta\rangle\}$, where c_j^\dagger is diagonal. Using equation (3.28), we obtain

$$\left\langle c_i c_j^\dagger \right\rangle_{\mathbf{h}} = \frac{\sum_{\alpha,\beta} \langle i|\alpha\rangle \langle \beta|j\rangle \text{Tr}[c_\alpha c_\beta^\dagger \mathbf{B}_L \mathbf{B}_{L-1} \dots \mathbf{B}_1]}{\text{Tr}[\mathbf{B}_L \mathbf{B}_{L-1} \dots \mathbf{B}_1]} \tag{3.57}$$

After taking the trace, (on the diagonal basis) the only nonzero contribution will be for $\alpha = \beta$. When $c_\alpha c_\beta^\dagger$ acts on the bra to its left, only that term survives in the sum since c_α is a diagonal operator in the basis $\{|\alpha\rangle\}$. On the other hand, the second equality in equation (3.41) gives the contribution to the trace of the exponential of $c_\alpha^\dagger c_\alpha$ appearing in the \mathbf{B} -matrices.

$$\text{Tr}[\mathbf{B}_L \mathbf{B}_{L-1} \dots \mathbf{B}_1] = \prod_\nu (1 + e^{-\rho_\nu}), \tag{3.58}$$

where $\{|\nu\rangle\}$ is the basis in which the product of the \mathbf{B} 's is diagonal.

$$\begin{aligned}
\langle c_i c_j^\dagger \rangle_h &= \sum_{\alpha} |\alpha\rangle\langle i| \frac{\text{Tr}[c_\alpha c_\alpha^\dagger \mathbf{B}_L \mathbf{B}_{L-1} \dots \mathbf{B}_1]}{\text{Tr}[\mathbf{B}_L \mathbf{B}_{L-1} \dots \mathbf{B}_1]} |j\rangle\langle \alpha| \\
&= \sum_{\alpha} |\alpha\rangle\langle i| \frac{\text{Tr}[(\mathbb{1} - c_\alpha^\dagger c_\alpha) \mathbf{B}_L \mathbf{B}_{L-1} \dots \mathbf{B}_1]}{\text{Tr}[\mathbf{B}_L \mathbf{B}_{L-1} \dots \mathbf{B}_1]} |j\rangle\langle \alpha| \\
&= \sum_{\alpha} |\alpha\rangle\langle i| 1 - \frac{\text{Tr}[c_\alpha^\dagger c_\alpha e^{-\Delta\tau\hat{h}}]}{\text{Tr}[e^{-\Delta\tau\hat{h}}]} |j\rangle\langle \alpha| \\
&= \sum_{\alpha} |\alpha\rangle\langle i| 1 - \frac{1}{1 + e^{\Delta\tau\varepsilon_{\alpha}}} |j\rangle\langle \alpha| \\
&= \sum_{\alpha} |\alpha\rangle\langle i| \frac{e^{\Delta\tau\varepsilon_{\alpha}}}{1 + e^{\Delta\tau\varepsilon_{\alpha}}} |j\rangle\langle \alpha| \\
&= \sum_{\alpha} |\alpha\rangle\langle i| \frac{1}{1 + e^{-\Delta\tau\varepsilon_{\alpha}}} |j\rangle\langle \alpha| \\
&= \left[\frac{1}{\mathbf{B}_L \mathbf{B}_{L-1} \dots \mathbf{B}_1} \right]_{ij},
\end{aligned} \tag{3.59}$$

where in the fourth equality we used an analogy with the Fermi function defined as

$$f_{\alpha} = \frac{\text{Tr}[e^{-\beta\mathcal{H}} \hat{n}_{\alpha}]}{\text{Tr}[e^{-\beta\mathcal{H}}]} = (1 + e^{\beta\varepsilon_{\alpha}})^{-1} \tag{3.60}$$

for $\mu = 0$ and with $\beta \mapsto \Delta\tau$. The product of \mathbf{B} -matrices was written as the exponential $e^{-\Delta\tau\hat{h}}$, which can be done because we have shown before that it is possible to diagonalize the product in a basis in which the trace amounts to the simple form of equation (3.58).

An alternative way of arriving to this result is to note that in the expression we obtain in the second equality, only the term $\nu = \alpha$ from equation (3.58) contributes [69], leading to the final result with $\rho_{\alpha} = \Delta\tau\varepsilon_{\alpha}$.

The electron density may be obtained from the Green function

$$\rho_{i\sigma} = \langle c_{i\sigma}^\dagger c_{i\sigma} \rangle = 1 - \langle c_{i\sigma} c_{i\sigma}^\dagger \rangle = 1 - G_{ii}^{\sigma}, \tag{3.61}$$

It is natural to think of averaging this over the lattice, and over the spins. This is justified by the fact that the Hubbard Hamiltonian is translationally invariant. Thus, $\rho_{i\sigma}$ should be independent of the spatial site. This statement is strict when exactly solving the model, but it becomes only approximate, i.e. valid only on average in our simulations. Thus, we take the average

$$\rho = \frac{1}{2N} \sum_{\sigma} \sum_{i=1}^N \rho_{i\sigma} \tag{3.62}$$

in an attempt to reduce statistical errors.

One must pay attention to the symmetry of the model at hand, since a similar model for a disordered system including randomness would not be translationally invariant anymore. Moreover, it is implicit that $\rho_{i\sigma}$ is already averaged over the HS-field configurations that were sampled through the simulation.

The average kinetic energy is similarly obtained.

$$\begin{aligned}\langle \mathcal{H}_K \rangle &= -t \sum_{\langle i,j \rangle, \sigma} \left\langle (c_{i\sigma}^\dagger c_{j\sigma} + c_{j\sigma}^\dagger c_{i\sigma}) \right\rangle \\ &= t \sum_{\langle i,j \rangle, \sigma} (G_{ij}^\sigma + G_{ji}^\sigma),\end{aligned}\tag{3.63}$$

where the minus sign is due to the switching of the order of the operators bringing the c^\dagger to the right.

3.1.1.C Correlation functions

One of the most important goals of QMC simulations is to inspect the system for order of various types, and to find associated phase transitions. This is done by computing correlation functions $C(j)$, measuring how correlated two sites separated by a distance j are.

$$C(j) = \langle \mathcal{O}_{i+j} \mathcal{O}_i^\dagger \rangle - \langle \mathcal{O}_{i+j} \rangle \langle \mathcal{O}_i^\dagger \rangle,\tag{3.64}$$

where \mathcal{O} is an operator corresponding to the order parameter of the phase transition. For example, we might be looking for magnetic order, in which case the relevant operators are $\mathcal{O}_i = n_{i\uparrow} - n_{i\downarrow}$, $\mathcal{O}_i^\dagger = n_{i\uparrow} - n_{i\downarrow}$, or superconductivity, where we would like to measure correlations in fermion pair formation: $\mathcal{O}_i = c_{i\downarrow} c_{i\uparrow}$, $\mathcal{O}_i^\dagger = c_{i\uparrow}^\dagger c_{i\downarrow}^\dagger$.

In general, we expect a high temperature disordered phase, for which correlations decay exponentially $C(j) \propto e^{-j/\xi}$, where ξ is a characteristic length called the correlation length. At some point, there can be a transition to a low temperature phase, where $C(j) \propto m^2$, where m is the order parameter for the transition. Right at the transition, that is at $T = T_c$, there might be singular behavior. In continuous phase transitions, the correlation length diverges $\xi \propto (T - T_c)^{-\nu}$, and the correlations decay slower (in fact algebraically): $C(j) \propto j^{-\eta}$, in an intermediate behavior between exponential decay and a constant. The *critical* exponents ν , and η are characteristic of the transition, or more accurately, of the universality class it belongs to.

The behavior of all these quantities on finite lattices does not precisely correspond to the infinite system behavior. The tails of the functions, i.e. the $j \rightarrow \infty$ limit is not well captured. Finite-size scaling is a method to improve on these predictions.

To evaluate correlation functions we use Wick's theorem. Expectations of more than two fermion creation and annihilation operators reduce to products of expectations of pairs of creation and annihilation operators. For example, for pair order:

$$\langle C(j) \rangle = \langle c_{i+j,\downarrow} c_{i+j,\uparrow} c_{i,\uparrow}^\dagger c_{i,\downarrow}^\dagger \rangle\tag{3.65}$$

How would one measure a correlation function experimentally? Fortunately, there is a quantity that is easy to measure called structure factor, which is just the Fourier transform of the correlation function

$$S(q) = \sum_j e^{iqj} C(j)\tag{3.66}$$

The accuracy of QMC simulations can be evaluated by comparing the results for correlation functions with the corresponding structure factors, which can be measured experimentally.

4

Discussing the algorithm

Discuss the algorithm

5

Stabilization

Describe the stabilization algorithm.

6

Applications

Contents

6.1	One-dimensional Hubbard Chain	66
6.2	Square lattice	66
6.3	Honeycomb lattice	66
6.4	Nanoribbon	66

Applying all this to something

6.1 One-dimensional Hubbard Chain

6.2 Square lattice

6.3 Honeycomb lattice

6.4 Nanoribbon

In this section, we apply our code to the case of honeycomb lattice with boundary conditions corresponding to a nanoribbon.

An example of an application of a QMC technique is the simulation of electron correlations in a transition metal dichalcogenide (TMD) nanoribbon, a two-dimensional nanostructure made out of some graphene-like compound [31, 35, 36, 41, 42]. The structure is much longer on one direction than on the other, resembling a ribbon, hence its name. The electronic states that accumulate on the edges of this ribbon might lead to interesting magnetic behavior in these TMD nanostructures (as they do in the analogous graphene nanostructures[37]) and this possibility remains unexplored numerically[38, 39]. Moreover, there is some interest in exploring the phase diagram of these systems because recent studies point at the possibility of topological superconductivity [34].

A nanoribbon is much longer on one direction than on the other, i.e. $l \gg w$. This condition corresponds to taking $N_x \gg N_y$ in our conventions (see figure (6.1), where this condition is, of course, not obeyed solely for the sake of giving a visual representation of the boundary conditions, and the numbering system).

We use three coordinates to label each site on the honeycomb lattice, by taking advantage of its bipartite nature. Regarding the honeycomb lattice as two interpenetrating triangular sublattices A and B , we take the axes x and y to be along the primitive vectors of each triangular sublattice. Along the x -direction, the ribbon is supposed to be very long, which justifies the fact that we take Periodic boundary conditions (PBCs). In contrast, in the narrow y -direction we take Open boundary conditions (OBCs). To number the sites on the ribbon, we introduce an additional coordinate labeling the sublattice: $z = 0$, if the site is in sublattice A , and $z = 1$ if the site is in sublattice B . We then adopt the numbering convention for the sites $i = 1, \dots, 2N_x N_y$ of the lattice \mathcal{L} :

$$i(x, y, z) = N_x N_y z + N_x y + x, \quad (6.1)$$

where $x = 0, \dots, N_x - 1$, $y = 0, \dots, N_y - 1$, and $z = 0, 1$ define each element $\mathbf{r} = (x, y, z) \in \mathcal{L}$.

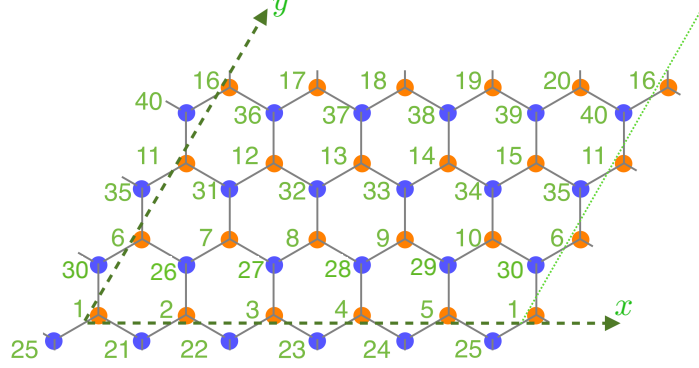


Figure 6.1: An illustration of the boundary conditions on the nanoribbon for $N_x = 5$, $N_y = 4$. Let the orange circles correspond to sublattice A , and the blue circles correspond to sublattice B .

The geometry of the system appears through the hopping matrix \mathbf{K} in our code. This numbering system makes it straightforward to find the neighbors of each site. Let us begin by considering a site that is not on a zigzag edge. There are four possible cases. For example, for

$$z_i = 0, y_i \neq N_y - 1, x_i \neq 0,$$

we have $\langle j_i \rangle = \{j(\mathbf{r})\}$, with \mathbf{r} in

$$\left\{ \mathbf{r}_j \in \mathcal{L} \mid z_j = 1 \wedge \left[\left(y_j = y_i \wedge (x_j = x_i \vee x_j = x_i - 1) \right) \vee \left(y_j = y_i + 1 \wedge x_j = x_i - 1 \right) \right] \right\}$$

As opposed to the sites of a honeycomb lattice with PBCs, which have 3 neighbors, the sites of the zigzag edges have only 2 neighbors. Again, there are four possible cases. For example, for

$$z_i = 0, y_i = N_y - 1, x_i \neq 0,$$

we have $\langle j_i \rangle = \{j(\mathbf{r})\}$, with \mathbf{r} in

$$\left\{ \mathbf{r}_j \in \mathcal{L} \mid z_j = 1 \wedge y_j = y_i \wedge (x_j = x_i \vee x_j = x_i - 1) \right\}$$

We summarize these and the remaining cases in the following table.

Table 6.1: Nearest neighbors on the nanoribbon.

PBCs				OBCs			
Case	z_j	y_j	x_j	Case	z_j	y_j	x_j
$z_i = 0, y_i \neq N_y - 1, x_i \neq 0$	1	y_i	x_i	$z_i = 0, y_i = N_y - 1, x_i \neq 0$	1	y_i	x_i
		$y_i + 1$	$x_i - 1$				$x_i - 1$
$z_i = 0, y_i \neq N_y - 1, x_i = 0$	1	y_i	0	$z_i = 0, y_i = N_y - 1, x_i = 0$	1	y_i	0
		$y_i + 1$	$N_x - 1$				$N_x - 1$
$z_i = 1, y_i \neq 0, x_i \neq N_x - 1$	0	y_i	x_i	$z_i = 1, y_i = 0, x_i \neq N_x - 1$	0	y_i	x_i
		$y_i - 1$	$x_i + 1$				$x_i + 1$
$z_i = 1, y_i \neq 0, x_i = N_x - 1$	0	y_i	$N_x - 1$	$z_i = 1, y_i = 0, x_i = N_x - 1$	0	y_i	0
		$y_i - 1$	0				$N_x - 1$

7

Conclusions and Future Work

Conclusions Chapter

Bibliography

1. Mermin, N. D. & Wagner, H. Absence of Ferromagnetism or Antiferromagnetism in One- or Two-Dimensional Isotropic Heisenberg Models. *Physical Review Letters* **17**, 1133–1136 (Nov. 28, 1966).
2. Coleman, S. There are no Goldstone bosons in two dimensions. *Communications in Mathematical Physics* **31**, 259–264. ISSN: 0010-3616, 1432-0916 (1973).
3. Hohenberg, P. C. Existence of Long-Range Order in One and Two Dimensions. *Physical Review* **158**, 383–386 (June 10, 1967).
4. Hirsch, J. Discrete Hubbard-Stratonovich transformation for fermion lattice models. *Physical Review B* **28**, 4059–4061 (June 16, 1983).
5. Hirsch, J. E., Sugar, R. L., Scalapino, D. J. & Blankenbecler, R. Monte Carlo simulations of one-dimensional fermion systems. *Physical Review B* **26**, 5033–5055 (Nov. 1, 1982).
6. Blankenbecler, R., Scalapino, D. J. & Sugar, R. L. Monte Carlo calculations of coupled boson-fermion systems. I. *Physical Review D* **24**, 2278–2286 (Oct. 15, 1981).
7. Hirsch, J. E. Two-dimensional Hubbard model: Numerical simulation study. *Physical Review B* **31**, 4403–4419 (Apr. 1, 1985).
8. Hirsch, J. E. Monte Carlo Study of the Two-Dimensional Hubbard Model. *Physical Review Letters* **51**, 1900–1903 (Nov. 14, 1983).
9. Hirsch, J. E. Stable monte carlo algorithm for fermion lattice systems at low temperatures. *Physical Review B* **38**, 12023–12026 (Dec. 1, 1988).
10. Hirsch, J. E. & Tang, S. Antiferromagnetism in the Two-Dimensional Hubbard Model. *Physical Review Letters* **62**, 591–594 (Jan. 30, 1989).
11. Dumitrescu, P. T., Serbyn, M., Scalettar, R. T. & Vishwanath, A. Superconductivity and nematic fluctuations in a model of doped FeSe monolayers: Determinant quantum Monte Carlo study. *Physical Review B* **94**, 155127 (Oct. 17, 2016).
12. Berg, E., Lederer, S., Schattner, Y. & Trebst, S. Monte Carlo Studies of Quantum Critical Metals. *arXiv:1804.01988 [cond-mat]*. arXiv: 1804 . 01988. <http://arxiv.org/abs/1804.01988> (2018) (Apr. 5, 2018).
13. Beyl, S., Goth, F. & Assaad, F. F. Revisiting the hybrid quantum Monte Carlo method for Hubbard and electron-phonon models. *Physical Review B* **97**, 085144 (Feb. 22, 2018).
14. Chang, C.-C., Gogolenko, S., Perez, J., Bai, Z. & Scalettar, R. T. Recent advances in determinant quantum Monte Carlo. *Philosophical Magazine* **95**, 1260–1281. ISSN: 1478-6435 (Apr. 23, 2015).
15. Esterlis, I. *et al.* Breakdown of the Migdal-Eliashberg theory: A determinant quantum Monte Carlo study. *Physical Review B* **97**, 140501 (Apr. 2, 2018).

16. Mondaini, R., Ying, T., Paiva, T. & Scalettar, R. T. Determinant quantum Monte Carlo study of the enhancement of \$d\$-wave pairing by charge inhomogeneity. *Physical Review B* **86**, 184506 (Nov. 7, 2012).
17. Meng, Z. Y., Hung, H.-H. & C. Lang, T. The characterization of topological properties in Quantum Monte Carlo simulations of the Kane-Mele-Hubbard model. *Modern Physics Letters B* **28**. doi:10.1142/S0217984914300014 (Jan. 10, 2014).
18. Kung, Y. F. *et al.* Characterizing the three-orbital Hubbard model with determinant quantum Monte Carlo. *Physical Review B* **93**, 155166 (Apr. 29, 2016).
19. Johnston, S. *et al.* Determinant quantum Monte Carlo study of the two-dimensional single-band Hubbard-Holstein model. *Physical Review B* **87**, 235133 (June 24, 2013).
20. Rademaker, L., Johnston, S., Zaanen, J. & van den Brink, J. Determinant quantum Monte Carlo study of exciton condensation in the bilayer Hubbard model. *Physical Review B* **88**, 235115 (Dec. 16, 2013).
21. Ying, T. *et al.* Determinant quantum Monte Carlo study of \$d\$-wave pairing in the plaquette Hubbard hamiltonian. *Physical Review B* **90**, 075121 (Aug. 13, 2014).
22. Scalettar, R. T. *Numerical Studies of Disordered Tight-Binding Hamiltonians* in. Lectures on the Physics of Strongly Correlated Systems XI. **918** (June 1, 2007), 111–202. doi:10.1063/1.2751991. <http://adsabs.harvard.edu/abs/2007AIPC..918..111S> (2018).
23. Zhou, Z., Cai, Z., Wu, C. & Wang, Y. Quantum Monte Carlo simulations of thermodynamic properties of \$\mathrm{SU}(2N)\$ ultracold fermions in optical lattices. *Physical Review B* **90**, 235139 (Dec. 22, 2014).
24. Anderson, P. W. More Is Different. *Science* **177**, 393–396. ISSN: 0036-8075, 1095-9203 (Aug. 4, 1972).
25. Wen, X. G. Topological orders in rigid states. *International Journal of Modern Physics B* **04**, 239–271. ISSN: 0217-9792 (Feb. 1, 1990).
26. Quintanilla, J. & Hooley, C. The strong-correlations puzzle. *Physics World* **22**, 32. ISSN: 2058-7058 (2009).
27. Lieb, E. H. & Wu, F. Y. Absence of Mott Transition in an Exact Solution of the Short-Range, One-Band Model in One Dimension. *Physical Review Letters* **20**, 1445–1448 (June 17, 1968).
28. Hubbard, J. Electron correlations in narrow energy bands. *Proc. R. Soc. Lond. A* **276**, 238–257. ISSN: 0080-4630, 2053-9169 (Nov. 26, 1963).
29. Katsnelson, M. I. Graphene: carbon in two dimensions. *Materials Today* **10**, 20–27. ISSN: 1369-7021 (Jan. 1, 2007).
30. *The Nobel Prize in Physics 2010 - Advanced Information* https://www.nobelprize.org/nobel_prizes/physics/laureates/2010/advanced.html (2018).
31. Wang, Q. H., Kalantar-Zadeh, K., Kis, A., Coleman, J. N. & Strano, M. S. Electronics and optoelectronics of two-dimensional transition metal dichalcogenides. *Nature Nanotechnology* **7**, 699–712. ISSN: 1748-3395 (Nov. 2012).
32. Roldán, R. *et al.* Electronic properties of single-layer and multilayer transition metal dichalcogenides MX₂ (M = Mo, W and X = S, Se). *Annalen der Physik* **526**. doi:10.1002/andp.201400128 (Oct. 1, 2014).
33. Xu, X., Yao, W., di, X. & Heinz, T. Spin and pseudospins in layered transition metal dichalcogenides. *Nature Physics* **10**. doi:10.1038/nphys2942 (Apr. 30, 2014).

34. Hsu, Y.-T., Vaezi, A., Fischer, M. H. & Kim, E.-A. Topological superconductivity in monolayer transition metal dichalcogenides. *Nature Communications* **8**, 14985. ISSN: 2041-1723 (Apr. 11, 2017).
35. Braz, J. E. H., Amorim, B. & Castro, E. V. Valley polarized magnetic state in hole-doped mono layers of transition metal dichalcogenides. *arXiv:1712.07157 [cond-mat]*. arXiv: 1712 . 07157. <http://arxiv.org/abs/1712.07157> (2018) (Dec. 19, 2017).
36. Chen, Y. *et al.* Fabrication of MoSe₂ nanoribbons via an unusual morphological phase transition. *Nature Communications* **8**, 15135. ISSN: 2041-1723 (May 4, 2017).
37. Yazev, O. V. Emergence of magnetism in graphene materials and nanostructures. *Reports on Progress in Physics* **73**, 056501. ISSN: 0034-4885 (2010).
38. Feldner, H. *et al.* Dynamical Signatures of Edge-State Magnetism on Graphene Nanoribbons. *Physical Review Letters* **106**, 226401 (May 31, 2011).
39. Golor, M., Lang, T. C. & Wessel, S. Quantum Monte Carlo studies of edge magnetism in chiral graphene nanoribbons. *Physical Review B* **87**, 155441 (Apr. 30, 2013).
40. Cheng, S., Yu, J., Ma, T. & Peres, N. M. R. Strain-induced edge magnetism at the zigzag edge of a graphene quantum dot. *Physical Review B* **91**, 075410 (Feb. 11, 2015).
41. Raczkowski, M. & Assaad, F. F. Interplay between the edge-state magnetism and long-range Coulomb interaction in zigzag graphene nanoribbons: Quantum Monte Carlo study. *Physical Review B* **96**, 115155 (Sept. 26, 2017).
42. Yang, G., Li, B., Zhang, W., Ye, M. & Ma, T. Strain-tuning of edge magnetism in zigzag graphene nanoribbons. *Journal of Physics: Condensed Matter* **29**, 365601. ISSN: 0953-8984 (2017).
43. Davelou, D., Kopidakis, G., Kaxiras, E. & Remediakis, I. N. Nanoribbon edges of transition-metal dichalcogenides: Stability and electronic properties. *Physical Review B* **96**, 165436 (Oct. 27, 2017).
44. Metropolis, N. & Ulam, S. The Monte Carlo Method. *Journal of the American Statistical Association* **44**, 335–341. ISSN: 0162-1459 (1949).
45. Troyer, M. & Wiese, U.-J. Computational Complexity and Fundamental Limitations to Fermionic Quantum Monte Carlo Simulations. *Physical Review Letters* **94**, 170201 (May 4, 2005).
46. Newman, M. E. J. & Barkema, G. T. *Monte Carlo Methods in Statistical Physics* Google-Books-ID: J5aLdDN4uFwC. 500 pp. ISBN: 978-0-19-851797-9 (Clarendon Press, Feb. 11, 1999).
47. Kosztin, I., Faber, B. & Schulten, K. Introduction to the diffusion Monte Carlo method. *American Journal of Physics* **64**, 633–644. ISSN: 0002-9505 (May 1, 1996).
48. Toulouse, J., Assaraf, R. & Umrigar, C. J. in *Advances in Quantum Chemistry* (eds Hoggan, P. E. & Ozdogan, T.) 285–314 (Academic Press, Jan. 1, 2016). doi:10 . 1016/bs . aiq . 2015 . 07 . 003. <http://www.sciencedirect.com/science/article/pii/S0065327615000386> (2018).
49. Fazekas, P. *Lecture Notes on Electron Correlation and Magnetism* Google-Books-ID: GV5pyxX3TfMC. 798 pp. ISBN: 978-981-02-2474-5 (World Scientific, Jan. 1, 1999).
50. Mahan, G. D. *Many-Particle Physics* 3rd ed. ISBN: 978-0-306-46338-9. //www.springer.com/gp/book/9780306463389 (2018) (Springer US, 2000).
51. Altland, A. & Simons, B. D. *Condensed Matter Field Theory* Cambridge Core. /core/books/condensed-matter-field-theory/0A8DE6503ED868D96985D9E7847C63FF (2018).
52. Hayes, B. Hip-Hop Physics. *American Scientist* **97**. <https://www.americanscientist.org/article/hip-hop-physics> (2018) (Dec. 2009).

53. Bohm, D. & Pines, D. A Collective Description of Electron Interactions: III. Coulomb Interactions in a Degenerate Electron Gas. *Physical Review* **92**, 609–625 (Nov. 1, 1953).
54. Gell-Mann, M. & Brueckner, K. A. Correlation Energy of an Electron Gas at High Density. *Physical Review* **106**, 364–368 (Apr. 15, 1957).
55. Sawada, K., Brueckner, K. A., Fukuda, N. & Brout, R. Correlation Energy of an Electron Gas at High Density: Plasma Oscillations. *Physical Review* **108**, 507–514 (Nov. 1, 1957).
56. Hubbard, J. The description of collective motions in terms of many-body perturbation theory. II. The correlation energy of a free-electron gas. *Proc. R. Soc. Lond. A* **243**, 336–352. ISSN: 0080-4630, 2053-9169 (Jan. 14, 1958).
57. Hubbard, J. The description of collective motions in terms of many-body perturbation theory III. The extension of the theory to the non-uniform gas. *Proc. R. Soc. Lond. A* **244**, 199–211. ISSN: 0080-4630, 2053-9169 (Mar. 11, 1958).
58. Nozières, P. & Pines, D. Electron Interaction in Solids. General Formulation. *Physical Review* **109**, 741–761 (Feb. 1, 1958).
59. Editorial. The Hubbard model at half a century. *Nature Physics* **9**, 523. ISSN: 1745-2481 (Sept. 2013).
60. Ashcroft, N. W. & Mermin, N. D. *Solid State Physics* Google-Books-ID: 1C9HAQAAIAAJ. 856 pp. ISBN: 978-0-03-083993-1 (Holt, Rinehart and Winston, 1976).
61. H de Boer, J. & J W Verwey, E. Semiconductors With Partially and With Completely Filled 3d-Lattice Bands. *Proceedings of the Physical Society* **49**, 59 (1937).
62. Mott, N. F. & Peierls, R. Discussion of the paper by de Boer and Verwey. *Proceedings of the Physical Society* **49**, 72. ISSN: 0959-5309 (1937).
63. Mott, N. F. The Basis of the Electron Theory of Metals, with Special Reference to the Transition Metals. *Proceedings of the Physical Society. Section A* **62**, 416. ISSN: 0370-1298 (1949).
64. PoorLeno. *Hydrogen Density Plots* https://commons.wikimedia.org/wiki/File:Hydrogen_Density_Plots.png. Accessed: 2018-05-03.
65. Alavi, A. et al. *Quantum Materials: Experiments and Theory* ISBN: 978-3-95806-159-0 (Aug. 31, 2016).
66. Mila, F. *Physique du Solide III et IV* (École Polytechnique Fédérale de Lausanne, 2007).
67. Gennes, P.-G. d. *Superconductivity of Metals and Alloys* Google-Books-ID: xacsAAAAYAAJ. 292 pp. ISBN: 978-0-7382-0101-6 (Advanced Book Program, Perseus Books, 1999).
68. Bai, Z., Chen, W., Scalettar, R. & Yamazaki, I. in Hou, T. Y., Liu, C. & Liu, J.-G. *Series in Contemporary Applied Mathematics* 1–110 (CO-PUBLISHED WITH HIGHER EDUCATION PRESS, June 2009). ISBN: 978-981-4273-25-1 978-981-4273-26-8. doi:10.1142/9789814273268_0001. http://www.worldscientific.com/doi/abs/10.1142/9789814273268_0001 (2018).
69. Santos, R. R. d. Introduction to quantum Monte Carlo simulations for fermionic systems. *Brazilian Journal of Physics* **33**, 36–54. ISSN: 0103-9733 (Mar. 2003).



Hartree-Fock Approximation and the Self Consistent Field Method

In the mean field approximation, the quartic term of the interaction part of the Hamiltonian

$$V_{\text{int}} = \frac{1}{2} V_{\nu' \mu'}^{\nu \mu} c_{\nu}^{\dagger} c_{\mu}^{\dagger} c_{\mu'} c_{\nu'},$$

becomes a sum of all possible 2-body terms (note that terms of the type $\langle cc \rangle$ and $\langle c^{\dagger}c^{\dagger} \rangle$ must vanish since they do not conserve the number of particles).

$$c_{\nu}^{\dagger} c_{\mu}^{\dagger} c_{\mu'} c_{\nu'} \approx -\langle c_{\nu}^{\dagger} c_{\mu'} \rangle c_{\mu}^{\dagger} c_{\nu'} - \langle c_{\mu}^{\dagger} c_{\nu'} \rangle c_{\nu}^{\dagger} c_{\mu'} + \langle c_{\nu}^{\dagger} c_{\nu'} \rangle c_{\mu}^{\dagger} c_{\mu'} + \langle c_{\mu}^{\dagger} c_{\mu'} \rangle c_{\nu}^{\dagger} c_{\nu'}, \quad (\text{A.1})$$

where we ignored the constant terms which are unimportant in the Hamiltonian, in what concerns the dynamics.

This Hartree-Fock, or mean field approximation is slightly tricky to obtain. It requires one to be precise about what the meaning of the mean field approximation is in terms of creation and annihilation operators. In mean field theory, we assume that the operator

$$\rho_{\mu \mu'} = c_{\mu}^{\dagger} c_{\mu'} \quad (\text{A.2})$$

is close to its average, so that we neglect second order terms in the fluctuations $\delta \rho_{\mu \mu'}$, i.e. $\rho_{\mu \mu'}$ is “large” only when its average is nonzero, otherwise it is negligibly small. Thus, for most combinations of indices, this operator will vanish. We follow the usual mean field procedure of writing the original operator as a deviation plus an average

$$c_{\nu}^{\dagger} \left(c_{\mu}^{\dagger} c_{\mu'} - \langle c_{\mu}^{\dagger} c_{\mu'} \rangle \right) c_{\nu'} + c_{\nu}^{\dagger} c_{\nu'} \langle c_{\nu}^{\dagger} c_{\nu'} \rangle \quad (\text{A.3})$$

Then we note that if $\nu' \neq \mu$, we can commute $c_{\nu'}$ with the parenthesis. But this is true except in a set of measure zero. In the thermodynamic limit $N \rightarrow \infty$, the number of allowed \mathbf{k} -states is very large, and if we take a continuum limit in which the set of possible \mathbf{k} -states becomes dense, then the commutation becomes exact. Repeating the procedure of writing (A.3) replacing $c_{\nu}^{\dagger} c_{\nu'} \mapsto c_{\nu}^{\dagger} c_{\nu'} - \langle c_{\nu}^{\dagger} c_{\nu'} \rangle + \langle c_{\nu}^{\dagger} c_{\nu'} \rangle$, we obtain

$$\underbrace{(c_{\nu}^{\dagger} c_{\nu'} - \langle c_{\nu}^{\dagger} c_{\nu'} \rangle)(c_{\mu}^{\dagger} c_{\mu'} - \langle c_{\mu}^{\dagger} c_{\mu'} \rangle)}_{\propto \delta \rho_{\mu \mu'} \delta \rho_{\nu \nu'} \rightarrow 0} + c_{\nu}^{\dagger} c_{\nu'} \langle c_{\mu}^{\dagger} c_{\mu'} \rangle + c_{\mu}^{\dagger} c_{\mu'} \langle c_{\nu}^{\dagger} c_{\nu'} \rangle - \langle c_{\mu}^{\dagger} c_{\mu'} \rangle \langle c_{\nu}^{\dagger} c_{\nu'} \rangle \quad (\text{A.4})$$

But this result is not complete. This is only the so called Hartree or direct term. Due to identical nature of the interacting electrons, we must consider an analogous contribution for $\langle c_{\nu}^{\dagger} c_{\mu'} \rangle$ finite. We start by exchanging the first two operators:

$$c_{\nu}^{\dagger} c_{\mu}^{\dagger} c_{\mu'} c_{\nu'} = -c_{\mu}^{\dagger} c_{\nu}^{\dagger} c_{\mu'} c_{\nu'} \quad (\text{A.5})$$

Then we proceed in exactly the same manner as before. The result is analogous, but a minus sign appears and we must switch $\mu \leftrightarrow \nu$:

$$- c_\mu^\dagger c_{\nu'} \langle c_\nu^\dagger c_{\mu'} \rangle - c_\nu^\dagger c_{\mu'} \langle c_\mu^\dagger c_{\nu'} \rangle + \langle c_\nu^\dagger c_{\mu'} \rangle \langle c_\mu^\dagger c_{\nu'} \rangle \quad (\text{A.6})$$

Ignoring the constant terms of the type $\langle c^\dagger c \rangle \langle c^\dagger c \rangle$, we recover equation (A.1).

Now we can simply substitute the mean field expansion of equation (A.1) in the second term to obtain the last term that is subtracted in equation (2.1) (we omit the boldface on the \mathbf{k} 's solely in the following equation, but keep in mind that they are vectors):

$$\begin{aligned} & \frac{1}{2} \sum_{\substack{k_1 k_2 k'_1 k'_2 \\ \sigma_1 \sigma_2}} V_{k'_1 k'_2}^{k_1 k_2} \left(- \underbrace{\langle c_{k_1 \sigma_1}^\dagger c_{k'_2 \sigma_2} \rangle}_{\delta_{k_1 k'_2} \delta_{\sigma_1 \sigma_2} f_{k_1}} c_{k_2 \sigma_2}^\dagger c_{k'_1 \sigma_1} - \underbrace{\langle c_{k_2 \sigma_2}^\dagger c_{k'_1 \sigma_1} \rangle}_{\delta_{k_2 k'_1} \delta_{\sigma_1 \sigma_2} f_{k_2}} c_{k_1 \sigma_1}^\dagger c_{k'_2 \sigma_2} + \underbrace{\langle c_{k_1 \sigma_1}^\dagger c_{k'_1 \sigma_1} \rangle}_{\delta_{k_1 k'_1} f_{k_1}} c_{k_2 \sigma_2}^\dagger c_{k'_2 \sigma_2} \right. \\ & \left. + \underbrace{\langle c_{k_2 \sigma_2}^\dagger c_{k'_2 \sigma_2} \rangle}_{\delta_{k_2 k'_2} f_{k_2}} c_{k_1 \sigma_1}^\dagger c_{k'_1 \sigma_1} \right) \end{aligned} \quad (\text{A.7})$$

In the language of Hartree Fock theory, the first two terms give the exchange term, and the last two terms the direct term. Apart from the $\frac{1}{2}$ factor, the term in (A.7) becomes

$$\begin{aligned} & - \sum_{\substack{k_1 k_2 \\ k'_1 \sigma_1}} V_{k'_1 k_1}^{k_1 k_2} f_{k_1} c_{k_2 \sigma_1}^\dagger c_{k'_1 \sigma_1} - \sum_{\substack{k_1 k_2 \\ k'_2 \sigma_1}} V_{k_2 k'_2}^{k_1 k_2} f_{k_2} c_{k_1 \sigma_1}^\dagger c_{k'_2 \sigma_1} + \sum_{\substack{k_1 k_2 k'_2 \\ \sigma_1 \sigma_2}} V_{k_1 k'_2}^{k_1 k_2} f_{k_1} c_{k_2 \sigma_2}^\dagger c_{k'_2 \sigma_2} \\ & + \sum_{\substack{k_1 k_2 k'_1 \\ \sigma_1 \sigma_2}} V_{k'_1 k'_2}^{k_1 k_2} f_{k_2} c_{k_1 \sigma_1}^\dagger c_{k'_1 \sigma_1} \\ & = \sum_{k_1 k_2 \sigma_1} \left(4V_{k_1 k_2}^{k_1 k_2} - 2V_{k_2 k_1}^{k_1 k_2} \right) f_{k_2} c_{k_1 \sigma_1}^\dagger c_{k_1 \sigma_1}, \end{aligned} \quad (\text{A.8})$$

where we used momentum conservation to eliminate a k' -sum. Moreover, we used that the sum on spin ($\pm 1/2$) on the last two terms gives factors of 2, since the interaction is spin independent and thus no spin-dependent term remains after we use momentum conservation. Making $k_1 \rightarrow k$, $k_2 \rightarrow k'$, $\sigma_1 \rightarrow \sigma$, and recalling the definition in equation (2.2), we obtain the result we sought.

The procedure above is meant to serve as an intuitive derivation. Now we approach the problem more formally. In fact, the argument that allowed us to perform the commutation leading to equation A.4 seems somewhat handwaving. We should not have to take the thermodynamic limit to perform a mean field expansion. A more systematic procedure to obtain the mean field expansion of a quartic interaction term was given by Pierre de Gennes in the context of a mean field treatment of a superconductor in a magnetic field [67]. Our case is actually much simpler to analyze, but we follow the same argument as de Gennes.

Consider the Hamiltonian to be given by $\mathcal{H} = \mathcal{H}_0 + \mathcal{H}_1$, where

$$\begin{aligned}\mathcal{H}_0 &= \sum_{\mathbf{k}, \sigma} \varepsilon_{\mathbf{k}} c_{\mathbf{k}, \sigma}^\dagger c_{\mathbf{k}, \sigma} \\ \mathcal{H}_1 &= \frac{1}{2} \sum_{\substack{\mathbf{k}_1 \mathbf{k}_2 \\ \mathbf{k}'_1 \mathbf{k}'_2 \\ \sigma_1 \sigma_2}} V_{\mathbf{k}_1 \mathbf{k}_2}^{k_1 k_2} c_{\mathbf{k}_1 \sigma_1}^\dagger c_{\mathbf{k}_2 \sigma_2}^\dagger c_{\mathbf{k}'_2 \sigma_2} c_{\mathbf{k}'_1 \sigma_1}\end{aligned}\tag{A.9}$$

We would like to find an effective Hamiltonian that is quadratic in the fermion operators:

$$\mathcal{H}_{\text{eff}} = \sum_{\mathbf{k}, \sigma} (\varepsilon_{\mathbf{k}} + v_{\mathbf{k}}) c_{\mathbf{k}, \sigma}^\dagger c_{\mathbf{k}, \sigma}\tag{A.10}$$

This effective Hamiltonian is diagonal, so assuming we know $v_{\mathbf{k}}$ (which is what we are trying to determine in the first place), we can compute its eigenstates $\{|\phi\rangle\}$, and compute the average of the actual Hamiltonian \mathcal{H} using the basis $\{|\phi\rangle\}$:

$$\langle \mathcal{H} \rangle = \frac{\sum_{\phi} \langle \phi | \mathcal{H} | \phi \rangle e^{-\beta E_{\phi}}}{\sum_{\phi} e^{-\beta E_{\phi}}}\tag{A.11}$$

Our criterion to determine \mathcal{H}_{eff} is the requirement that the free energy $F = \langle \mathcal{H} \rangle - TS$, with the average computed with the eigenstates of \mathcal{H}_{eff} be stationary, i.e. $\delta F = 0$. Thus, we find the mean field form of the quartic term invoking only a variational principle without any need to resort to the thermodynamic limit. In fact, we never even have to explicitly compute the average in equation (A.11). In terms of pairs of fermion operator averages, we have

$$\langle \mathcal{H} \rangle = \sum_{\mathbf{k}, \sigma} \varepsilon_{\mathbf{k}} \left\langle c_{\mathbf{k}, \sigma}^\dagger c_{\mathbf{k}, \sigma} \right\rangle + \frac{1}{2} \sum_{\substack{\mathbf{k}_1 \mathbf{k}_2 \\ \mathbf{k}'_1 \mathbf{k}'_2 \\ \sigma_1 \sigma_2}} V_{\mathbf{k}_1 \mathbf{k}_2}^{k_1 k_2} \left\langle c_{\mathbf{k}_1 \sigma_1}^\dagger c_{\mathbf{k}_2 \sigma_2}^\dagger c_{\mathbf{k}'_2 \sigma_2} c_{\mathbf{k}'_1 \sigma_1} \right\rangle,\tag{A.12}$$

where the last term can be reduced to products of averages of pairs of fermion operators by Wick's theorem:

$$\begin{aligned}\left\langle c_{\mathbf{k}_1 \sigma_1}^\dagger c_{\mathbf{k}_2 \sigma_2}^\dagger c_{\mathbf{k}'_2 \sigma_2} c_{\mathbf{k}'_1 \sigma_1} \right\rangle &= \left\langle c_{\mathbf{k}_1 \sigma_1}^\dagger c_{\mathbf{k}'_1 \sigma_1} \right\rangle \left\langle c_{\mathbf{k}_2 \sigma_2}^\dagger c_{\mathbf{k}'_2 \sigma_2} \right\rangle - \left\langle c_{\mathbf{k}_1 \sigma_1}^\dagger c_{\mathbf{k}'_2 \sigma_2} \right\rangle \left\langle c_{\mathbf{k}_2 \sigma_2}^\dagger c_{\mathbf{k}'_1 \sigma_1} \right\rangle \\ &+ \left\langle c_{\mathbf{k}_1 \sigma_1}^\dagger c_{\mathbf{k}_2 \sigma_2}^\dagger \right\rangle \left\langle c_{\mathbf{k}'_2 \sigma_2} c_{\mathbf{k}'_1 \sigma_1} \right\rangle\end{aligned}\tag{A.13}$$

The computation is now done by using the rules (for all \mathbf{k} and σ).

$$\begin{aligned}\left\langle c_{\mathbf{k}, \sigma}^\dagger c_{\mathbf{k}', \sigma'} \right\rangle &= \delta_{\mathbf{k}, \mathbf{k}'} \delta_{\sigma, \sigma'} f_{\mathbf{k}} \\ \left\langle c_{\mathbf{k}, \sigma}^{(\dagger)} c_{\mathbf{k}', \sigma'}^{(\dagger)} \right\rangle &= 0,\end{aligned}\tag{A.14}$$

where $f_{\mathbf{k}} = (e^{\beta(\varepsilon_{\mathbf{k}} - \mu)} + 1)^{-1}$ is the Fermi-Dirac function.

Since the original Hamiltonian is quadratic, again we have that terms of the type $\langle cc \rangle$ and $\langle c^\dagger c^\dagger \rangle$ do not contribute. Hence, varying the free energy, we obtain

$$\delta F = \delta \langle \mathcal{H} \rangle - T\delta S = \sum_{\mathbf{k}\sigma} \varepsilon_{\mathbf{k}} \delta \left\langle c_{\mathbf{k},\sigma}^\dagger c_{\mathbf{k},\sigma} \right\rangle + \frac{1}{2} \sum_{\substack{\mathbf{k}_1 \mathbf{k}_2 \\ \mathbf{k}'_1 \mathbf{k}'_2 \\ \sigma_1 \sigma_2}} V_{\mathbf{k}'_1 \mathbf{k}'_2}^{k_1 k_2} \left(\left\langle c_{\mathbf{k}_1 \sigma_1}^\dagger c_{\mathbf{k}'_1 \sigma_1} \right\rangle \delta \left\langle c_{\mathbf{k}_2 \sigma_2}^\dagger c_{\mathbf{k}'_2 \sigma_2} \right\rangle + \right. \\ \left. \delta \left\langle c_{\mathbf{k}_1 \sigma_1}^\dagger c_{\mathbf{k}'_1 \sigma_1} \right\rangle \left\langle c_{\mathbf{k}_2 \sigma_2}^\dagger c_{\mathbf{k}'_2 \sigma_2} \right\rangle - \left\langle c_{\mathbf{k}_1 \sigma_1}^\dagger c_{\mathbf{k}'_2 \sigma_2} \right\rangle \delta \left\langle c_{\mathbf{k}_2 \sigma_2}^\dagger c_{\mathbf{k}'_1 \sigma_1} \right\rangle - \delta \left\langle c_{\mathbf{k}_1 \sigma_1}^\dagger c_{\mathbf{k}'_2 \sigma_2} \right\rangle \left\langle c_{\mathbf{k}_2 \sigma_2}^\dagger c_{\mathbf{k}'_1 \sigma_1} \right\rangle \right) - T\delta S, \quad (\text{A.15})$$

which can be simplified exactly in the same manner as in equation (A.7), i.e. by using the rules of equation (A.14), and that the occupation of a given momentum state \mathbf{k} is given by the Fermi-Dirac function:

$$\delta F = \sum_{\mathbf{k}\sigma} \varepsilon_{\mathbf{k}} \delta \left\langle c_{\mathbf{k},\sigma}^\dagger c_{\mathbf{k},\sigma} \right\rangle + \sum_{\mathbf{k}\mathbf{k}'\sigma} \left(2V_{\mathbf{k}\mathbf{k}'}^{\mathbf{k}\mathbf{k}'} - V_{\mathbf{k}'\mathbf{k}'}^{\mathbf{k}\mathbf{k}'} \right) f_{\mathbf{k}'} c_{\mathbf{k}\sigma} \delta \left\langle c_{\mathbf{k},\sigma}^\dagger c_{\mathbf{k},\sigma} \right\rangle \quad (\text{A.16})$$

We can now compare $\delta F = \delta \langle \mathcal{H} \rangle - T\delta S$ and $\delta F' = \delta \langle \mathcal{H}_{\text{eff}} \rangle - T\delta S$, which is simply given by

$$\delta F' = \delta \langle \mathcal{H}_{\text{eff}} \rangle - T\delta S = \sum_{\mathbf{k}\sigma} (\varepsilon_{\mathbf{k}} + v_{\mathbf{k}}) \delta \left\langle c_{\mathbf{k},\sigma}^\dagger c_{\mathbf{k},\sigma} \right\rangle \quad (\text{A.17})$$

Requiring both free energies to be stationary, we find our desired result

$$v_{\mathbf{k}} = \sum_{\mathbf{k}'} \left(2V_{\mathbf{k}\mathbf{k}'}^{\mathbf{k}\mathbf{k}'} - V_{\mathbf{k}'\mathbf{k}'}^{\mathbf{k}\mathbf{k}'} \right) f_{\mathbf{k}'}, \quad (\text{A.18})$$

which agrees with the result obtained from our initial more intuitive, but somewhat less rigorous argument.

B

Computing the partition function for a
quadratic Hamiltonian

Let us start by restating the result we want to prove.

If $\mathcal{H} = \mathbf{c}^\dagger \mathbf{H} \mathbf{c}$, where \mathbf{H} is a $N \times N$ Hermitian matrix, then we have that

$$\text{Tr}[e^{-\beta \mathcal{H}}] = \prod_{i=1}^N (1 + e^{-\beta \lambda_i}), \quad (\text{B.1})$$

where λ_i are the eigenvalues of \mathbf{H} .

We will now prove equation (B.1). Without loss of generality, let us consider \mathbf{H} to be diagonal. Then, its eigenvalues coincide with the diagonal entries, so that $\mathbf{H} = \text{diag}(\lambda_i)$. The quadratic Hamiltonian may then be diagonalized

$$\mathcal{H} = \mathbf{c}^\dagger \text{diag}(\lambda_1, \lambda_2, \dots, \lambda_N) \mathbf{c} = \sum_{i=1}^N \lambda_i n_i$$

We continue by induction. When $N = 1$, we have

$$\text{Tr}(e^{-\beta \mathcal{H}}) = \langle 0 | e^{-\beta \lambda_1 n_1} | 0 \rangle + \langle 1 | e^{-\beta \lambda_1 n_1} | 1 \rangle = 1 + e^{-\beta \lambda_1} \quad (\text{B.2})$$

Assuming that for $N - 1$:

$$\text{Tr}[e^{-\beta \sum_{i=1}^{N-1} \lambda_i n_i}] = \prod_{i=1}^{N-1} (1 + e^{-\beta \lambda_i})$$

we can compute the trace for i going up to N .

$$\begin{aligned} \text{Tr}[e^{-\beta \sum_{i=1}^N \lambda_i n_i}] &= \sum_{i=1}^N \left\langle \psi_1^{\lambda_1} \psi_2^{\lambda_2} \dots \psi_N^{\lambda_N} \middle| e^{-\beta \sum_{i=1}^N \lambda_i n_i} \right| \psi_1^{\lambda_1} \psi_2^{\lambda_2} \dots \psi_N^{\lambda_N} \right\rangle \\ &= \sum_{i=1}^{N-1} \left(\left\langle \{\psi_i^{\lambda_i}\} 0 \middle| e^{-\beta \sum_{i=1}^N \lambda_i n_i} e^{-\beta \lambda_N n_N} \right| \{\psi_i^{\lambda_i}\} 0 \right\rangle + \left\langle \{\psi_i^{\lambda_i}\} 1 \middle| e^{-\beta \sum_{i=1}^N \lambda_i n_i} e^{-\beta \lambda_N n_N} \right| \{\psi_i^{\lambda_i}\} 1 \right\rangle \right) \\ &= (1 + e^{-\beta \lambda_N}) \sum_{i=1}^{N-1} \left\langle \{\psi_i^{\lambda_i}\} \middle| e^{-\beta \lambda_i n_i} \right| \{\psi_i^{\lambda_i}\} \right\rangle \\ &= (1 + e^{-\beta \lambda_N}) \prod_{i=1}^{N-1} (1 + e^{-\beta \lambda_i}) \\ &= \prod_{i=1}^N (1 + e^{-\beta \lambda_i}) \end{aligned}$$

To complete the proof we note that for any \mathbf{H} , there exists a unitary matrix \mathbf{Q} , such that $\mathbf{Q}^T \mathbf{H} \mathbf{Q} = \mathbf{\Lambda} = \text{diag}(\lambda_i)$. Let $\tilde{\mathbf{c}} = \mathbf{Q} \mathbf{c}$, and $\tilde{n}_i = \tilde{c}_i^\dagger \tilde{c}_i$. Then, we find

$$\mathcal{H} = \mathbf{c}^\dagger \mathbf{H} \mathbf{c} = \tilde{\mathbf{c}}^\dagger \mathbf{\Lambda} \tilde{\mathbf{c}} = \sum_{i=1}^N \lambda_i \tilde{n}_i$$

The trace is independent of the choice of basis functions. Thus, we have

$$\begin{aligned}\mathrm{Tr}(e^{-\beta \mathcal{H}}) &= \mathrm{Tr}\left(\prod_{i=1}^N e^{-\beta \lambda_i \tilde{n}_i}\right) \\ &= \prod_{i=1}^N \left(1 + e^{-\beta \lambda_i}\right)\end{aligned}$$

C

Obtaining an effective Heisenberg
Hamiltonian as the $U/t \gg 1$ limit of
the Hubbard model

To obtain the effective Hamiltonian corresponding to the $U/t \gg 1$ limit of the Hubbard model to second order in degenerate perturbation theory, we start with its general form, as obtained in equation (2.69).

$$\mathcal{H}_{\text{eff}} = -\mathcal{H}_0 \frac{\sum_j n_{j,\sigma} n_{j,-\sigma}}{U} \mathcal{H}_0 \quad (\text{C.1})$$

For each element j of the sum, only terms of type

$$\sum_{i(j)} c_{j\sigma}^\dagger c_{i\sigma}$$

contribute. Here $\sum_{i(j)}$ is a sum over the set of neighbors i of site j .

A term of the effective Hamiltonian \mathcal{H}_{eff} corresponding to the j -th element in the sum reads

$$-\frac{t^2}{U} \sum_{i(j), \sigma_1, \sigma_2} c_{i,\sigma_1}^\dagger c_{j,\sigma_1} n_{j,\sigma} n_{j,-\sigma} c_{j,\sigma_2}^\dagger c_{i,\sigma_2}$$

There are only four cases in which the contribution of a term of this type is nonzero.

- $\sigma = \sigma_1 = \sigma_2$

The operator in the sum then becomes

$$c_{i,\sigma}^\dagger c_{j,\sigma} n_{j,\sigma} n_{j,-\sigma} c_{j,\sigma}^\dagger c_{i,\sigma} = n_{i,\sigma} n_{j,-\sigma} c_{j,\sigma} n_{j,\sigma} c_{j,\sigma}^\dagger$$

Now, we use a fermionic operator identity:

$$\begin{aligned} cn &= cc^\dagger c = (1 - c^\dagger c)c = c \\ \implies c_{j,\sigma} n_{j,\sigma} c_{j,\sigma}^\dagger &= c_{j,\sigma} c_{j,\sigma}^\dagger = 1 - n_{j,\sigma} \end{aligned}$$

The term of the Hamiltonian corresponding to this first case then takes on the form

$$n_{i,\sigma} n_{j,-\sigma} (1 - n_{j,\sigma})$$

We can further simplify this term by noting that in the subspace where \mathcal{H}_{eff} acts, every site is occupied by only a single electron so that

$$n_{j,\sigma} + n_{j,-\sigma} = 1 \iff 1 - n_{j,\sigma} = n_{j,-\sigma}$$

Since, for fermions we have that $\hat{n} = \hat{n}^k$, whichever the power $k \in \mathbb{N}$, the final form of the sought term of the Hamiltonian is

$$n_{i,\sigma} n_{j,-\sigma}$$

- $-\sigma = \sigma_1 = \sigma_2$

The contribution to the Hamiltonian is exactly of the same form but making $\sigma \mapsto -\sigma$:

$$n_{i,-\sigma} n_{j,\sigma}$$

- $\sigma = -\sigma_1 = \sigma_2$

We can use the same reasoning as we did for the first term to obtain

$$\begin{aligned} & c_{i,-\sigma}^\dagger c_{j,-\sigma} n_{j,\sigma} n_{j,-\sigma} c_{j,\sigma}^\dagger c_{i,\sigma} \\ &= c_{i,-\sigma}^\dagger c_{i,\sigma} \underbrace{c_{j,-\sigma} n_{j,-\sigma}}_{c_{j,-\sigma}} \underbrace{n_{j,\sigma} c_{j,\sigma}^\dagger}_{c_{j,\sigma}^\dagger} \\ &= -c_{i,-\sigma}^\dagger c_{i,\sigma} c_{j,\sigma}^\dagger c_{j,-\sigma} \end{aligned}$$

- $-\sigma = -\sigma_1 = \sigma_2$

Analogously, the contribution to the Hamiltonian is

$$\begin{aligned} & c_{i,\sigma}^\dagger c_{j,\sigma} n_{j,\sigma} n_{j,-\sigma} c_{j,-\sigma}^\dagger c_{i,-\sigma} \\ &= -c_{i,-\sigma}^\dagger c_{i,\sigma} c_{j,\sigma}^\dagger c_{j,-\sigma} \end{aligned}$$

Grouping all these four terms, we obtain

$$\mathcal{H}_{\text{eff}} = \frac{2t^2}{U} \sum_{\langle i,j \rangle, \sigma} (-n_{i,\sigma} n_{j,-\sigma} + c_{i,-\sigma}^\dagger c_{i,\sigma} c_{j,\sigma}^\dagger c_{j,-\sigma}), \quad (\text{C.2})$$

where the factor of 2 appears because for each pair of nearest neighbors $\langle i,j \rangle$, a term comes from the term $n_{j,\sigma} n_{j,-\sigma}$ of the sum $\sum_j n_{j,\sigma} n_{j,-\sigma}$, and another term from $n_{i,\sigma} n_{i,-\sigma}$.

Recall the second quantized form of the spin operators:

$$\begin{cases} S_i^z = \frac{1}{2}(n_{i,\uparrow} - n_{i,\downarrow}) \\ S_i^+ = c_{i,\uparrow}^\dagger c_{i,\downarrow} \\ S_i^- = c_{i,\downarrow}^\dagger c_{i,\uparrow}, \end{cases} \quad (\text{C.3})$$

Using these relations and that the density operator is $n_i = n_{i,\uparrow} + n_{i,\downarrow}$, the following relations hold

$$\begin{aligned} S_i^z S_j^z - \frac{1}{4} n_i n_j &= -\frac{1}{2} (n_{i,\uparrow} n_{j,\downarrow} + n_{i,\downarrow} n_{j,\uparrow}) \\ S_i^+ S_j^- + S_i^- S_j^+ &= c_{i,\uparrow}^\dagger c_{i,\downarrow} c_{j,\downarrow}^\dagger c_{j,\uparrow} + c_{i,\downarrow}^\dagger c_{i,\uparrow} c_{j,\uparrow}^\dagger c_{j,\downarrow} \end{aligned} \quad (\text{C.4})$$

Thus, we may rewrite the effective Hamiltonian:

$$\mathcal{H}_{\text{eff}} = \frac{4t^2}{U} \sum_{\langle i,j \rangle} \left(S_i^z S_j^z - \frac{1}{4} n_i n_j + \frac{1}{2} (S_i^+ S_j^- + S_i^- S_j^+) \right) \quad (\text{C.5})$$

But $S_i^z S_j^z + \frac{1}{2}(S_i^+ S_j^- + S_i^- S_j^+) = \mathbf{S}_i \cdot \mathbf{S}_j$ and $n_i = n_j = 1$ in the ground state subspace, so the effective Hamiltonian becomes

$$\mathcal{H}_{\text{eff}} = \frac{4t^2}{U} \sum_{\langle i,j \rangle} \left(\mathbf{S}_i \cdot \mathbf{S}_j - \frac{1}{4} \right), \quad (\text{C.6})$$

which corresponds to the antiferromagnetic Heisenberg model: $\mathcal{H}_{\text{Heis}} = J \sum_{\langle i,j \rangle} \mathbf{S}_i \cdot \mathbf{S}_j$, with $J = 4t^2/U$.